COMPARISON OF ORDINARY KRIGING AND DEEP LEARNING METHODS IN GRADE ESTIMATION: A PILOT STUDY ON THE SIRAKAYALAR Au MINERALIZATION (NW TÜRKİYE)

A THESIS SUBMITTED TO
THE GRADUATE SCHOOL OF NATURAL AND APPLIED SCIENCES
OF
MIDDLE EAST TECHNICAL UNIVERSITY

BY

ALİ BUĞRA ÖZGÜN

IN PARTIAL FULFILLMENT OF THE REQUIREMENTS
FOR
THE DEGREE OF MASTER OF SCIENCE
IN
GEOLOGICAL ENGINEERING

August 2025

Approval of the thesis:

COMPARISON OF ORDINARY KRIGING AND DEEP LEARNING METHODS IN GRADE ESTIMATION: A PILOT STUDY ON THE SIRAKAYALAR Au MINERALIZATION (NW TÜRKİYE)

submitted by **Ali BUĞRA ÖZGÜN** in partial fulfillment of the requirements for the degree of **Master of Science** i**n Geological Engineering, Middle East Technical University** by,

Prof. Dr. Naci Emre Altun
Dean, **Graduate School of Natural and Applied Sciences** _____

Prof. Dr. Erdin Bozkurt
Head of the Department, **Geological Engineering, METU** _____

Assist. Prof. Dr. Ali İmer
Supervisor, **Geological Engineering, METU** _____

Examining Committee Members:

Prof. Dr. A. Erhan Tercan
Mining Engineering, Hacettepe University _____

Assist. Prof. Dr. Ali İmer
Geological Engineering, METU _____

Prof. Dr. Kaan Sayit
Geological Engineering, METU _____

Assoc. Prof. Dr. Sinan Akıska
Geological Engineering, Ankara University _____

Assoc. Prof. Dr. Fırat Atalay
Mining Engineering, Hacettepe University _____

Date: 28.08.2025

I hereby declare that all information in this document has been obtained and presented in accordance with academic rules and ethical conduct. I also declare that, as required by these rules and conduct, I have fully cited and referenced all material and results that are not original to this work.

Name Last name : Özgün, Ali Buğra

Signature :

ABSTRACT

COMPARISON OF ORDINARY KRIGING AND DEEP LEARNING METHODS IN GRADE ESTIMATION: A PILOT STUDY ON THE SIRAKAYALAR Au MINERALIZATION (NW TÜRKİYE)

Özgün, Ali Buğra
Master of Science, Geological Engineering
Supervisor: Assist. Prof. Dr. Ali İmer

August 2025, 102 pages

Resource estimation of an orebody is a crucial step for advanced exploration project as it dictates project's finances and ultimately its feasibility. In this scope, a wide variety of geostatistical approaches have been conducted for accurate estimation of mineral resources since the 20th century. More recently, geostatistical approaches have become even more common with increasing power of modern computers. Machine Learning (ML) algorithms have similar evolution to the discipline of geostatistics. These often show good performance for complex tasks when compared to traditional geostatistical methods. This study involves comparative grade estimation of the Sırakayalar gold prospect in Lapseki (Canakkale) through ordinary kriging and Deep Learning (DL) approaches, particularly to determine potential advantages and limitations of DL approaches. Gold mineralization at Sirakayalar is hosted in a talus zone comprising transported and mechanically disrupted low-sulfidation epithermal-style vein fragments within a fine-grained matrix comprising silica, clays, and Fe-Ti-oxides. Methodology of the study includes pre-processing, domaining, variograms, block model designing and search criteria for Ordinary Kriging applications, and selection of optimizer & activation functions and creating of estimation model for DL applications. OK uses auto-correlation functions for estimation while DL uses 3D weight function. Both methods show local anomalies. Hence, there is a trade-off between both methods like interpretability and predictive

power. DL models behave like block-box, since OK shows all transparencies, and DL requires stationary large datasets while OK could apply sparse datasets. In future, usage of hybrid models, inserting block wise estimation and modelling by using polar coordinates could be studied.

Keywords: Deep Learning, Ordinary Kriging, Geostatistic, Grade Estimation, Sırakayalar Mineralization. (Max 5 keywords)

ÖZ

KAYNAK TAHMİNİNDE ORTALAMASIZ KRIGING VE DERİN ÖĞRENME YÖNTEMLERİNİN KARŞILATIRMASI: SIRAKAYALAR Au MİNERALİZASYONU (KB TÜRKİYE) ÜZERİNDE BİR PİLOT ÇALIŞMA

Özgün, Ali Buğra
Yüksek Lisans, Jeoloji Mühendisliği
Tez Yöneticisi: Assist. Prof. Dr. Ali İmer

Ağustos 2025, 102 sayfa

Bir cevher yatağının kaynak tahmini, projenin finansmanını ve nihayetinde fizibilitesini belirlediği için ileri arama projesi için çok önemli bir adımdır. Bu kapsamda, 20. yy' dan buyana maden kaynak tahmini için jeoistatiksel yaklaşımlar kullanılmaktadır. Son zamanlarda, artan teknolojiyle beraber güçlenmiş bilgisayarların yardımlarıyla jeoistatiksel yaklaşımlar daha yaygın hale gelmiştir. Makine Öğrenmesi algoritmaları da aynı evrime tabi olmuştur. Makine öğrenmesi karmaşık görevler üzerinde geleneksel yöntemlerden çoğu zaman daha iyi sonuçlar göstermektedir. Bu çalışma, Çanakkale Lapseki' deki bulunan Sırakayalar altın çevherleşmesinde tenör tahmini çalışmasında Ortalamasız Kriging (OK) ve Derin Öğrenme (DÖ) uygulamalarını, sonuçların karşılaştırılmasını ve avantaj & dezavantajlarını, sınırlarını ve uygulamada uygun olabilecek ortamları ortaya koymak amacıyla Sırakayalar Cevherleşmesi' nde gerçekleştirilmiştir. Sırakayalar'daki altın cevherleşmesi, silika, killer ve Fe-Ti oksitlerden oluşan ince taneli bir matris içinde taşınmış ve mekanik olarak parçalanmış düşük sülfürlü epitermal tarzı damar parçalarından oluşan bir yamaç moloz zonunda yer almaktadır.

Çalışmanın metodolojisi, uygulamadan önceki veri işleme, kümelendirme, OK uygulamaları için variogramlar, blok model ve arama kriterlerinin kurgusu ve DÖ için optimizasyon ve aktivasyon fonksiyonlarını seçimi ve 3B ağırlık fonksiyonunu oluşturmayı kapsamaktadır. OK tahmin için otokorelasyon fonsiyonunu kullanırken DÖ 3B ağırlık fonksiyonlarını kullanmaktadır. Her iki yöntem de yerel anomalileri göstermektedir. Dolayısıyla, yorum kabiliyeti ve tahmin gücü arasında değişimler bulunmaktadır. OK, tüm adımlar için şeffaflık gösterirken, DÖ kara kutu gibi davranmaktadır. OK, boşluklu yapılardaki verilerde uygulanabilirken, DÖ büyük veri setleri ve durağan yapıda kümeler için daha uygun yapıya sahiptir. Gelecekte, hibrit modellerin kullanımı, blok bazlı fonksiyonların ve kutupsal koordinatlar kullanılarak modelleme incelenebilir.

Anahtar Kelimeler: Derin Öğrenme, Ortalamasız Kriging, Jeoistatistik, Tenör Tahmini, Sırakayalar Cevherleşmesi. (En fazla 5 anahtar kelime)

To my family

ACKNOWLEDGMENTS

First of all, I would like to express my sincere gratitude to my supervisor, Assist. Prof. Dr. Ali İmer, for his continuous support throughout my master studies and for sharing his immense knowledge.

I am also grateful to Hasan Yücel and TÜMAD for providing the necessary data, and I would like to thank the staff of TÜMAD for their assistance.

My special thanks go to Sabri Karahan and Dama Engineering Company for their endless support during this study.

I am deeply thankful to Dr. Yusuf Ziya Özkan and Mehmet Ali Akbaba for their mentorship and invaluable guidance in educating and training me in geostatistics and machine learning.

Finally, I would like to extend my heartfelt appreciation to my wife, Sevda Özgün, for her patience, encouragement, and support.

TABLE OF CONTENTS

ABSTRACT v

ÖZ vii

ACKNOWLEDGMENTS x

TABLE OF CONTENTS xi

LIST OF TABLES xiv

LIST OF FIGURES xv

1 INTRODUCTION 1

1.1 Statement of Purpose 1

1.2 Objectives of the Study 4

1.3 Methodological Framework 4

1.4 Structure of the Thesis 4

2 LITERATURE REVIEW 7

2.1 Overview of Mineral Grade Estimation 7

2.2 Fundamentals of Geostatistics in Mineral Resource Estimation 8

2.2.1 Variography and Spatial Continuity 8

2.2.2 Kriging Techniques 8

2.2.3 Exploratory Data Analysis and Implementation 9

2.3 Machine Learning in Geosciences 9

2.3.1 Foundational Concepts – Supervised and Unsupervised Learning. 10

2.3.2 Deep Learning Architectures (MLP, CNN, RNN) 10

2.4 Previous Comparative Studies – Geostatistics versus ML-DL 11

2.5 Research Gaps 12

3 REGIONAL AND LOCAL GEOLOGY 15

3.1 Regional Geology 15

3.1.1 The Basement Rocks 16
3.1.2 Tectonic Framework 17
3.1.3 Magmatism and Hydrothermal Activity 18
3.1.4 Epithermal Gold Mineralization 19
3.2 Local Geology of Sırakayalar Prospect 20
3.2.1 Metamorphic Units 20
3.2.2 Volcanics 21
3.2.3 Sedimentary Rocks 22
3.2.4 Mineralization and Paragenesis 22
3.2.5 Previous Exploration Studies 23
4 DATA AND METHODOLOGY 25
4.1 Data Sources and Characteristics 25
4.1.1 Drillhole Database 25
4.1.2 Digital Terrain Models (DTMs) 27
4.2 Data Preparation and Cleaning 27
4.2.1 Domain Modelling and Wireframing 28
4.2.2 Compositing and Capping (Outlier Handling) of Assay Data 31
4.3 Geostatistical Estimation Workflow 37
4.3.1 Variogram Modelling and Spatial Continuity Analysis 37
4.3.2 Block Model Design 39
4.3.3 Ordinary Kriging Implementation 40
4.4 Deep Learning Approaches 41
4.4.1 Data Structuring and Preprocessing for Deep Learning 41
4.4.2 Network Architecture Selection 44
4.4.3 Deep Learning Application 46

5 RESULTS AND INTERPRETATION.....55
5.1 Geostatistical Estimation Results..... 55
5.1.1 Block Model Outputs (Grade & Tonnage) 55
5.1.2 Swath Plots and Validation..... 56
5.2 Deep Learning Estimation Results..... 61
5.2.1 Raw Assay Data Application..... 61
5.2.2 Domain Assigned Assay Application 65
6 DISCUSSION 77
6.1 Strengths and Weaknesses of Each Method 77
6.2 Interpretability vs. Predictive Power..... 77
6.3 Applicability to Sparse or Noisy Datasets 78
6.4 Literature Comparison of the Study..... 78
6.5 Lessons Learned and Methodological Reflections 79
7 CONCLUSIN AND RECOMMENDATIONS 83
7.1 Summary of Findings..... 83
7.2 Contribution to Knowledge..... 83
7.3 Recommendations for Future Work..... 84
REFERENCES 85
A. Appendix Title 103
B. Appendix Title 104
C. Appendix Title 105

LIST OF TABLES

TABLES

Table 4.1 Summary of Mineralization Zone Compositing Assumptions 29
Table 4.2 Implicit Assumptions for Solid Model 31
Table 4.3 Summary Statistic of Before/after Capping Gold Grade 36
Table 4.4 Summary Statistic of Interval Field of Assay Data in ppm 37
Table 4.5 Summary of Semi-variogram and Search Ellipsoid Parameters 38
Table 4.6 Block Model Attributes 39
Table 4.7 Ordinary Kriging Search Parameters 40
Table 4.8 Summary of the Deep Learning Inputs and Limitations 42
Table 4.9 Summary of Model Parameters 48
Table 4.10 Summary Statistics of Composite Intervals 51
Table 4.11 Summary of Parameters Used for Second Phase 51
Table 5.1 Resource Statement of Sırakayalar Mineralization by Ordinary Kriging 56
Table 5.2 Raw Assay Data Application by Deep Learning 61
Table 5.3 Summary Statistic of Input and Output Data for Raw Assay Application 62
Table 5.4 Domain Assigned Deep Learning Approach 66

LIST OF FIGURES

FIGURES

Figure 3.1 The location of the Sırakayalar Mineralization (OPS Map, 2024)..... 15
Figure 3.2 Simplified regional geological map of the Biga Peninsula showing Late Cenozoic magmatic and older ophiolitic and basement rocks. IAESZ refers İzmir-Ankara-Erzincan Suture Zone (Gülyüz et al., 2020; after Türkecan and Yurtsever, 2002). 18
Figure 3.3 Generalized columnar section of the Biga Peninsula. Sh refers Shoshonitic (Dönmez et al., 2005; Sanchez et al., 2016; Günaydın, 2017; from Dilekler, 2022). 19
Figure 3.4 Geological map of the area hosting the Sırakayalar, Karatepe, and Kovanlık prospects located immediately north of the Lapseki Au deposit (from Dilekler, 2022). 21
Figure 4.1 Ore shots of the Sırakayalar Mineralization due to maximum intensity projection (a, b, c views). 26
Figure 4.2 Plan view of the Sırakayalar area distribution of drill holes used in this study. 28
Figure 4.3 Sırakayalar mineralized domains and section lines at plan view. 29
Figure 4.4 30 m shaded cross-sectional views of the domains. Section lines are shown in Figure 4.3. 30
Figure 4.5 Decile analysis for the LG domain. Orange line represents after cut. ... 32
Figure 4.6 Histogram of Au distribution (in ppm) for the LG domain. Orange bars represent after cut, and gray bars represent before cut. 33
Figure 4.7 Cumulative frequency plot of Au assays (in ppm) for the LG domain. Orange line represents the cut value. 33
Figure 4.8 Probability plot of Au (in ppm) for the LG domain. Orange line represents cut value. 34
Figure 4.9 Decile analysis for the HG domain. Orange line represents after cut. .. 34
Figure 4.10 Histogram of Au distribution (in ppm) for the HG domain. Orange bars represent after cut, and gray bars represent before cut. 35

Figure 4.11 Cumulative frequency plot of Au assays (in ppm) for the HG domain. Orange line represents the cut value. 35
Figure 4.12 Probability plot of Au (in ppm) for the LG domain. Orange line represents cut value. 36
Figure 4.13 Workflow of the OK application. 37
Figure 4.14 Search ellipsoid configuration at 3D space. 38
Figure 4.15 Three axes and downhole semi-variogram results. 39
Figure 4.16 The workflow of the DL application. 41
Figure 4.17 2D coordinated regression performance with different inputs and hidden layers. Left part inputs include X_1, X_2, X_1X_2; middle part inputs X_1 an X_2; right part inputs X_1 and X_2. Top to bottom; number of hidden layers; 1-2-4-6. Tests were conducted by learning rate 0.001, regularization rate 0.03. Tests were applied multi gaussian random dataset for left and middle parts and rest of them were applied planer random dataset. 20 percent of the data were used test samples. Noise was selected 20 and batch size selected 30. The quantity of epoch(iteration) is approximately 1000. The background color shows discrimination. The color represents data, weight; -1 /0 /1 respectively orange, white and blue (created by Similkov and Carter-playground.tensorflow.org, 2025). 43
Figure 4.18 Relation between data fit and weight decay (Goodfellow at al., 2016). 46
Figure 4.19 Comparison for underfit and overfit parts of the numeric model (Goodfellow at al., 2016) 47
Figure 4.20 Mean squared error of Test and Train Loss. 50
Figure 4.21 Performance of the loss comparison as mean squared error for LG. ... 52
Figure 4.22 Performance of the loss comparison as mean squared error for HG. .. 52
Figure 5.1 Swath plots respectively east, north and RL. In east and north direction 30 m and in RL 10 m thickness were used. Comp: Composite file as frequency and value, DL-Domain: Deep Learning domain as value and frequency, OK: Ordinary Kriging, NN: Nearest Neighbor estimation as Au grade in ppm. 57
Figure 5.2 30m shaded sections for visual block model and raw assay grade comparison. 59

Figure 5.3 3D view of the estimated blocks by using geostatistical approaches. ... 60
Figure 5.4 Grade vs tonnage curves for comparison to recognize small changes at cut-off grade. ... 60
Figure 5.5 Overfit run of the 2m composited data by raw assay application. ... 62
Figure 5.6 Optimal fit run of the 2m composited data by raw assay application. .. 63
Figure 5.7 A-A' cross-section of raw assay Deep Learning results to compare raw assay data – optimal fit, raw assay application. ... 63
Figure 5.8 B-B' cross-section of raw assay Deep Learning results to compare raw assay data – optimal fit, raw assay application. ... 64
Figure 5.9 C-C' sections of raw assay Deep Learning results to compare raw assay data – optimal fit, raw assay application. ... 64
Figure 5.10 Grade vs tonnage curve of Deep Learning approach to comparison to recognize small changes at cut-off grade for raw assay application. ... 65
Figure 5.11 3D view of estimated BM for domain assigned DL method. ... 67
Figure 5.12 A-A' cross-section DL-Domain BM as HG and LG by using Deep Learning approaches. ... 67
Figure 5.13 B-B' cross-section DL-Domain BM as HG and LG by using Deep Learning approaches. ... 68
Figure 5.14 C-C' cross-section DL-Domain BM as HG and LG by using Deep Learning approaches. ... 68
Figure 5.15 Grade vs tonnage curves of domain assigned Deep Learning approach to comparison to recognize small changes at cut-off grade. ... 69
Figure 5.16 Block wise comparison of both methods, B-B' section. The background blocks represent OK, and foreground blocks represent DL. ... 70
Figure 5.17 Block wise comparison of both methods, C-C' section. The background blocks represent OK, and foreground blocks represent DL. ... 70
Figure 5.18 Block wise comparison of both methods, A-A' section. The background blocks represent OK, and foreground blocks represent DL. ... 71
Figure 5.19 Histogram graphs of OK and DL-Domain applications' grades. ... 71

Figure 5.20 3D view of the regularized BM for DL-domain method. Factor fields applied to volume of the blocks and relatively smaller blocks represent smaller portion of mineralization. Original Z dimensions were preserved as location..... 72
Figure 5.21 Residual analysis to compare the results of OK and DL-domain methods. 73
Figure 5.22 Cross plot of OK and DL-domain methods. Red dash line represents 1:1. R^2 value is 0.74 with intersection to zero. 74
Figure 5.23 3D view of the Au difference in ppm, obtained by OK results subtracted with DL-domain results (block factor applied). The positive and negative values represent respectively domination of OK and DL estimation as grade. 75

CHAPTER 1

INTRODUCTION

The Sırakayalar Mineralization (the study area) known as part of Lapseki Gold Mine which belongs to TÜMAD A.Ş. which is junior partner of Nurol Holding. Sırakayalar mineralization is located at Biga Peninsula. Sırakayalar mineralization shows high variability as grade at 3D space (which means low range auto-correlation), and the gold mineralization mainly related with float material. The main scope of this study covers grade estimation with geostatistical and deep learning approaches and their comparison for high variability deposits.

1.1 Statement of Purpose

Modelling is a milestone of any project or design. The range of the models could vary widely depending on their aim. In a mining project, from brown field to feasibility study, mineral resources are essential to investing a project. The main risk assessments of a mining project mainly depend on geology, engineering and finance (Appleyard, 2001; quoted in Edwards, 2001). Investment in exploration projects for brownfield projects poses great risks for investors (Lassonde, 1990). Even if early exploration projects pose risk, there are numerous stock exchange companies in TSX (Toronto Stock Exchange) who handle the exploration actions (Almonty Industries, 2025; Laramide Resources, 2025; Seabridge Gold, 2025). Eventually, investors are protected by national regulations including Joint Ore Reserves Committee (JORC), National Instrument 43-101 (NI-43 101), Canadian Institute of Mining (CIM) etc. (NI 43-101, 2001; JORC, 2012; CIM, 2019). In those regulations, several obligations were applied to technical reports to meet requirements. In resource estimation parts of these reports, which are obliged to regulations, could be handled differently. That means reporting and resource estimation part could be dependent on writer of the

reports. Hence, the reliability of these models could be questioned. In that case, the quality of the resource estimation depends on data density (configuration) with constraints, that could be a powerful key explaining mineral resources for a project.

Models could be represented numerically. The numerical models to explain in engineering scope were widely used in industrial and scholarly research from earth science to aerospace. In numerical methods, the main concern is scoping to reason. The problem is the key features and rest the restrictions of the model should be applied to according the model like using Ordinary Differential Equations (ODE), Finite Element Analysis, etc. (Verlet, 1967; Clough, 1960). Each model has benefits and gaps to compare others like residuals at ODE approaches.

Grade estimation of a mineralization is based on a central limit theorem. The central limit theorem explains, reason for showing normal (or log-normal) trends as mean of the numerous assay results of drill holes or estimated block grades. This provides the basis for the use of samples in estimating global mean grades, maintaining the mean of approximately normality in block grades, and using Gaussian-based estimation and ratio refinement methods in geostatistics. In other words, a population should show similar behaviors with sample clusters (Fischer, 2011). In the same way, domained samples used for the estimation show similar trends to compare drill hole data. Then, geostatistical application must be represented by sampling configurations. The two main approaches in the resource estimation are *deterministic* and *stochastic*. The *deterministic* approach behaves in a way that all input parameters are certain in definitive bias and results must be definitive according to this bias. Inverse distance powered applications could be example of *deterministic* approaches. In contrast, a *stochastic* approach depends on probability of the sample data. Theory of Ordinary Kriging could be example for *stochastic* application by using random field and variogram models, and the application of Ordinary Kriging could be example for *deterministic* approaches (same input gives same results). The main reason for usage of *stochastic* application should be explained in 3 different steps: un-completed sampling, sampling bias and detail of the modelling. First, the sampling could be expensive, unavailable, etc. at a population. There is a trade-off

between sampling and the gains. Secondly, sampling bias could be explained confidence of the sampling such as analysis methods (sensitivity of the analysis method, precision of the analysis methods), nugget effect, orientation at 3D space, etc. Thirdly, the detail of the model depends on known or unknown certainties like discarded information (Goodfellow, et al., 2016). The declination of the drillhole could be example of this one. The measurements were taken generally defined as meters like 10m each. The errors caused by declination of drillholes were accepted as sensitivity of the scope. All these make probabilistic approaches more meaningful for resource estimation.

In mineral exploration, both traditional and more modern estimation methods are frequently used in the statement of mineral resources when considering economic viability of a project. Traditional methods include those using simple geometric algorithms such as the polygon method and the triangle method. The modern methods on the other hand cover numerical methods at blocks in mineralized solids. The numerical estimation is handled using the behaviors of the deposits. Most commonly used numerical estimation methods for resource estimation are Kriging, Inverse Distance Powered, Nearest Neighbor, and Radial Base Function. (Krige, 1951; Matheron, 1963; Shepard, 1968; Fix and Hodges, 1958; Broomhead and Lowe, 1988). By using these estimation methods, block-wise in mineralization domains were estimated according to restrictions.

In recent years, in addition to common numerical approaches machine learning (ML) algorithms have become widely popular in resolving engineering problems. Machine learning algorithms deal with the problem by building a bridge between the results and the inputs (Goodfellow et al., 2016) in which the bridge is made up of mathematical functions. These functions are used to classify the inputs or slope of regression. Hence, the machine learning algorithm could explain complex-wise engineering problems by using inputs and outputs.

The Sırakayalar mineralization shows short range autocorrelation which disturbed by mechanically. Ordinary Kriging depends on autocorrelation and estimation are based on this autocorrelation function for global estimation. As alternatively, ML

algorithms could learn from the data and could represent estimation more local based which could be increase efficiency and reliability of the models in global. This study is conducted to explain comparison between grade estimation with ordinary kriging and machine learning algorithms.

1.2 Objectives of the Study

- To perform grade estimation using ordinary kriging and deep learning approaches.
- To evaluate and compare the estimation performance of both methods using statistical and spatial metrics.
- To identify the advantages, limitations, and suitable use-cases for each method within the context of mineral deposits exhibiting high variability.

1.3 Methodological Framework

The methodology consists of data preprocessing (compositing, capping, domain modelling), implementation of ordinary kriging via geostatistical software, and development of a deep learning model using feedforward neural networks. Model validation will be based on statistical comparison, visual validation, cross-plot, residual analysis, and swath plots.

1.4 Structure of the Thesis

This thesis is structured as follows:

- Chapter 1 introduces the research, objectives, and scope.
- Chapter 2 presents a literature review on grade estimation, geostatistics, and machine learning applications.
- Chapter 3 outlines the geological and mineralization feature of the study area.

- Chapter 4 details the data and methodology used.
- Chapter 5 presents the results and their comparative analysis.
- Chapter 6 discusses the findings and implications.
- Chapter 7 concludes the study and suggests future work.

CHAPTER 2

LITERATURE REVIEW

2.1 Overview of Mineral Grade Estimation

Mineral resource estimation is the process of quantifying the amount and grade of mineralized material within a defined geological volume, typically based on sparse sampling data such as drillholes. It is a critical component of mine planning, feasibility analysis, and economic valuation. Estimation methodologies have evolved considerably over the past century, from early manual methods such as polygonal and sectional approaches to modern three-dimensional block modeling and geostatistical algorithms.

In recent years, the integration of data-driven approaches, particularly machine learning (ML) and deep learning (DL), has opened new pathways for modeling mineral resources, especially in complex or data-rich geological settings. This chapter synthesizes the historical and theoretical foundations of both geostatistics and ML/DL approaches, drawing attention to their applications, limitations, and recent comparative studies.

The literature is organized into four major thematic areas:

1. Fundamental and historical development of geostatistical estimation.
2. Advances in machine learning, particularly deep learning.
3. Comparative studies evaluating the performance of both methods.
4. Practical and epistemological challenges in resource estimation

2.2 Fundamentals of Geostatistics in Mineral Resource Estimation

2.2.1 Variography and Spatial Continuity

A cornerstone of geostatistical resource modeling is the concept of spatial correlation, which is quantified through variography. Variograms describe how sample similarity changes with distance and direction, enabling geologists and modelers to understand the continuity of grades across space. The variogram informs key modeling decisions, such as search ellipsoid orientation and kriging weights.

The origin of modern geostatistics dates back to the pioneering work of Krige (1951), who introduced statistical techniques for ore body evaluation in South African gold mines. He later demonstrated (Krige, 1952) that acceptable resource estimates could be obtained using limited data by properly accounting for spatial relationships.

Building on Krige's foundational work, Matheron (1963) formalized the theory of Best Linear Unbiased Estimation (BLUE), laying the groundwork for what is now known as kriging. His subsequent contributions (1971a, 1971b) introduced the Intrinsic Random Function Theory, enabling spatial modeling based on both local and global variance structures.

2.2.2 Kriging Techniques

Ordinary Kriging (OK) remains as the most widely used estimation method in the mining industry. It provides a statistically optimal solution under the assumption of a constant but unknown mean within a local neighborhood (Rossi & Deutsch, 2014). Other kriging variants include:

- Disjunctive Kriging (Journel, 1974), used for nonlinear problems involving complex distributions.
- Indicator Kriging (Journel, 1982), designed for categorical or binary variables;

- Universal Kriging (Huijbregts & Matheron, 1997), which incorporates a known trend or drift;

In contrast, Inverse Distance Weighting (IDW) is a simpler deterministic method where nearby data points have a greater influence on the estimate. Although less rigorous, IDW is often used in preliminary studies due to its intuitive implementation.

2.2.3 Exploratory Data Analysis and Implementation

Tukey (1973) was instrumental in promoting Exploratory Data Analysis (EDA), emphasizing visualization, anomaly detection, and data integrity prior to model construction. This philosophy is echoed in geostatistical workflows that prioritize data validation, declustering, and transformation prior to estimation.

Journel and Huijbregts (1978) further developed geostatistical theory for mining applications, systematizing the use of variograms, kriging, and conditional simulation in the estimation process.

In their fundamental textbook, Isaaks and Srivastava (1989) defined geostatistics as the study of spatial autocorrelation, offering practical strategies for applying regression-based models to geological datasets.

2.3 Machine Learning in Geosciences

Machine learning has emerged as a powerful tool in geosciences, enabling the analysis of complex, high-dimensional, and often non-linear datasets that are common in geological investigations (Bergen et al., 2019; Khan et al., 2022). From mineral prospectivity mapping (Özkan, 2025) and lithological classification to seismic interpretation and resource estimation, ML techniques offer enhanced predictive capabilities compared to traditional methods (Jain & Yellishetty, 2021). Algorithms such as support vector machines, random forests, and deep neural networks can learn patterns from sparse or noisy data, making them well-suited for

geological domains where uncertainty and variability are inherent (Li et al., 2016; Zhang et al., 2022). Despite its growing adoption, the integration of machine learning in geosciences poses challenges related to data quality, model interpretability, and the need for domain-specific adaptation (Meade & Perron, 2023; Khan et al., 2022). Nevertheless, the field continues to advance, driven by increasing data availability, computational power, and interdisciplinary collaboration between geoscientists and data scientists (Jain & Yellishetty, 2021; Bergen et al., 2019).

2.3.1 Foundational Concepts – Supervised and Unsupervised Learning

Supervised learning algorithms are trained on labeled datasets to learn mappings from inputs to outputs. In geoscience, these methods are commonly used for grade prediction, lithological classification, and alteration zoning. Unsupervised learning, by contrast, identifies inherent patterns in data without predefined labels, making it suitable for anomaly detection or clustering geochemical signatures.

ML methods offer flexibility in handling both linear and nonlinear relationships and can adapt to non-stationary data frequent challenge in mineral deposits.

2.3.2 Deep Learning Architectures (MLP, CNN, RNN)

The theoretical underpinnings of machine learning trace back to Ramsey (1926), who interpreted probability not only as frequency but as a degree of belief; laying the philosophical foundation for Bayesian inference.

Major milestones include:

- Werbos (1981): Introduced backpropagation for training artificial neural networks (ANNs).
- Breiman et al. (1984): Developed decision trees using dataset partitioning and variance-based splitting.

- Rumelhart et al. (1986) and Hinton (1989): Advanced multi-layer perceptrons (MLPs) and introduced the concept of connectionism, foundational for DL.
- Cortes and Vapnik (1995): Developed Support Vector Machines (SVMs) capable of separating complex data structures in high-dimensional spaces.
- Mitchell (1997): Emphasized the adaptability of learning systems across supervised, unsupervised, and reinforcement paradigms.

With the emergence of deep learning, models have gained the ability to automatically extract hierarchical features from raw data. Key architectural developments include:

- CNNs (Convolutional Neural Networks): Effective in spatial data interpretation, such as hyperspectral imaging and core photography analysis.
- RNNs (Recurrent Neural Networks): Designed for sequential data, though less common in geological modeling.
- ReLU (Rectified Linear Unit) activation functions, promoted by Fukushima (1975, 1980) and later validated by Jarrett et al. (2009) and Glorot et al. (2011), have become standard due to their efficiency in training deep networks.

2.4 Previous Comparative Studies – Geostatistics versus ML-DL

Recent studies have increasingly sought to benchmark geostatistical methods against machine learning and deep learning models:

- Mahboob et al., (2022) review that ML models generally outperformed non-ML methods including kriging.
- Afeni et al. (2021) applied ANN-MLP (Artificial Neural Networks) and OK to drillhole dataset for Itaktepe iron ore deposits, showing OK better performance for grade estimation.

- Galetakis. (2022) applied ANFISs (Adaptive Fuzzy Interface Systems), ANN and OK to drillhole dataset. ML algorithms were highlighted as potential for usage to grade estimation that is effectively capturing the spatial variability.

Despite promising results, deep learning methods are often criticized for their "black box" nature and lack of transparency which means that it is particularly problematic in high-stakes resource reporting environments.

2.5 Research Gaps

Both geostatistics and deep learning present fundamental challenges in mineral resource estimation:

- Geostatistics relies on the assumption of stationarity and often struggles with sparse or irregular sampling, nugget effects, and complex deposit geometries.
- Deep learning requires large, high-quality training datasets and lacks intuitive interpretability, complicating model validation and communication, particularly in the absence of established frameworks.

A persistent trade-off exists between interpretability and predictive performance. The selection of an estimation method must consider project stage, data quality, and regulatory requirements.

This literature review traces the parallel evolution of geostatistical and deep learning approaches in resource estimation. Geostatistics remains the industry standard due to its transparency and regulatory acceptance, while deep learning shows promise in capturing complex, non-linear, and non-stationary patterns in geological data.

However, there is a notable gap in comparative evaluations of these methodologies, particularly for geologically complex and highly variable mineral deposits such as the Sırakayalar Gold Project. This thesis addresses this gap by systematically evaluating the performance of ordinary kriging and deep learning models on real-

world data, with specific emphasis on spatial accuracy, bias, and computational efficiency.

CHAPTER 3

REGIONAL AND LOCAL GEOLOGY

The Sırakayalar gold deposit was selected as the application area to compare the performance of mineral resource estimations based on Kriging and Deep Learning methods. The Sırakayalar mineralization is located in the Lapseki district of Çanakkale Province, in an area that geographically and geologically lies at the northwestern end of the Biga Peninsula (Figure 3.1).

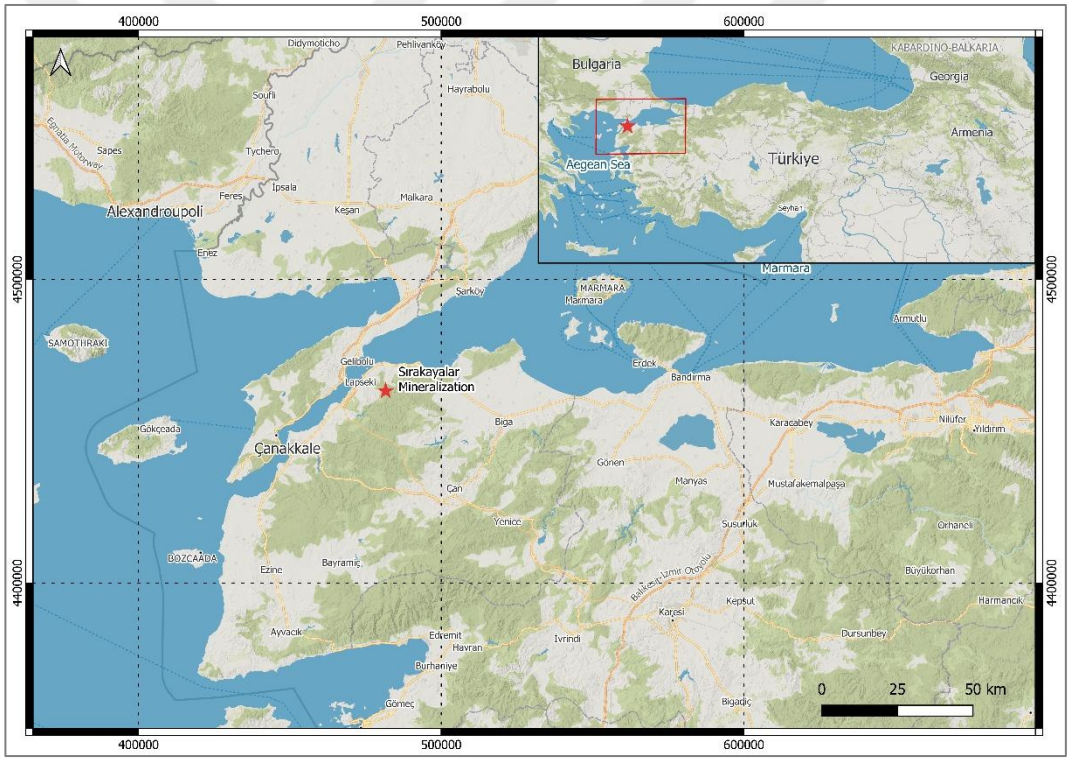


Figure 3.1 The location of the Sırakayalar Mineralization (OPS Map, 2024).

3.1 Regional Geology

The Biga Peninsula, located in northwestern Türkiye, is one of the most geologically active and mineralogically prospective regions of the Eastern Mediterranean and

forms a key sector of the Tethyan Metallogenic Belt (Şengör and Yılmaz, 1981; Okay et al., 1996; Yiğit, 2012; Tunç et al., 2014). Biga Peninsula is composed of three tectonic terrains; Tauride-Anatolide Block in the south, the Sakarya Zone and the Rhodope-Strandja Zone in the northwest (Okay and Tüysüz, 1999). It is characterized by a complex tectonic and magmatic history that has created favorable conditions for a variety of mineral deposit types, including epithermal Au-Ag and porphyry Cu-Mo-Au deposits as well as skarn and carbonate-replacement-type base metal mineralization (REFS). The Peninsula forms part of the broader Western Anatolian Extensional Province (WAEP; REFS), a region predominantly shaped by late subduction-related to collisional and post-collisional tectonics, crustal thinning, and widespread volcanism following closure of the Tethys oceanic domains (REFS; Figure 3.2).

3.1.1 The Basement Rocks

The basement rocks in the Biga Peninsula are generally composed of metamorphic units including the Çamlıca metamorphics, the Kazdağ massif, and the Karakaya Complex.

The Çamlıca metamorphics are comprised by mica schist and calc-schist units, quartzite, and slivers of ultramafic rocks (Yilmaz & Karacik, 2001). The Paleozoic Kazdağ Massif, on the other hand, is composed of mica schist, gneiss, marble as well as meta-ophiolites (Schuiling, 1959; Gümüş, 1964; Aslaner, 1965; Bingöl et al., 1973; Okay at al., 1991; Okay and Satır, 2000). Overlying Permo-Triassic Karakaya Complex is composed of limestone olistoliths (Carboniferous – Permian), low-grade metamorphics of clastic and carbonate lithologies as well as metabasalts (Permian – Triassic) and pre-Jurassic intrusions (Bingöl et al., 1974; Aydın et al., 1995; Okay et al., 1996, 2002; Delaloye and Bingöl, 2000). According to Şengör and Yılmaz (1981), these rocks associated with closure of Paleo-Tethys throughout the IAESZ (Figure 3.2).

Ophiolitic bodies are defined as Çetmi ophiolite mélange and Denizgören ophiolite (Okay et al., 1990; 1991). Çetmi ophiolitic mélange is mainly exposed at west of Kazdağ Massif that is mainly composed of basic volcanic and pyroclastic, limestone blocks, shale, graywacke (Okay et al., 1990). It is trusted over Çamlıca Metamorphics. In contrast it has normal faulted contact with Kazdağ Massif. Denizgören ophiolite is mainly exposed northern part of the Ezine district, and it is mainly composed of serpentinized harzburgite (Okay et al., 1991). It is trusted over Çamlıca Metamorphics and sedimentary rocks (Okay et al., 1991).

3.1.2 Tectonic Framework

The tectonic evolution of the Biga Peninsula has been shaped by convergence and subsequent collision between the Eurasian and African–Arabian plates, as well as by the westward escape of the Anatolian microplate along major strike slip fault systems such as the North Anatolian Fault Zone "NAFZ" (McKenzie, 1972; Şengör et al, 1985).

This evolution is interpreted as closure of Paleo-Tethys Ocean in Late Triassic (Şengör and Yılmaz, 1981; Okay et al., 1996, 1998). In later on (Late Cretaceous-Early Eocene), the later stage subduction and collusion throughout Izmir-Ankara Structure Zone (IASZ) were interpreted as closure northern branch of Neo-Tethys Ocean (Şengör and Yılmaz, 1981; Harris et al., 1994; Okay and Tüysüz, 1999, Kaymakcı et al., 2009).

Transnational tectonic regime was caused by N-S extension due to subduction and dextral strike slip faulting throughout NAFZ by E-W directed, and it is represented by NE-SW directed splays of NAFZ (McKenzie, 1972; 1978; LePichon and Angelier, 1979; Şengör et al, 1985; Meulenkamp et al., 1988; Kaymakcı et al., 2007).

This geodynamic regime produced a fault-bounded mosaic of tectonostratigraphic units that include metamorphic basement rocks, ophiolitic mélanges, magmatic arcs, and sedimentary basins (Figure 3.2). The Kazdağ Massif (Paleozoic) and Çamlıca Metamorphic complex (Maastrichtian) constitute the metamorphic basement, mainly

composed of Paleozoic-Mesozoic schists, marbles, and gneisses, which are overlain by Paleogene to Neogene volcanic and volcano sedimentary units hosting most regional mineralization (Okay et al., 1991; Okay and Satır, 2000; Aydın et al., 2019).

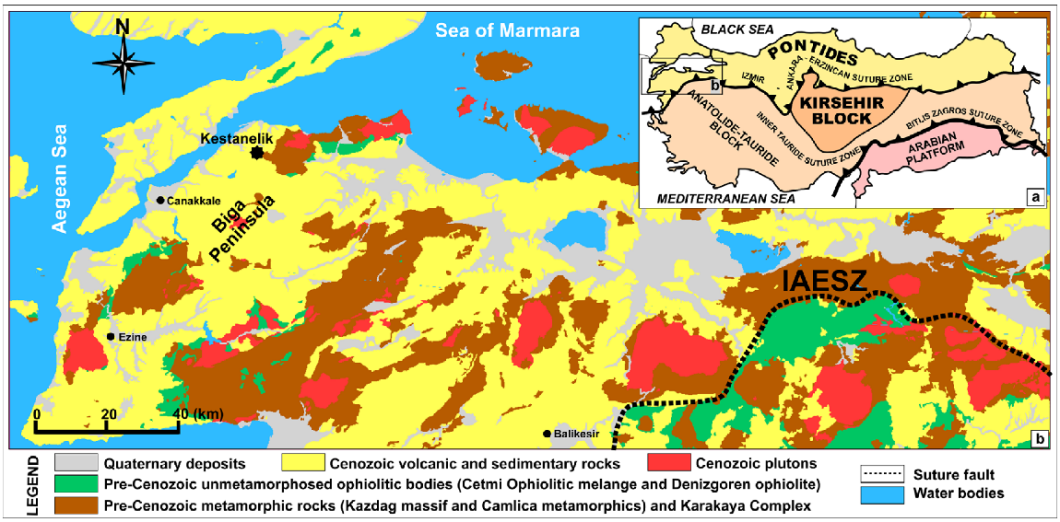


Figure 3.2 Simplified regional geological map of the Biga Peninsula showing Late Cenozoic magmatic and older ophiolitic and basement rocks. IAESZ refers İzmir-Ankara-Erzincan Suture Zone (Gülyüz et al., 2020; after Türkecan and Yurtsever, 2002).

3.1.3 Magmatism and Hydrothermal Activity

Multiple magmatic phases occurred from the Late Eocene to the Neogene, linked to slab rollback and back arc extension in the Aegean region (Altunkaynak and Genç, 2008; Yiğit, 2012). Neogene calc-alkaline to high K-volcanic rocks and sub-volcanic intrusions, mainly including andesitic, dacitic to rhyolitic domes, flows, and pyroclastic units, are spatially and temporally associated with hydrothermal alteration zones and precious metal deposits (Altunkaynak and Genç, 2008; Yiğit, 2012; Akıska et al., 2013; Clark, 2014; Demirela et al., 2014; Kuşcu et al., 2019; Aluç et al., 2023; 2024). Hydrothermal fluid circulation is often by extensional faults and fracture zones, enabling fluid pathways, while the interplay of tectonic extension, high heat flow, and magmatic degassing produced favorable conditions especially for epithermal Au-Ag mineralization, often including low- and intermediate-sulfidation and less commonly high-sulfidation type epithermal

mineralization (Yiğit, 2012; Sanchez et al., 2016; Kuşcu et al., 2019; Aluç et al., 2024).

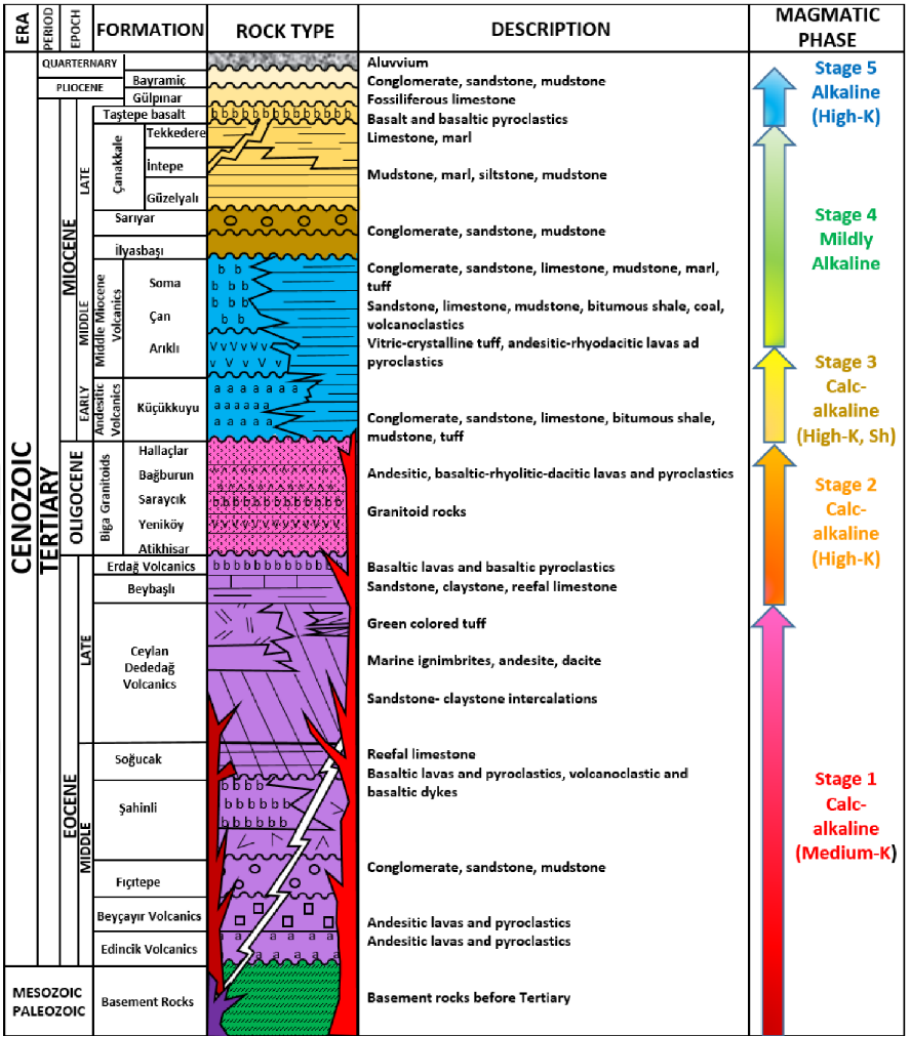


Figure 3.3 Generalized columnar section of the Biga Peninsula. Sh refers Shoshonitic (Dönmez et al., 2005; Sanchez et al., 2016; Günaydın, 2017; from Dilekler, 2022).

3.1.4 Epithermal Gold Mineralization

Epithermal deposits commonly occur adjacent to volcanic centers, calderas, or subvolcanic intrusions and are structurally controlled by fault zones (Arribas et al, 1995; Hedenquist et al., 2000). Typical features include silicification, argillic and advanced argillic alteration zones, quartz–adularia veins and breccias, and Au - Ag mineralization hosted in volcanic and volcano sedimentary rocks, with pathfinder

elements such as As, Sb, Hg, and Ag (Aluç, 2023). Notable examples include the Kışladağ, Ovacık, Çöpler, and Kirazlı systems. The Sırakayalar prospect, the subject of this study, lies within this metallogenic context and exhibits geochemical and mineralogical signatures consistent with a low-sulfidation epithermal system (Clark, 2014; Dilekler, 2022).

3.2 Local Geology of Sırakayalar Prospect

The Sırakayalar mineralization and the nearby Kovanlık and Karatepe prospects lie immediately to the north of the Lapseki Au deposit and are characterized by similar rock units mainly including metamorphic, igneous and sedimentary lithologies (Clark, 2014; Gülyüz et al, 2020; Dilekler, 2022). The southerly Karatepe and Kovanlık sectors sit atop a topographic high, which is bordered in the east by a NW-trending, structurally-controlled valley (Dilekler, 2022). Both sectors contain siliceous quartz veins emplaced within metamorphic and subvolcanic units that represent the northern extension of the vein system exposed in the Lapseki gold mine. The Sırakayalar sector, on the other hand, is located immediately to the east of the NW-trending valley and contains dismembered blocks of siliceous mineralized veins hosted within talus material (Dilekler, 2022). Distinct lithological units recognized in the project area are described below.

3.2.1 Metamorphic Units

The mica schists one of the widely spread out unit at Biga Peninsula from Ezine to Karabiga, and it was defined as Çamlıca Metamorphic by Okay et al. (1990). Additionally, Çamlıca Metamorphics are addressed as cover rocks of the Kazdağ Massif (Kalafatcioglu, 1963). Later on, evolution and origin of the unit are interpreted as involution with Rhodope, Serbo-Macedonian Massif (Okay and Satır, 2000; Okay et al., 2001). Schist units of the Çamlıca Metamorphics (Okay and Satır, 2000) represent the lowermost (Figure 3.3) part of the local stratigraphy (Dilekler, 2022). Metamorphic units (Fig 3.4) are comprised by mica schist and graphite schist,

the former more dominant around the Kovanlık and Karatepe areas, and the latter is present in the Sırakayalar area (Clark, 2014; Dilekler, 2022). Deformed schist units host some of the vein-type mineralization in the Kovanlık and Karatepe areas, as well as in the Lapseki gold deposit.

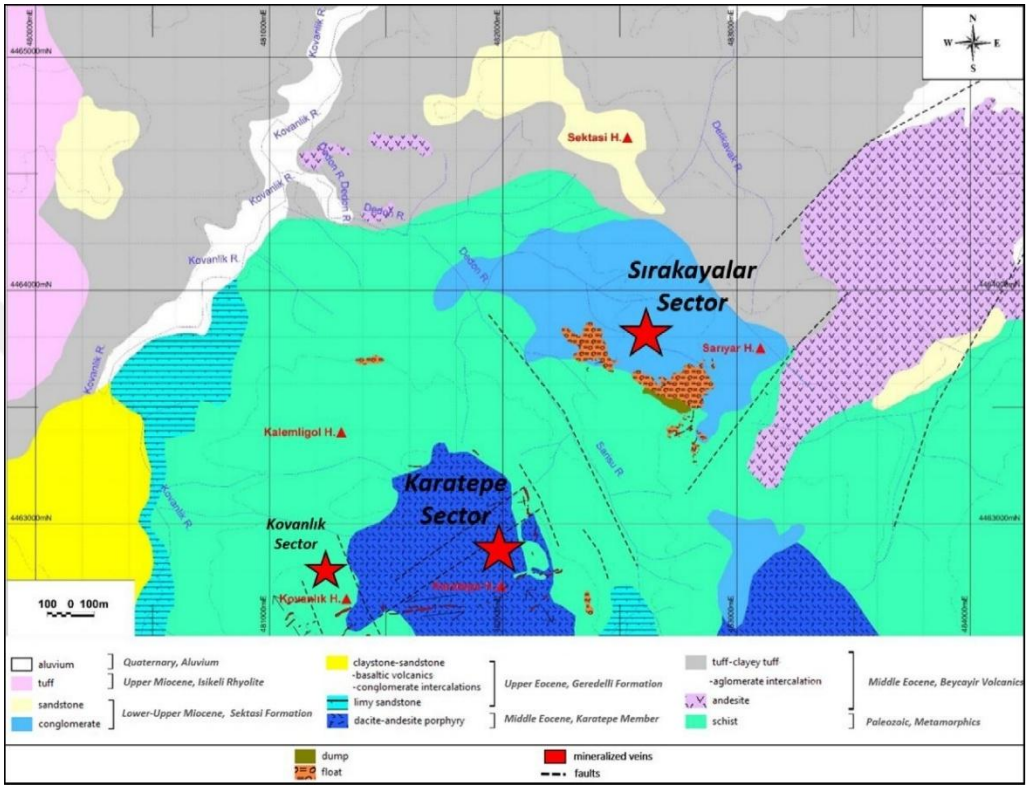


Figure 3.4 Geological map of the area hosting the Sırakayalar, Karatepe, and Kovanlık prospects located immediately north of the Lapseki Au deposit (from Dilekler, 2022).

3.2.2 Volcanics

Basement metamorphics are cross-cut and overlain by Eocene igneous lithologies of the Beyçayır Volcanics mainly including sub-volcanics, agglomerate, and tuff (Figure 3.4; Clark, 2014; Dilekler, 2022). Among these, only sub-volcanic rocks, belonging to the Karatepe Member, were encountered in the Kovanlık, Karatepe and Sırakayalar sectors (Dilekler, 2022). These sub-volcanics are variably-altered andesitic porphyries. Least-altered rocks as encountered in the drill cores and also locally in the outcrop have phenocrystic plagioclase, biotite, and hornblende with

minor quartz (Dilekler, 2022). These are surrounded by a groundmass containing fine-grained plagioclase and magnetite (Dilekler, 2022). Intact outcrops of andesite porphyry were only identified to the east and northeast of Sırakayalar, but not within the mineralized area (Fig 3.4).

3.2.3 Sedimentary Rocks

To the north of Sırakayalar, the andesitic subvolcanic rocks are overlain by the Sektaşı Formation along an unconformity. Sektaşı Formation is represented by conglomerate and sandstone (Dilekler, 2022).

The main unit exposed in the Sırakayalar area is a talus that contains variably-sized (from a few centimeters up to 2 m) blocks of andesite porphyry and mineralized siliceous veins (Dilekler, 2022). These fragments are compacted by an intensely-oxidized, red-colored matrix consisting of very fine-grained Fe-oxides (mainly hematite), clay, and silica (Dilekler, 2022). Talus material is separated from the underlying graphite schists with a low-angle detachment along which graphite schists are intensely sheared. The talus represents faulted and dismembered remnants of the Au-bearing veins that are similar to the ones exposed at Karatepe and Kovanlık prospect (Clark, 2014; Dilekler, 2022). The vein fragments show well-developed epithermal textures including colloform banding, crustiform banding, lattice/ghost bladed textures (Dilekler, 2022). Drilling by ESAN revealed local zones of high-grade Au-Ag mineralization containing up to 590 g/t Au per 1-m intervals. Due to intense oxidation, sulfides are generally not well-preserved in the siliceous vein fragments.

3.2.4 Mineralization and Paragenesis

Mineralization in the Sırakayalar, Kovanlık, and Karatepe areas is in the form of low-sulfidation epithermal veins that are predominantly made up of silica alongside rare sulfides (generally <5 vol.%) and sparse adularia (Clark, 2014; Dilekler, 2022). Silica occurs either as crystalline quartz (locally amethystine) or as cryptocrystalline

silica (chalcedony). Dilekler (2022) identified 3 distinct quartz textures in the vein fragments including early mosaic/jigsaw and saccharoidal to later bladed quartz, succeeded first by crustiform-comb quartz, and then by cockade-comb quartz.

Where preserved, andesite porphyry wall-rock fragments in Sırakayalar show moderate to high intensity quartz-chlorite-illite-carbonate±adularia alteration (Dilekler, 2022). Within the vein fragments, the main sulfide mineral is pyrite with subordinate arsenopyrite, and Au-Ag mineralization occurs as rare electrum and native gold (Dilekler, 2022).

3.2.5 Previous Exploration Studies

According to internal company reports at TÜMAD, discovery of the Sırakayalar mineralization was done by the MTA trough regional surface sampling survey. Previous exploration studies before ESAN remain unknown. ESAN conducted soil sampling, geophysical surveys (IP/Resistivity), trench and channel sampling, diamond and reverse circulation drills, mineral resource estimation (Addison Mining Services-internal report, 2019). After TÜMAD acquired the Sırakayalar license, the company began exploration activities and carried out drilling, structural analysis, and mineral resource estimation.

CHAPTER 4

DATA AND METHODOLOGY

All the work conducted in this chapter stood for several assumptions in research scope. There are certain neither economic nor valuable considerations both Sırakayalar Mineralization and Lapseki Gold Mine. In contrast, mineral resources rely on economic extraction.

4.1 Data Sources and Characteristics

The data used for geostatistical and modelling purposes consists of drill hole data; DTM, geological reports and geological maps (Figure 4.1). In this part, preparation of data, geostatistical approaches to resource estimation, semi-supervised deep learning method are provided. No verification studies were applied to data.

4.1.1 Drillhole Database

The drill hole database consisted of a total of 391 drill holes with a combined length of 34,214.50 m. Of these, 242 are diamond drill holes and 149 are RC drill holes with mean hole depth respectively 105.7 and 58.0 m. From these a total of 20,325 assay records were available in the database. Only Au assay values are used in this study. Geochemical analyses for detection of Au were completed by fire assay analyses conducted at the ALS Laboratory at İzmir. Specific gravity measurements are available from 3,698 samples. The mean specific gravity value of these samples is taken as 2.67 g/cm^3 regardless of the lithology and alteration. This is due to the close densities of the main lithological units (andesite porphyry and schist) intersected in the drill holes, the mineralogical similarities across all alteration styles observed in Sırakayalar (i.e., argillic and intermediate alteration), and also due to the

significantly low abundance of relatively dense sulfide minerals such as pyrite and arsenopyrite in the mineralized system.

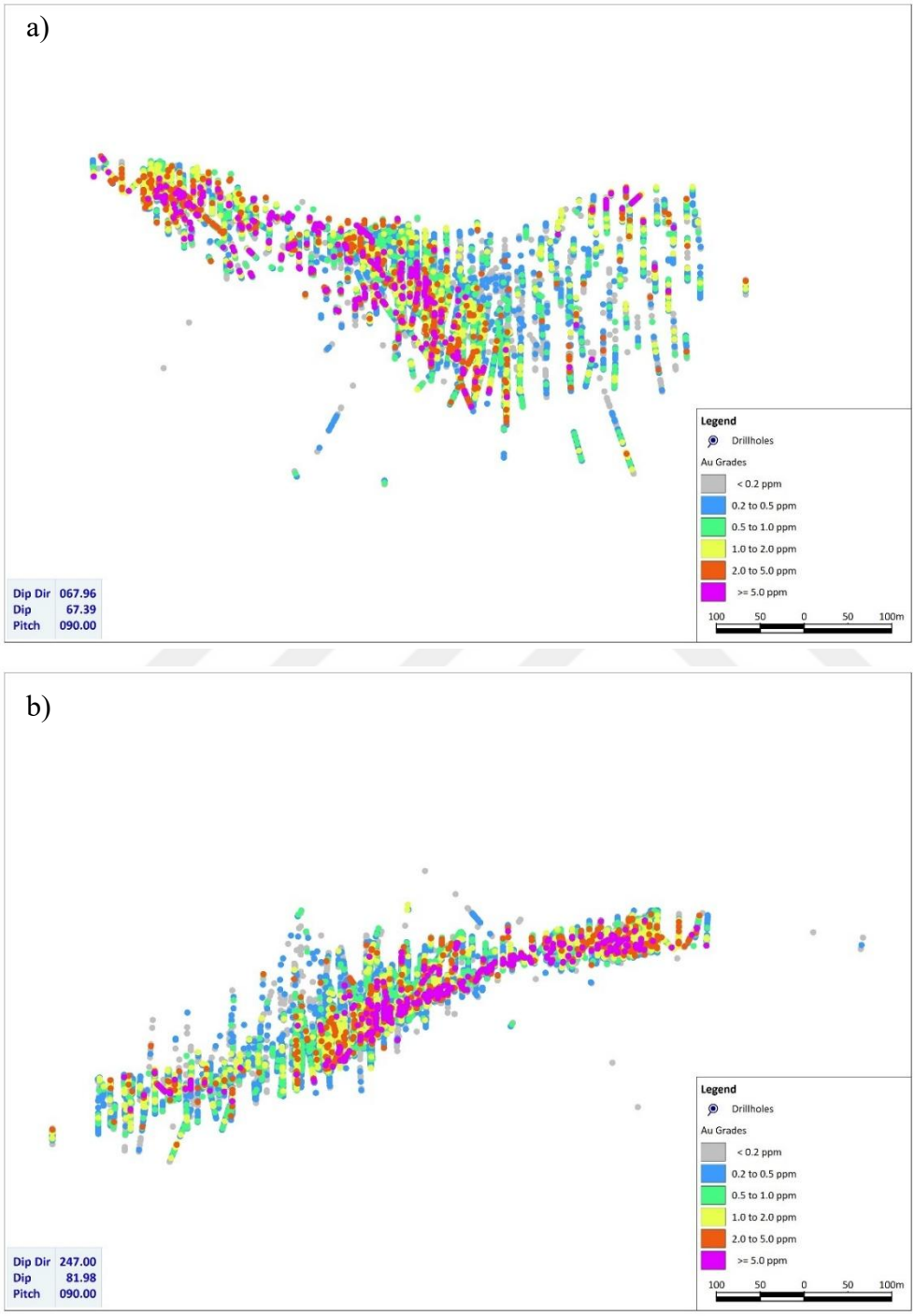


Figure 4.1 Ore shots of the Sırakayalar Mineralization due to maximum intensity projection (a, b, c views).

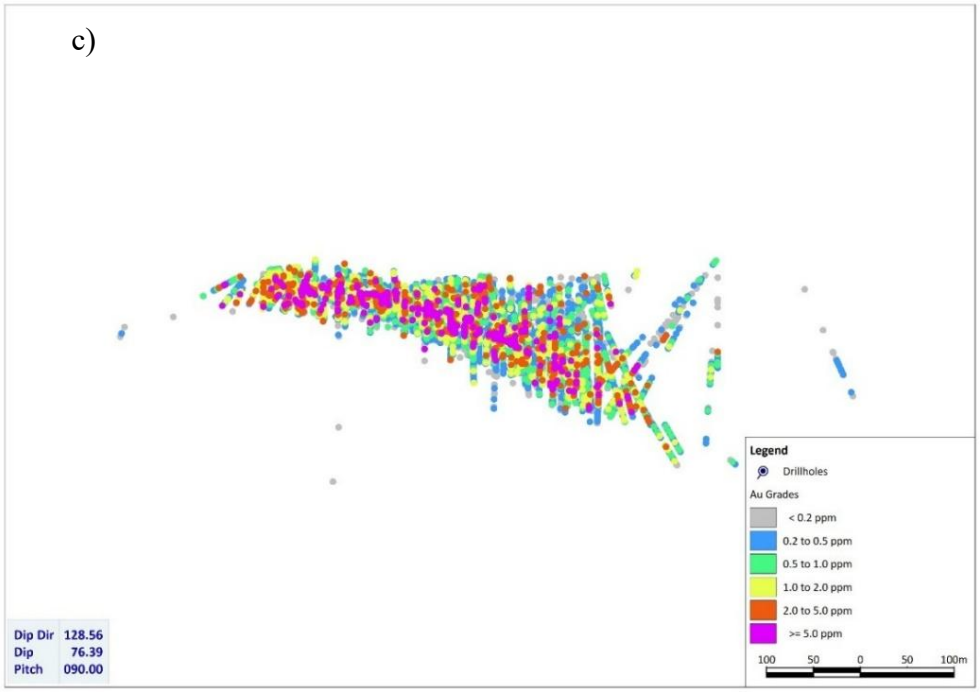


Figure 4.1 continued

4.1.2 Digital Terrain Models (DTMs)

The DTMs are available as 25k topographic maps and lidar based. However, information about the lidar based DTM is unknown such as, spatial resolution, area, scale, etc. 25k DTM was created from topographic lines (vectoral data).

4.2 Data Preparation and Cleaning

To estimate a value which is dependent on a numerical data, several adjustment should be made in geostatistical and deep learning approaches. These are listed below:

- Variable.
- Limitations.
- Methods.

The data should be prepared according to listed above. At the beginning, several drillhole sectors should be selected due to exploration targets. Drillhole data was validated and sorted by Sırakayalar Sector. Then, DTM (mesh structure) preparation and validation were conducted. 1:25,000 scaled topographic maps were used to cover resource areas, where lack of information had existed as mesh structure (Figure 4.2). The rest of the preparation just before the estimation was conducted according to method.

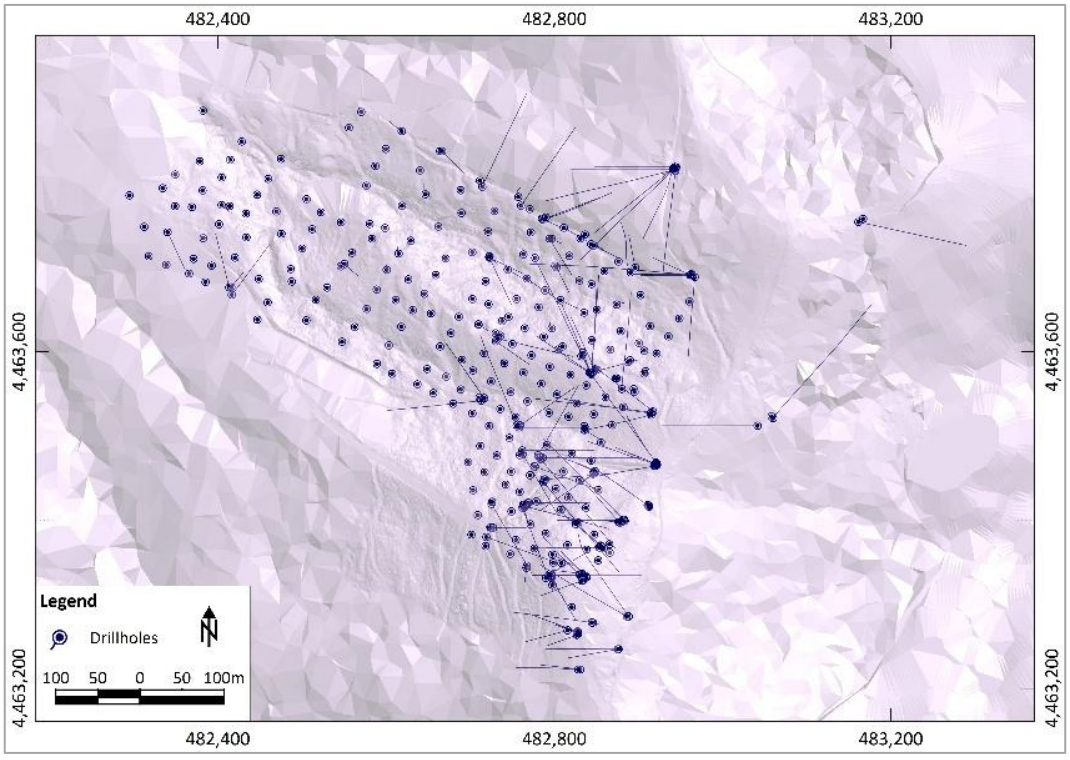


Figure 4.2 Plan view of the Sırakayalar area distribution of drill holes used in this study.

4.2.1 Domain Modelling and Wireframing

The Sırakayalar gold mineralization was separated into domains of high-grade and low-grade mineralization. The estimation was conducted in several steps:

The solid model was based assay data and uses on assumptions of high-grade (HG) and low-grade (LG) to increase precision. The cut-off grade (CoG) of run of mine

(ROM) is 0.5 ppm Au at the Lapseki Gold Mine. 3D continuity of assay grade was modelled by implicit model. Mineralization domains were identified as a central HG domain and surrounded by outer LG domain (Figure 4.3 and 4.4). Mineralization compositing assumptions and implicit solid model assumptions are provided in Tables 4.1 and 4.2, respectively.

Lithological solid models were not considered as limitations and there are also no additional wireframes that consist of barren igneous dykes, operated galleries, structural hard boundaries, etc.

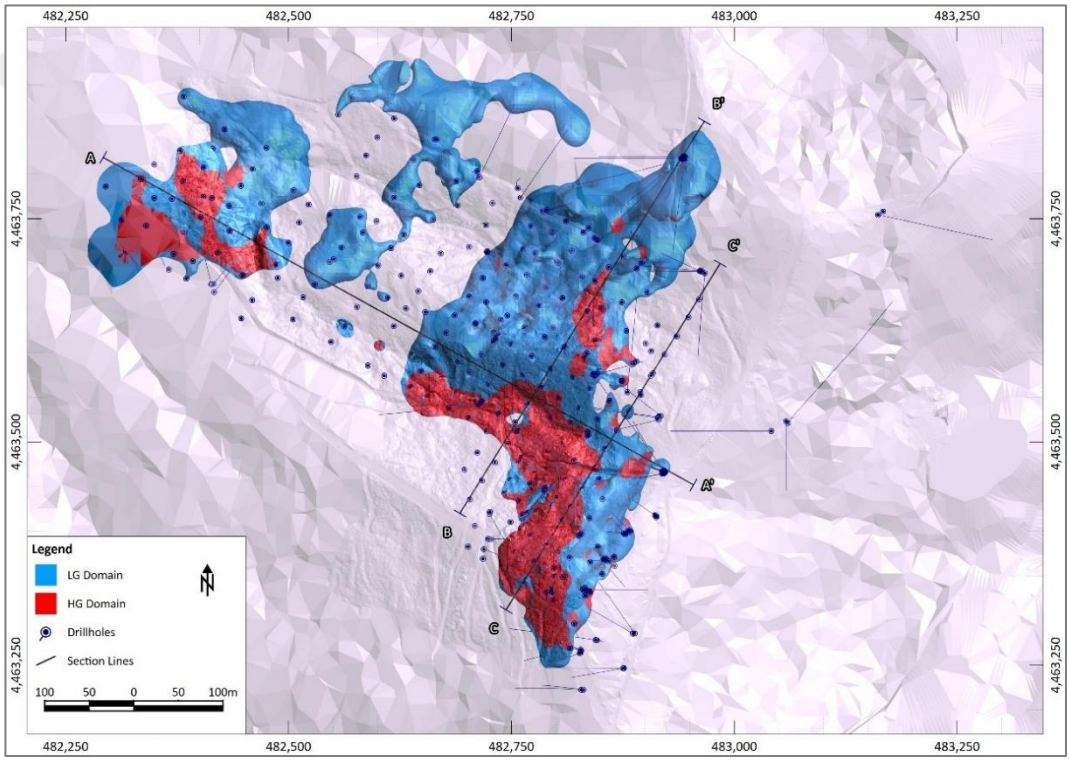


Figure 4.3 Sırakayalar mineralized domains and section lines at plan view.

Table 4.1 Summary of Mineralization Zone Compositing Assumptions

Grade Composite Data	Trigger Grade	Triger length	Average Grade	Internal Waste
LG	0.3	3	0.5	5
HG	0.5	3	1	5

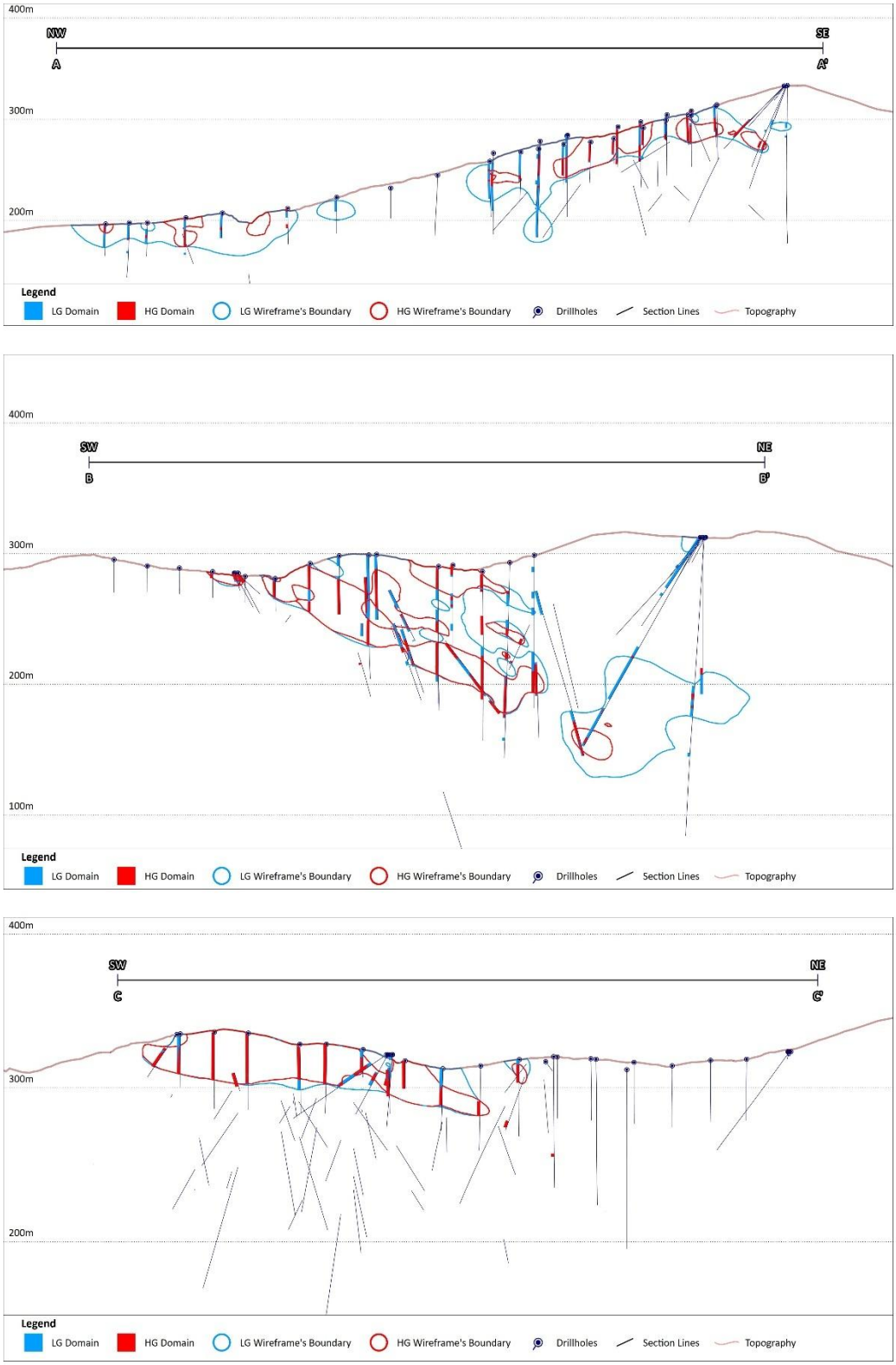


Figure 4.4 30 m shaded cross-sectional views of the domains. Section lines are shown in Figure 4.3.

Table 4.2 Implicit Assumptions for Solid Model

Range	Weighting								
	Axis1			Axis2			Axis3		
	Fac.	Az.	Plg.	Fac.	Az.	Plg.	Fac.	Az.	Plg.
120	1.5	300	0	2	30	30	1	30	-60

Two additional restrictions were applied to solid models. The solids were trimmed according to DTM. HG domain was trimmed, that must be enclosed by LG domain.

The same parameters were used for HG and LG domains. The classic linear method was used for implicit parameters. Maximum spacing was selected as 1 m, whereas 0.5 m is selected as the minimum spacing for interval length. Less than 125 m^3 solids were discarded.

4.2.2 Compositing and Capping (Outlier Handling) of Assay Data

The sampling of cores or chips were carried out in different interval length. Intervals that do not contain any numerical assay value are assigned assay values that are half of the detection limit, that is 0.0025 ppm. Then, 3D coordinates and domain types (either HG or LG) were written in another fields. The capping analyses were conducted separately as to HG and LG domains.

During the capping analyses, coefficient of values (COV), decile analysis and probability plots were investigated. Mineralized domains generally trend log-normal distribution and right skewness. In this part of the study, normal distribution was controlled to get higher resolution in relatively larger grades. Right tails of the histograms show low frequency that means probability in domain should be very-small in Figure 4.6 and 4.10.

In decile analysis, three main queries were applied during capping of assay data: (i) top decile cannot contain more than 40% of metal content, (ii) top decile cannot be larger than two times of the previous decile, and (iii) top percentile cannot contain

more than 10% of metal content. Accordingly, Au grade was capped for the LG domain at 4.15 ppm and for the HG domain at 6.4 ppm Au (Figure 4.5 and 4.9).

The COV values should be between 0.5 to 1.5 to increase efficiency of estimation by ordinary kriging (Table 4.3).

Tail parts of cumulative and probability plots represent outlier values (Figure 4.7, 4.8, 4.11 and 4.12). Any bottom cut was not applied, since analysis results were in ppm degree.

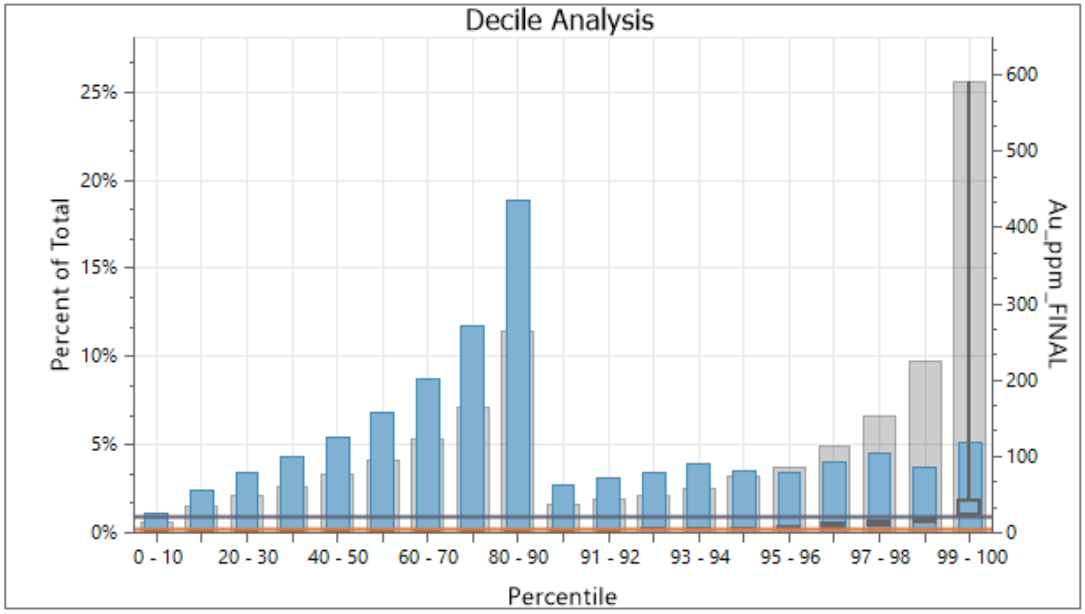


Figure 4.5 Decile analysis for the LG domain. Orange line represents after cut.

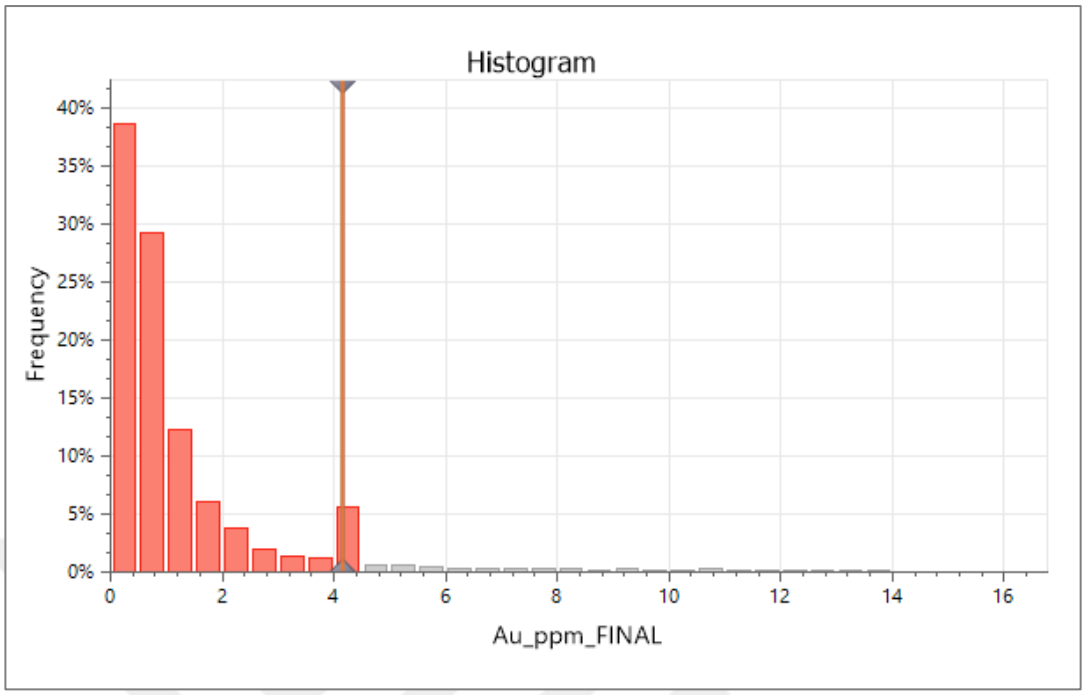


Figure 4.6 Histogram of Au distribution (in ppm) for the LG domain. Orange bars represent after cut, and gray bars represent before cut.

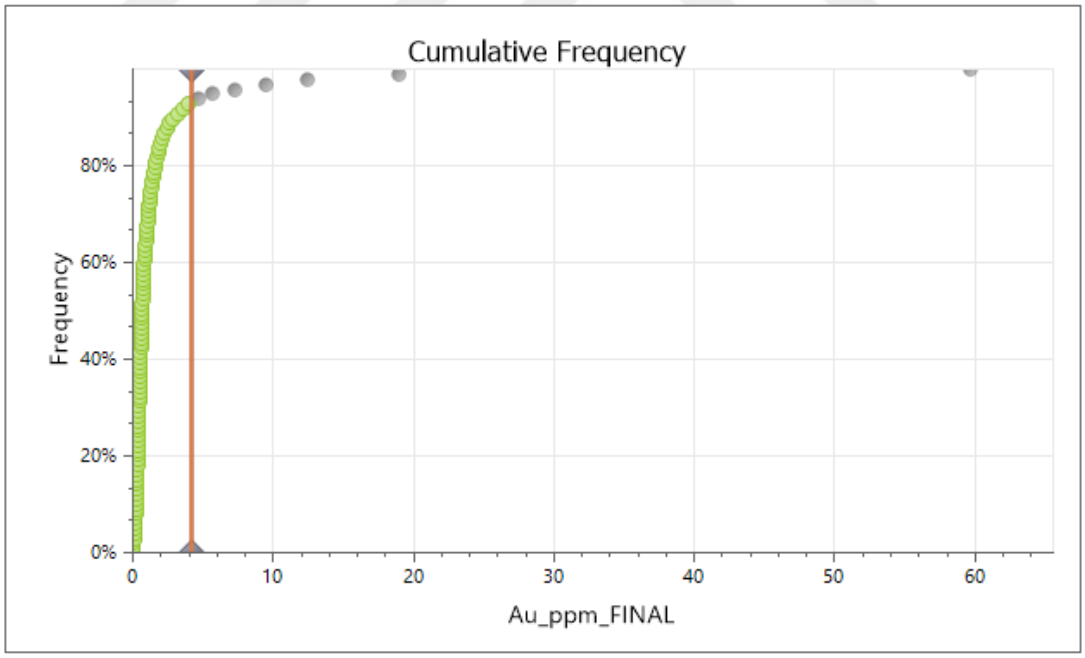


Figure 4.7 Cumulative frequency plot of Au assays (in ppm) for the LG domain. Orange line represents the cut value.

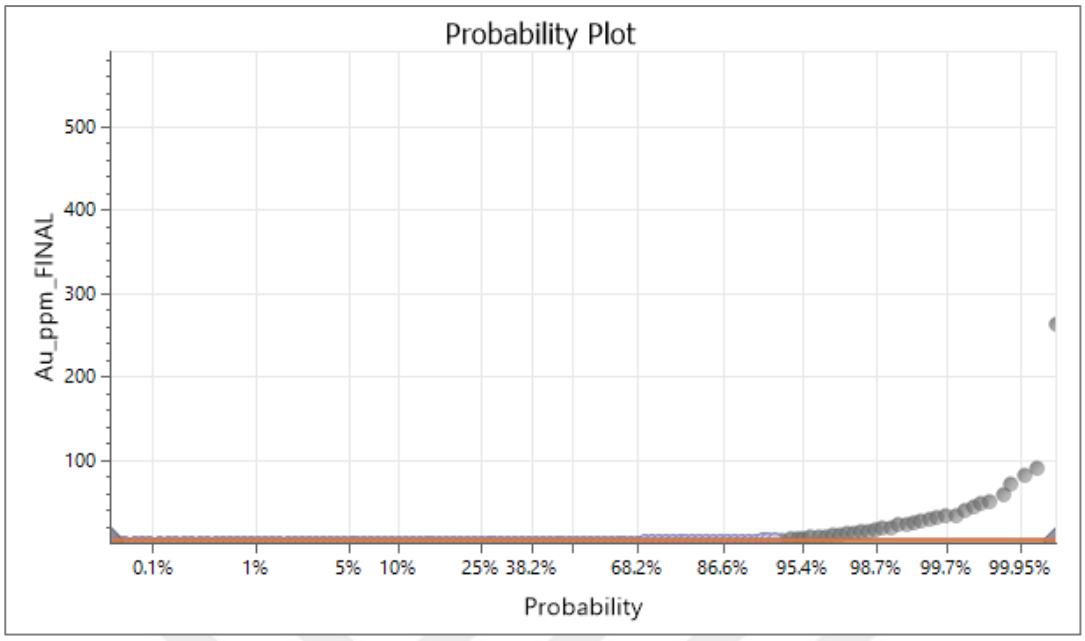


Figure 4.8 Probability plot of Au (in ppm) for the LG domain. Orange line represents cut value.

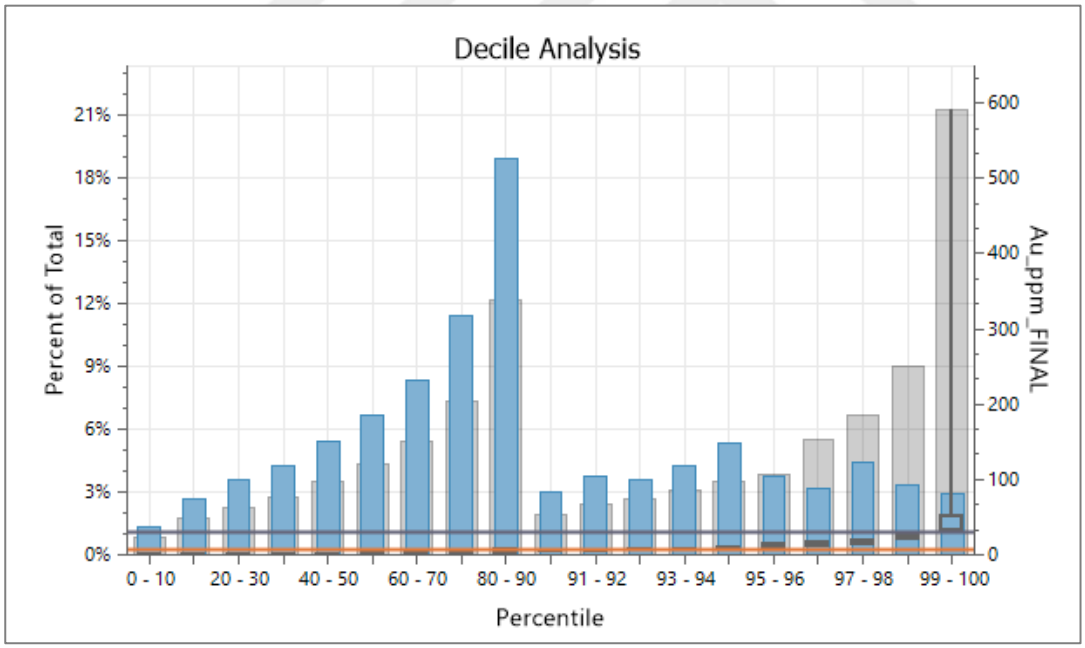


Figure 4.9 Decile analysis for the HG domain. Orange line represents after cut.

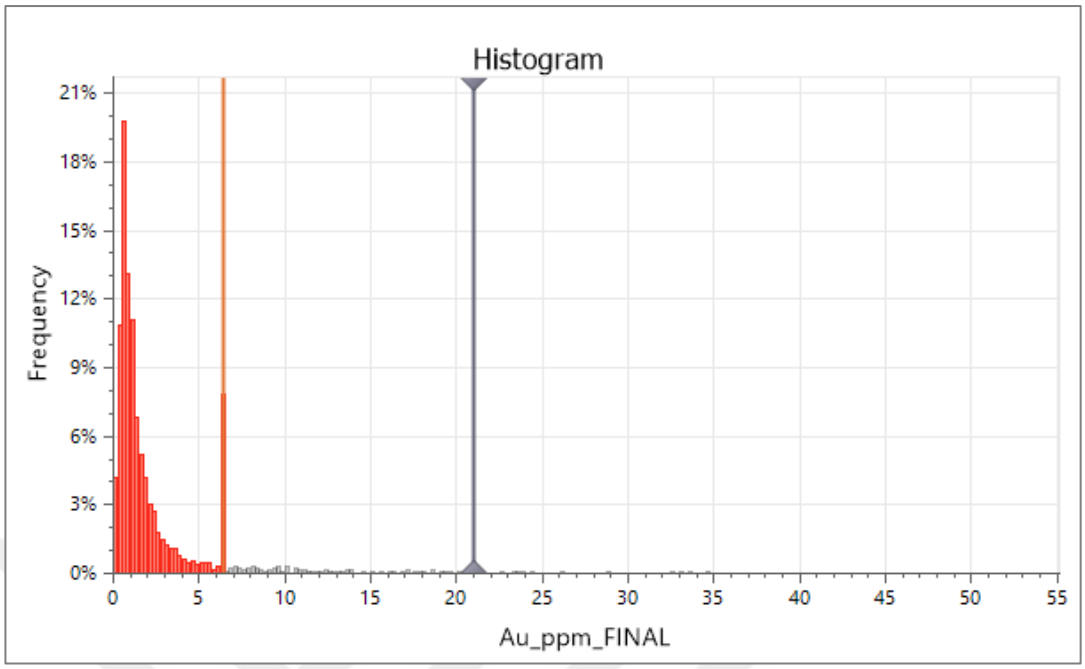


Figure 4.10 Histogram of Au distribution (in ppm) for the HG domain. Orange bars represent after cut, and gray bars represent before cut.

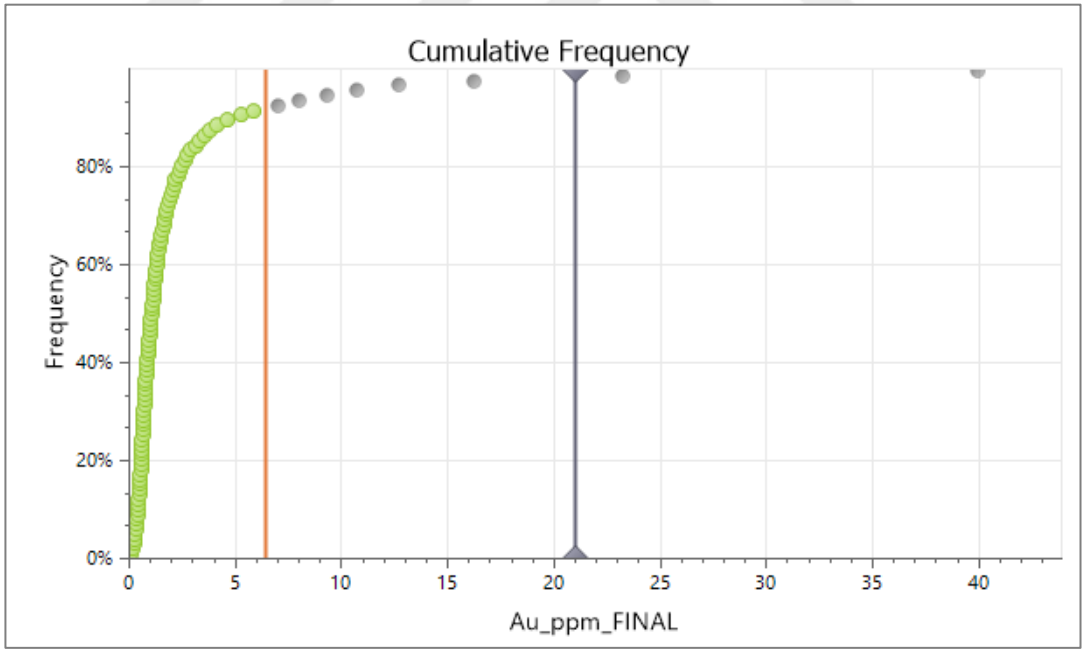


Figure 4.11 Cumulative frequency plot of Au assays (in ppm) for the HG domain. Orange line represents the cut value.

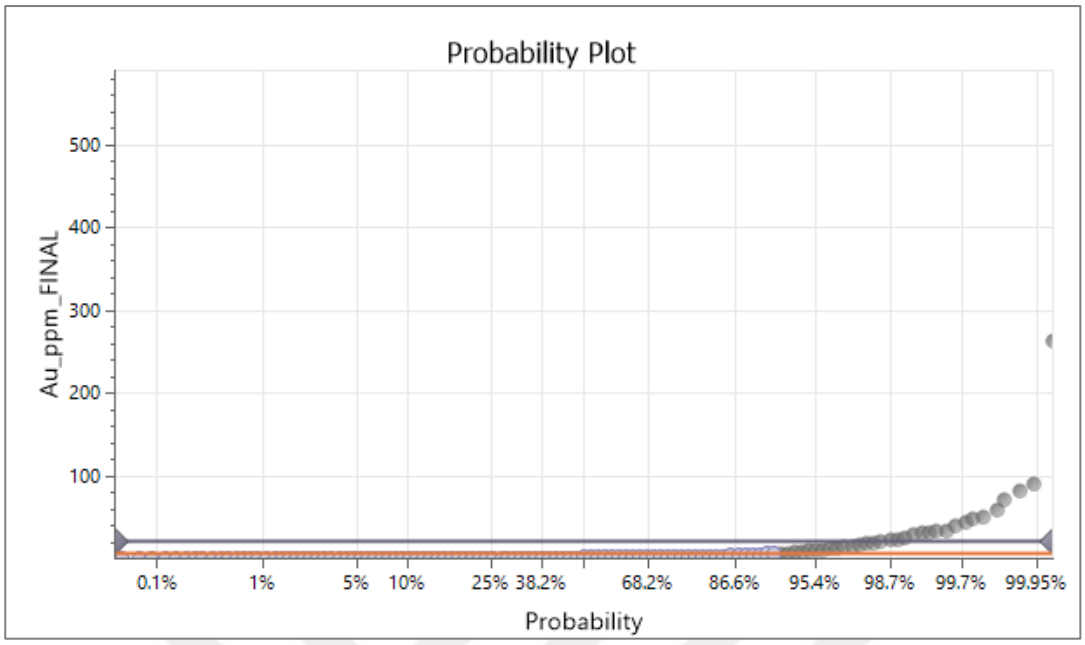


Figure 4.12 Probability plot of Au (in ppm) for the LG domain. Orange line represents cut value.

Table 4.3 Summary Statistic of Before/after Capping Gold Grade

Domain	Raw/Cap Count	Mean	Variance	SD	COV	Maximum	Percentage.
LG	6,549	1.78	92.78	9.63	5.19	590	-
	420	1.08	1.23	1.11	1.03	4.15	6.41
HG	3,864	2.69	155.	12.45	4.46	590	-
	286	1.73	3.05	1.75	1.02	6.4	7.4

The composite length was selected in both mineralization domains as 1m (Table 4.4). Reverse circulation data is included in compositing. However, reverse circulation drillings were not generally obeying the sampling length as 1m, which may increase the variance of assay results.

The downhole compositing the assay data was applied due to mineralization domains after capping analysis (Table 4.4). Minimum interval length was assumed to be 0.5 m, and residual interval was added to last interval.

Table 4.4 Summary Statistic of Interval Field of Assay Data in ppm

Minimum Value	0.05
Maximum Value	9.00
2nd Highest	7.50
3rd Highest	5.00
4th Highest	5.00
N	20325
Mean	1.329
Variance	0.357
Standard Deviation	0.598
Coeff. of Variation	0.450
Median	1.00

4.3 Geostatistical Estimation Workflow

The grade estimation workflow includes pre-processing, variogram analysis, selection of search parameters, estimation (3-run-pass) and validation part. The flow chart of OK grade estimation was given below Figure 4.13.

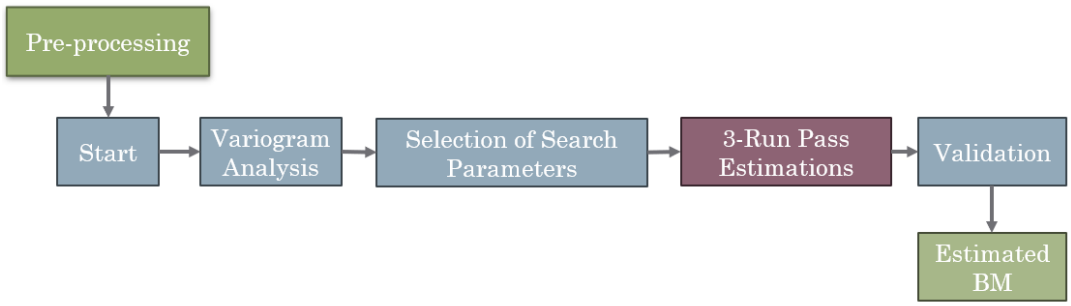


Figure 4.13 Workflow of the OK application.

4.3.1 Variogram Modelling and Spatial Continuity Analysis

Variogram models represent autocorrelation functions, whereby relatively higher and low grades are accumulated together. Variogram models were created with semi-

variogram analyses. Variogram analyses were conducted only by LG domain which has higher quantities of assay data. Then, it was applied to both LG and HG domain. Downhole variogram was conducted selection of nugget effect (C_0). Then, to honor the orientation of the mineralization and variogram maps, the axes were selected due to continuity of the mineralization such as strike (major), dip (semi-major) and pitch (minor). The variance was scaled to 1, and partial sill (total variance of the samples - C) were recorded (Figure 4.15). According to semi-variogram analyses, variogram models were created by using two spherical functions. Understanding anisotropy in 3D is crucial for designing the search strategy during the kriging estimations.

Result of the amenable variogram analyses, search ellipsoid (Figure 4.14) was selected as spherical and parameters summarized in Table 4.5.

Table 4.5 Summary of Semi-variogram and Search Ellipsoid Parameters

Domain	Axis	Azimuth /Plunge (°)	Nugget	Partial Sill	Range (m)
LG	Major	120/0			6.5/33.2
&	Semi-major	210/30	0.13	0.37/0.60	5.12/19.4
HG	Minor	210/-60			14.0/15.0

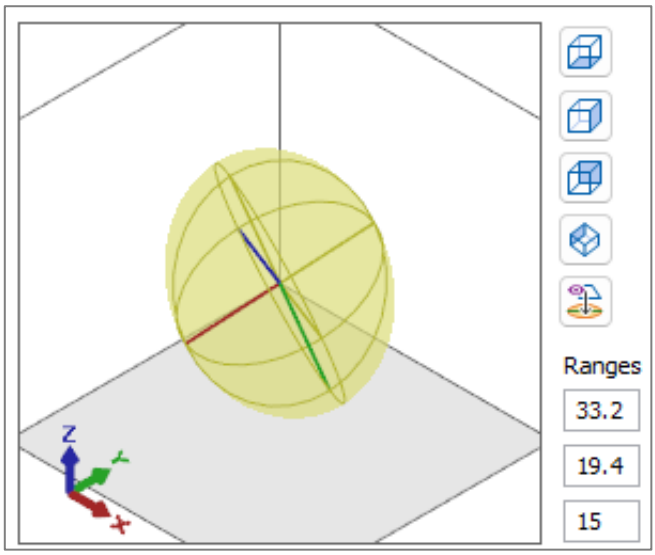


Figure 4.14 Search ellipsoid configuration at 3D space.

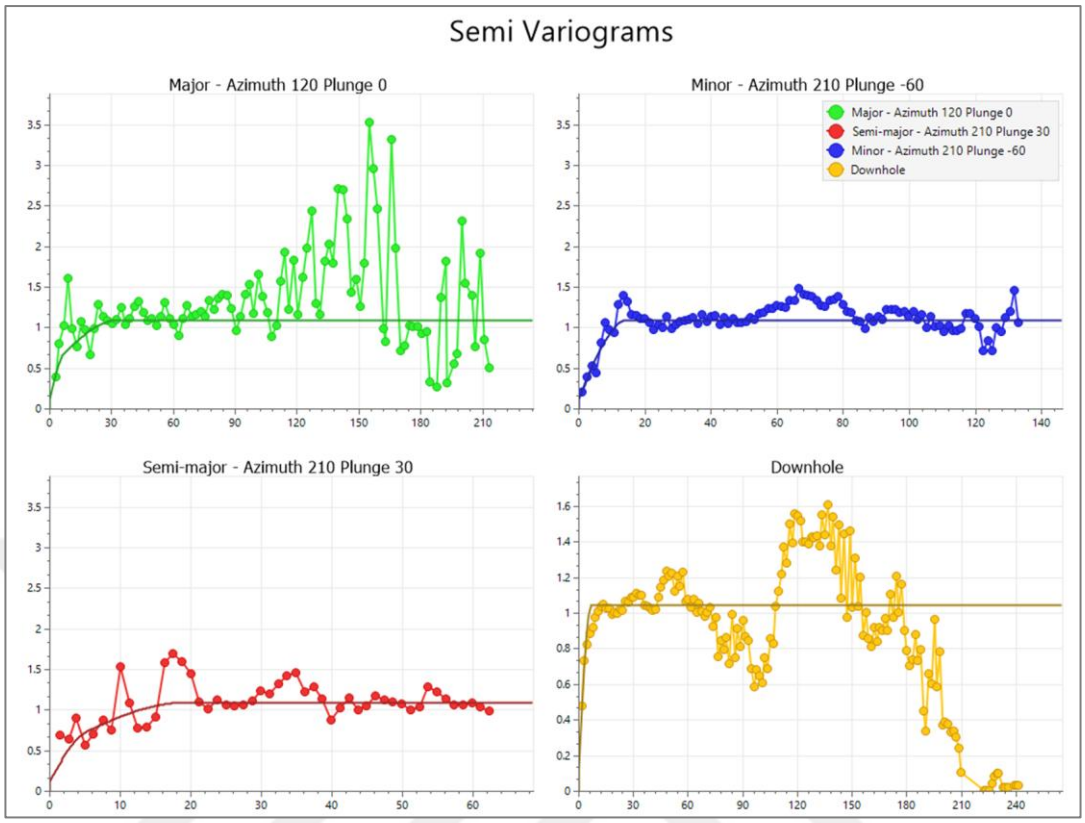


Figure 4.15 Three axes and downhole semi-variogram results.

4.3.2 Block Model Design

A parent block model with dimensions of 15 × 15 × 5 m (X, Y, RL) was created, consistent with the drill hole spacing. The model was rotated to align with the solid domain models. To better represent the deposit geometry, sub-blocking was applied at 3 × 3 × 5 (Table 4.6). Solid domain models were then assigned to the block model, requiring that at least 90% of the block volume lies within the corresponding wireframe.

Table 4.6 Block Model Attributes

Axes	Center		Blocks			Rotation (°)
	Min	Max	Size	Min Size	#	
E	481971	483396	15	5	92	-33
N	4462945	4464290	15	5	92	0

RL	25	375	5	1	71	0

4.3.3 Ordinary Kriging Implementation

The block estimation was carried out with Ordinary Kriging method 3 passes for each domain. The estimation covers only parent blocks. 3x3x5 discretization were applied and negative values were assigned as zero. The maximum informing sample per drillhole was selected as 5. The sector of the search ellipsoid was selected as quadrant. The maximum informing sample was selected as 16. Maximum sample per sector was selected 4.

Discretization basically creates virtual sub-blocks, and estimation was carried out for these blocks. Average value of the estimated grade was written as the grade. This application and estimation parent block only holds the block-wise estimation strategy, instead of the point-based estimations.

Quadrant based estimation and restriction of the samples were handled de-clustering part of the application. De-clustering was applied for stationary sampling bias which means that, higher grades and lower grades were represented as a sampling bias.

The search parameters were the same for both HG and LG, and they were listed at Table 4.7.

Table 4.7 Ordinary Kriging Search Parameters

Search Ellipsoid Orientation			Run	Sample Information		Search Range (m)		
Az.	Dip	Pitch		Min Trigger Sample	Min Sector	Major	Semi Major	Minor
210	30	0	1	3	3	33	20	15
			2	3	3	66	40	30
			3	1	1	66	40	30

4.4 Deep Learning Approaches

The main idea is assigning a block model; likewise using central limit theorem. Before the application of this method, a couple of method used like random forest, convolutional neural networks. However, the results were not satisfied compared with raw assay data. Then, pre-designed (convolutional) feed-forward Deep Learning method was applied to assign blocks.

The workflow of Deep Learning grade estimation was given at Figure 4.16.

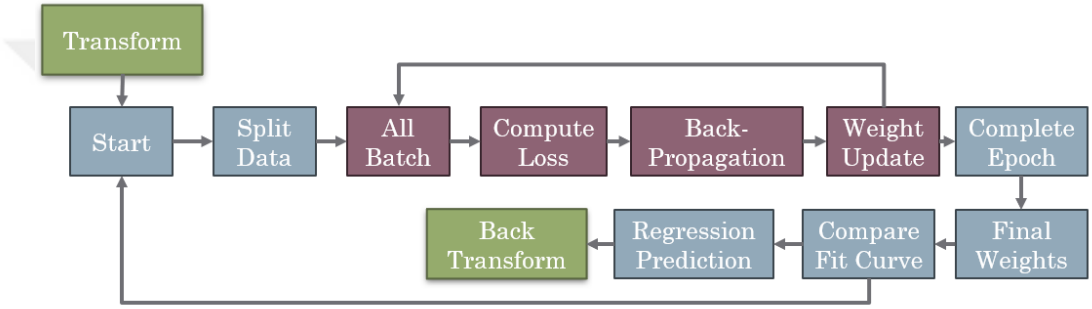


Figure 4.16 The workflow of the DL application.

4.4.1 Data Structuring and Preprocessing for Deep Learning

Idea of the machine learning algorithm is based on learning from the small portion of the population and making a prediction of the unknown parts.

In Deep Learning approaches several defined functions were applied by using Python language. Resulted .csv files were imported to Micromine 2025 application for comparison. For this section listed libraries (consist of defined functions) were used:

- Numpy (Harris et al., 2020),
- Pandas (McKinney, 2010),
- Torch - Pytorch (Paszke et al., 2010),
- Scikit (Pedregosa, 2011).

Table 4.8 Summary of the Deep Learning Inputs and Limitations

Variable	Limitations	Result
2m composited all data without filter and fake points	• Closest second drillhole • Decay factor • Fitting normal distribution	Assigned Block Model 15x15x5 Sub blocks min size 5x5x1
Domain assigned capped and 2m composited data	• Closest second drillhole • Domain assigned blocks • Decay factor • Fitting normal distribution	Assigned Block Model 5x5x2 Sub blocks min size 1x1x0.4

The Deep Learning (DL) application utilized both raw assay data and domain-assigned (pre-processed) data. The datasets and their limitations were summarized in Table 4.8, which served as the basis for the DL implementation.

The input variables included coordinates, domain assignments, and gold (Au) assay results. A stochastic probability function–based approach was applied to both location and grade estimation, using the RELU (rectified linear unit) activation function (Jarrett et al., 2009; Nair and Hinton, 2010; Glorot et al., 2011).

The central concept was to separate the density (probability) function across multiple DL layers, conditioned by spatial location. The coordinates of the input signals (point-based assay results) were expected to exhibit spatial correlation, while deeper hidden layers computed varying weights for regression.

To ensure consistency, all records were encoded as tensors, enabling the model to handle the accumulation of both barren and mineralized intervals. In summary, the expected outputs were represented in 2D form (Figure 4.17), illustrating the spatial distribution of predicted gold grades.

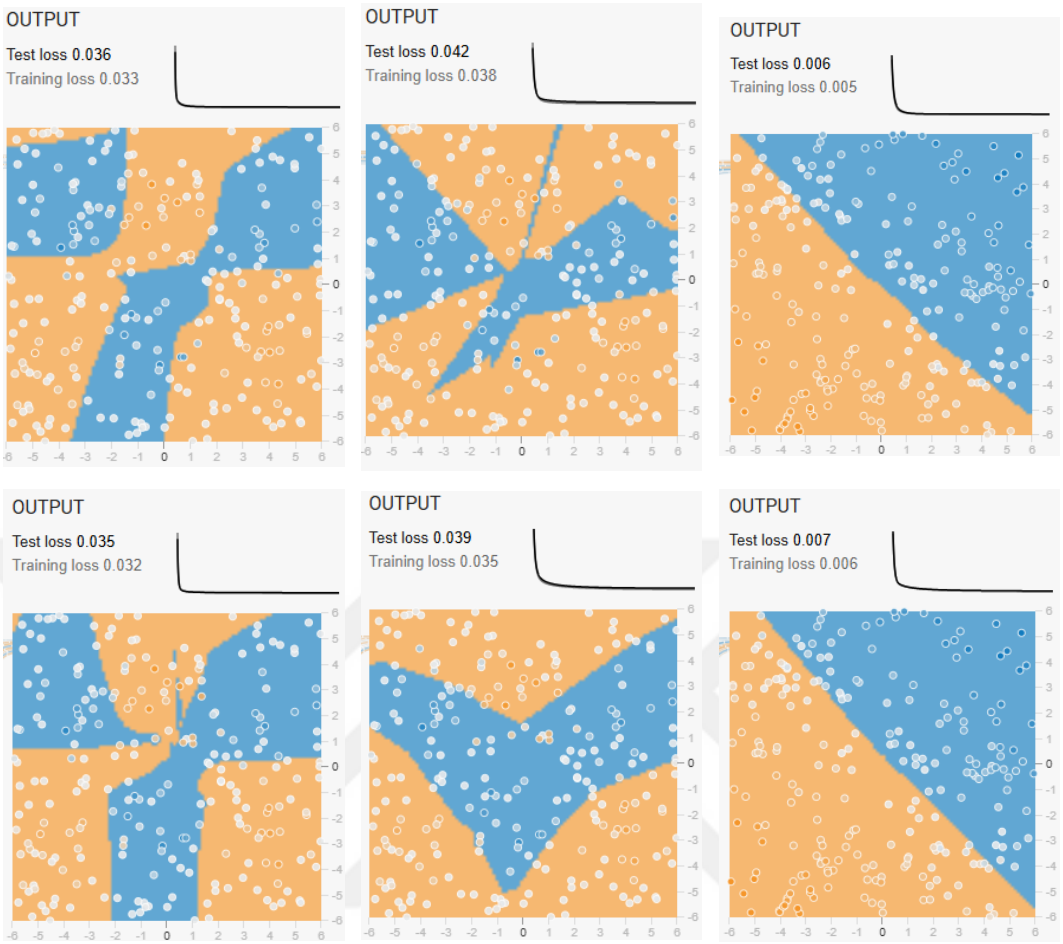


Figure 4.17 2D coordinated regression performance with different inputs and hidden layers. Left part inputs include X_1, X_2, X_1X_2; middle part inputs X_1 an X_2; right part inputs X_1 and X_2. Top to bottom; number of hidden layers; 1-2-4-6. Tests were conducted by learning rate 0.001, regularization rate 0.03. Tests were applied multi gaussian random dataset for left and middle parts and rest of them were applied planer random dataset. 20 percent of the data were used test samples. Noise was selected 20 and batch size selected 30. The quantity of epoch(iteration) is approximately 1000. The background color shows discrimination. The color represents data, weight; -1 /0 /1 respectively orange, white and blue (created by Similkov and Carter-playground.tensorflow.org, 2025).

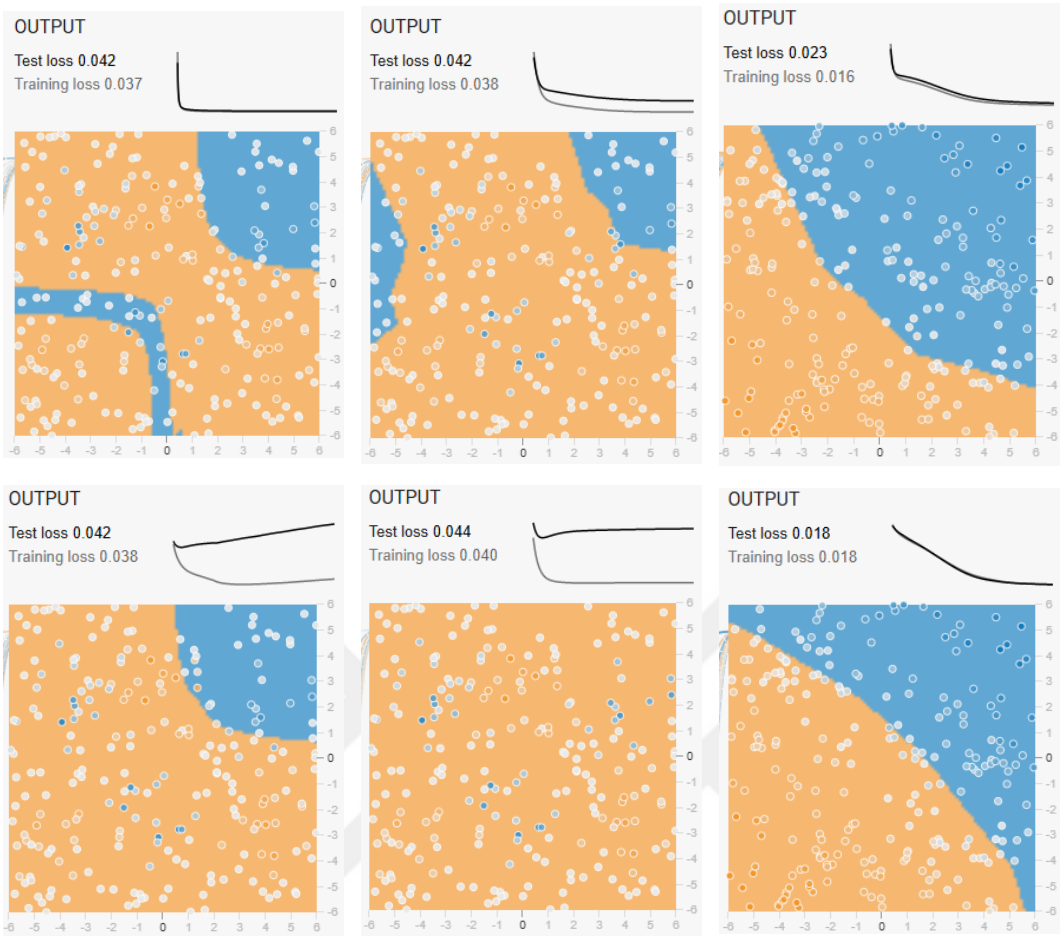


Figure 4.1 continued.

4.4.2 Network Architecture Selection

The data were converted into tensors and optimized using the Adam optimization module. The input assay data served as the basis for training. To evaluate model performance, the dataset was partitioned into training and testing subsets, with varying proportions applied. The train & test splits were generated by shuffling the records with different random seeds to ensure robustness and reduce bias. Finally, the prediction results were integrated into the block models for spatial representation. Adam module has several inputs like;

- γ (lr),
- β_1, β_2 (betas=(0.9, 0.999),
- θ_0 (params),

- f(θ) (objective),
- λ (weight decay),
- amsgrad(false),
- maximize(false),
- ϵ (epsilon=1e-08)(Pytorch,2025 version).

The default parameters were selected, except learning rate and weight decay. Learning rate and weight decay were used for fitting the results. By using the β_1 and β_2 stochastic part of the application covers random functions.

In Deep Learning approach, feed-forward based method was used to fill regression curve. Due to this method, applying feeds and further processing is continued regardless of backward fixing (Goodfellow at., 2016).

Weight decay was used to simplify the best fit (Figure 4.18). In this way higher rapid changes would be simplified. Since that was one of the hyper parameters, it depends on the number of iterations for each specific iteration; depended on iterations (Goodfellow at al., 2016).

Adam optimization (Kingma and Ba, 2014) was used to assign block models with normal distribution by using single layer application.

The model function is:

$Au(x;\theta)=W_3\sigma(W2\sigma(W_1x+b_1)+b_2)+b_3$

where

- x= input vector (coordinates and assay data),
- $\theta = \{W_1, W_2, W_3, b_1, b_2, b_3\}$= the set of learned weights and biases,
- σ= activation function (ReLU).

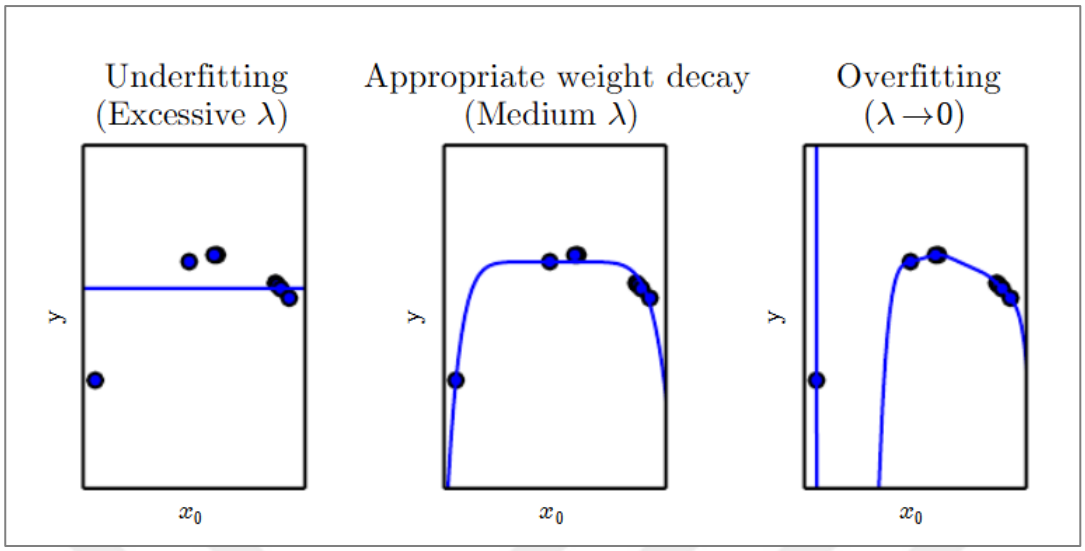


Figure 4.18 Relation between data fit and weight decay (Goodfellow at al., 2016).

4.4.3 Deep Learning Application

The tabular data were normalized by scaling values to the range of –1 to 1, which served as the network weights. Metric scaling was then applied to standardize the data. The dataset was partitioned into training and testing subsets, and the model was trained using the Adam optimizer.

For validation, several measures were employed, including mean squared error (MSE) to monitor overfitting and underfitting, histograms of estimated results, and the evaluation of mean, minimum and maximum values of outputs (Figure 4.19). These steps control the robustness of the DL model when compared to geostatistical results.

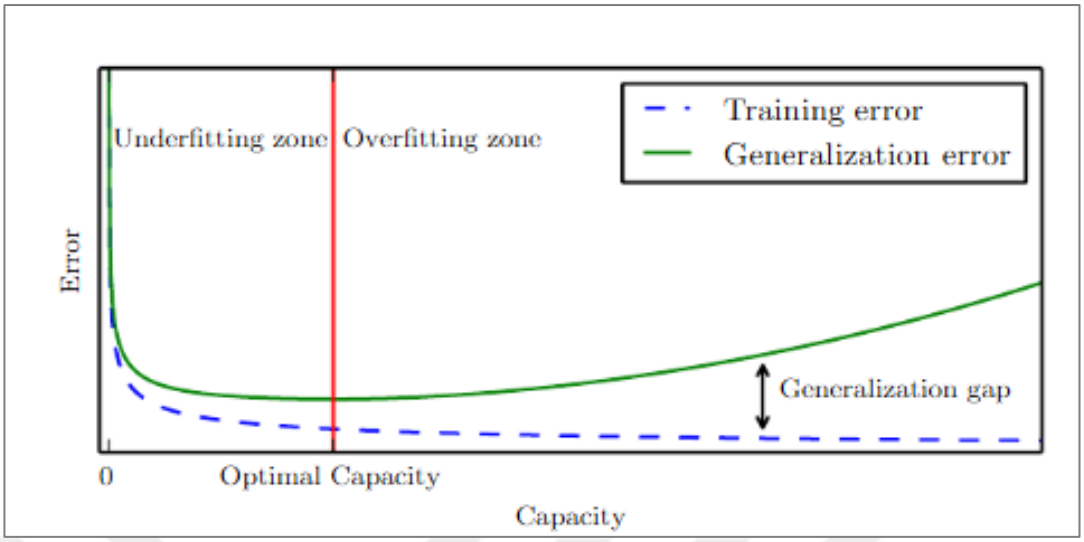


Figure 4.19 Comparison for underfit and overfit parts of the numeric model (Goodfellow at al., 2016).

4.4.3.1 Raw Data Assay Application

The raw assay application includes several steps for raw assay data to prepare. Assay data was composited with 1m intervals and less than 0.5m last residual intervals were added to last intervals. No query was not applied during this composition process which means that domains were not used as hard boundaries. However, the raw data does not show log-normal distribution, and their local variances of the data were quite high (sudden grade changes were seen).

In the edge of mineralization cloud, mineralization is continuing. Extrapolation zones should be truncated to background value. Extra points fake points were added to input data as baren (half of the detection limit of gold assay). Approximately 60m buffer zone was used to insert fake points around the mineralization. The fake points were set into DTM with 50x50m grid outside of buffer zone. Then, 1m interval fake points (3D) were generated and added into data. These application steps increased COV and decreased variance. Unless, this caused over estimation as the result on the blocks due to sudden decreasing of the Au grade, vice versa sudden increasing of Au grade.

Instead of adding fake points into inputs, the minimum sample count was increased. Composite interval increased to 2m to decrease variance of data. This applies regularization (smoothing the data) through input data and decreasing the vertical axis sampling quantities. Then, results were satisfied and quietly expected to compare raw assay data. The model parameters were given at Table 4.9 which are used for the raw assay application.

Table 4.9 Summary of Model Parameters

List of Parameters	Unit	Value
Composite	m	2
Minimum Points	Count	16
Train Size	%	40
Test Size	%	60
Random Seed	#	5
Learning Rate (lr)	#	0.05
Iteration (Epoch)	#	900
Max Distance to point	m	90
Weight Decay	#	0.0285
Hidden Layers' Neurons	#	64
Hidden Layers	#	2

During the fitting data as mentioned above learning rate, weight decay, minimum sample in range and minimum informing points were used. In overfit results, spotted dog pattern could be seen. Estimated grades of the closest blocks were slightly similar to input data. However, block model results were increased through to outer zone of a sphere regardless of input data. In contrast, grades of the closest blocks were slightly similar to input data and decreased to outer portion of the sphere. In both results, grades of the blocks were significantly regularized to fit model. Only, separation of mineralization and baren zones could see in rate of regularization.

A crucial observation was that, even when the same parameters were applied, the results varied depending on the random seed (including seed = 0). Depending on the seed, the outcomes ranged from optimal fits to overfit or underfit solutions:

- In under fit, approximately 1-5 different grade distribution were seen by using same input data. The curve of the normal distribution was so narrow (mod & median collapse). Most of the estimated blocks were barren. In the mineralization part high anomalies were detected.
- In over fit, pattern of the estimated block results was inverse of expected and extrapolation parts could reach to infinite numbers especially low learning rate, low weight decay and high iteration numbers.
- In optimal fit, curve of the normal distribution is wider than under fit's. As mentioned above, spotted dog pattern could be seen as spherical. The outer part of the spheres is slightly similar to the closest points. Most of the blocks were estimated ranging from input data. The optimal fit results would be used later part of the study.

Statistical parameters like min, max, mean, variance and COV values were compared to input and output data during the fitting.

Mean Squared Error (MSE) where mainly observed (y) and predicted (x) data as:

$$MSE = \frac{1}{n}\sum_{n=1}^{\infty}(y_i - x_i)^2$$

The MSE is significantly higher than expected (Figure 4.20). Over-under-optimal estimates with same parameters could be explained by variance and proportion of train/test data, grades of selected train-test data. The increasing proportion of tests is giving more related results for each different run. However, it decreases the efficiency of train data.



Figure 4.20 Mean squared error of Test and Train Loss.

4.4.3.2 Domain-Assigned Assay Data Application

In this part, previously classified domains were used. At the beginning, 1m mineralized composite intervals were used. However, even if the coefficient variation around 1 some local variances were caused to high mean squared error regardless of using high regularization. The deep learning estimation method is based on point estimation instead of using block estimation. The estimated value represents single point value in 3D space rather than average of the block value (Isaaks and Srivastava, 1989). There is no discretization part on Deep Learning approaches. Then, the block dimensions were decreased to handle both point-based estimation and discretization application. However, in geostatistical approaches, smaller blocks were not welcome. Approximately, block model dimensions should be between ½ to ¼ as drillhole spacing (Rossi and Deutsch, 2014). In this case around 1/5 to 1/8, which is not suitable for resource estimation. 2 m composite intervals were used for the estimation in both HG and LG domains. The summary statistics of LG and HG (1m and 2 m composited) are given at Table 4.10 which shows max, mean, COV and etc. for the input data. The summary parameters are given at Table 4.11 for domain DL application.

Table 4.10 Summary Statistics of Composite Intervals

Sample Type	Max	Count	Mean	Var.	SD	COV
LG 1m Composites	4.15	8,044	1.04	1.15	1.07	1.03
LG 2m Composites	4.15	4,124	1.04	0.98	0.99	0.95
HG 1m Composites	6.4	4,638	1.70	2.82	1.68	0.99
HG 2m Composites	6.4	2,404	1.70	2.35	1.53	0.90

Table 4.11 Summary of Parameters Used for Second Phase

List of Parameters	Unit	Value
Composite	m	2m
Minimum Points	Count	2
Train Size	%	25
Test Size	%	75
Random Seed	#	500
Learning Rate(lr)	#	0.002
Iteration(Epoch)	#	900
Max Distance to point	m	90
Weight Decay	#	0.0000001
Hidden Layers' Neurons	#	2,048
Hidden Layers	#	2

In complex problems, the number of neurons should generally be kept low, while the number of iterations should be increased, in contrast to simpler problems (Goodfellow, 2016). However, in cases where the data were constrained by wireframes, a higher number of neurons was used in order to provide a valid comparison with the previous setup.

The input data had previously been capped in the Ordinary Kriging (OK) application and composited into 2 m intervals. During the fitting process, nearly the same procedure was followed as in the previous application. However, capped bins were evident in the output histograms, which did not conform to a log-normal distribution of the clusters (decreases robustness of the model). The data would regularize by

fixing this problem which means weight decay and number of the iteration were increased.

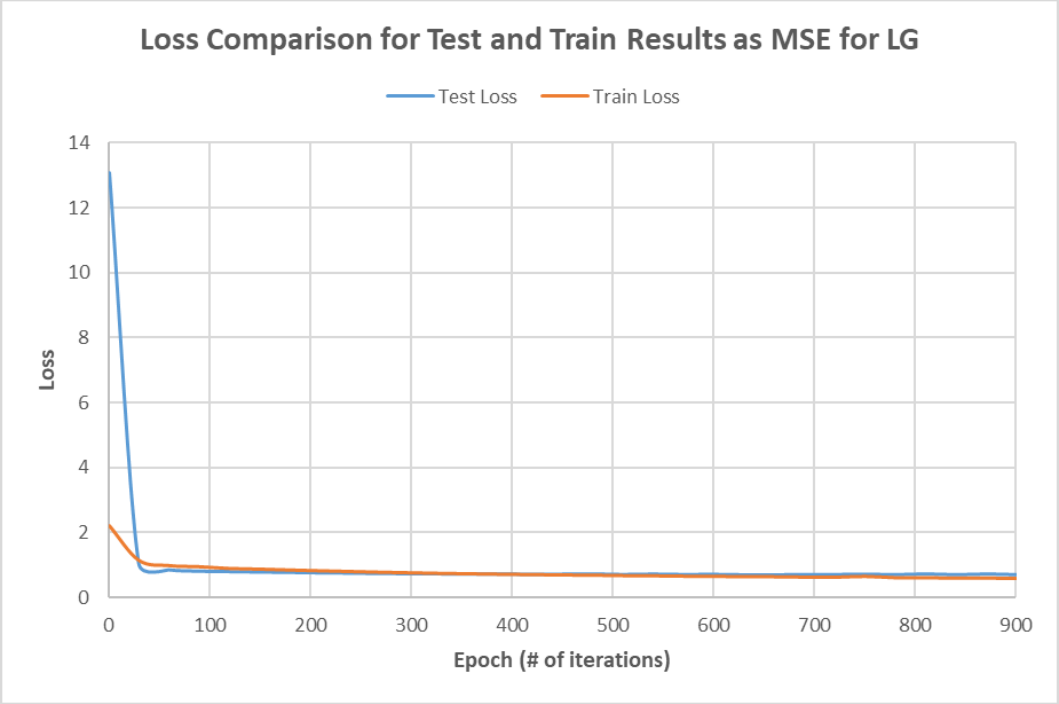


Figure 4.21 Performance of the loss comparison as mean squared error for LG.

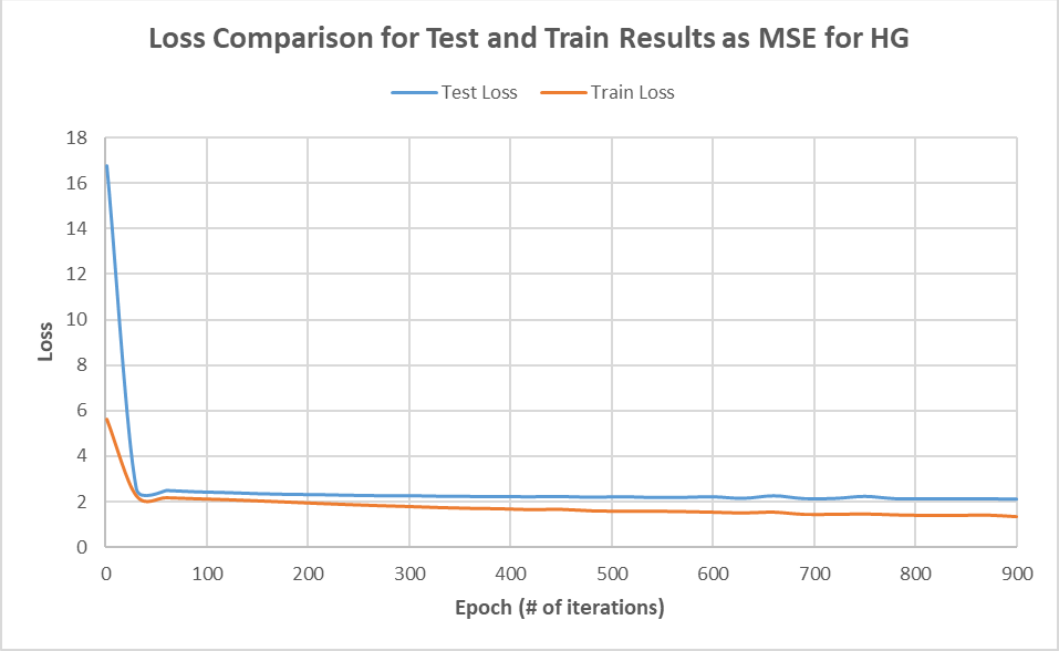


Figure 4.22 Performance of the loss comparison as mean squared error for HG.

In the LG domain, the mean squared error (MSE) was approximately 0.7209, while in the HG domain it was 2.0981. These MSE values are relatively low, and the training and testing MSE curves showed similar trends. This indicates that the fitting process was well balanced (Figures 4.21 and 4.22).

CHAPTER 5

RESULTS AND INTERPRETATION

There are no classifications that were applied which show the confidence level of the estimation. Neither redox boundary nor metallurgical test work results were applied for resource statements. All the resource was assumed to be mined as open pit above the cut-off grades.

As mentioned before, Sırakayalar Mineralization was one the sectors at Lapseki Gold Mine that processed by TÜMAD Madencilik A.S. Minimum processed gold grade is 0.5 ppm to process at tank leach process according to last known information provided by the company. The cut-off grade was selected with same as process cut-off.

5.1 Geostatistical Estimation Results

5.1.1 Block Model Outputs (Grade & Tonnage)

The resource estimation was reported by using volume, density, and average gold grade in different CoG values as ppm. The resource statement of Sırakayalar mineralization is given Table 5.1 by using ordinary kriging method.

Table 5.1 Resource Statement of Sırakayalar Mineralization by Ordinary Kriging

CoG (ppm)	Volume (Mm^3)	Tonnes (M)	Grade (ppm)	Au Content (Koz)
1.20	1.55	4.10	1.93	254
1.00	2.03	5.37	1.73	299
0.80	2.58	6.82	1.55	341
0.50	**3.74**	**9.90**	**1.27**	**405**
0.30	4.26	11.28	1.17	423
0.20	4.32	11.45	1.15	425
0.10	4.35	11.53	1.15	425
0.00	4.39	11.63	1.14	425

Notes:

1. No resource limitations were not applied like frame of license, social boundaries, etc.
2. Any metallurgical domains were not applied.
3. Resource classification was not applied according to national regulations like UMREK, JORC, NI 43-101.
4. Pit optimization was not conducted; all of the resource was assumed as minable with open-pit estimation respectively CoG.
5. This resource statement was conducted in research scope. There is no economic value of them.
6. The numbers were rounded.

5.1.2 Swath Plots and Validation

The resource estimation could be validated by visual or using statistical approaches. Statistical validation parts were carried out by 3D axes to swath graphs.

In swath plots (Figure 5.1), OK, DL-Domain and NN (Nearest Neighbor) are used for the comparison. The assumption is that NN is addressing the composite input files.

In the swath plots, similar estimation trends were expected, with both the collapsed and peak sections showing comparable behavior. Overall, the patterns of the estimations (i.e., amenable reflection points) were generally consistent (Figure 5.1). In the north and RL directions, the trends aligned very well. In contrast, the east direction displayed a similar overall trend but with different Au grades, primarily due to the lower frequency of input data. Where the input data density was higher, both the grades and the trends showed almost perfect matching.

Visual validations were carried out by comparison assay data with estimated blocks (Figure 5.2 and Figure 5.3). The estimated blocks should be represented with same mineralization trends as the assay data.

Grade versus tonnage curve shows sensitivity of the changing grades and tonnage. Any elbow type sudden changes could be clue for estimation errors (Figure 5.4).

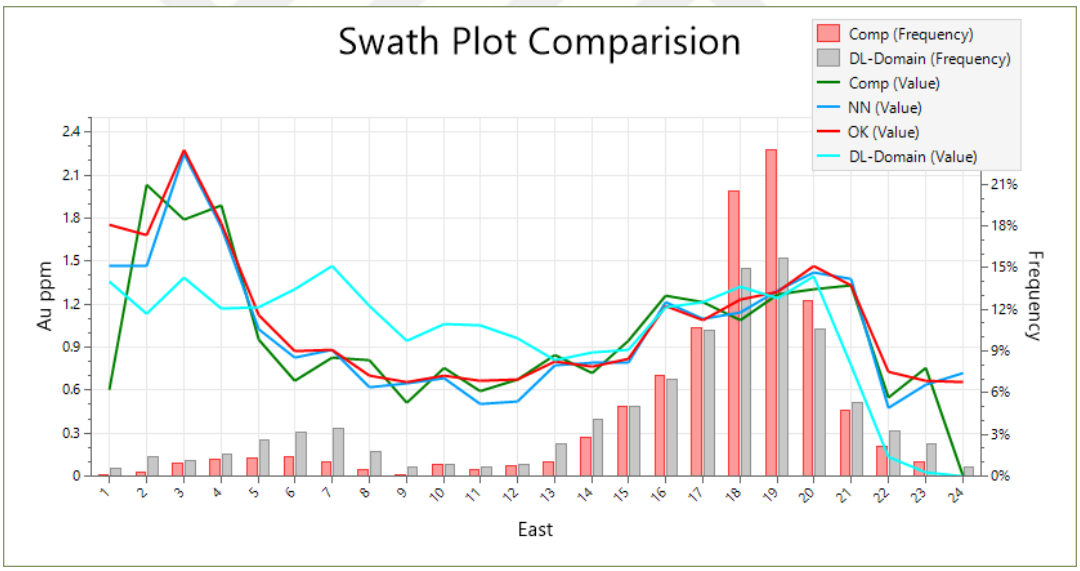


Figure 5.1 Swath plots respectively east, north and RL. In east and north direction 30 m and in RL 10 m thickness were used. Comp: Composite file as frequency and value, DL-Domain: Deep Learning domain as value and frequency, OK: Ordinary Kriging, NN: Nearest Neighbor estimation as Au grade in ppm.

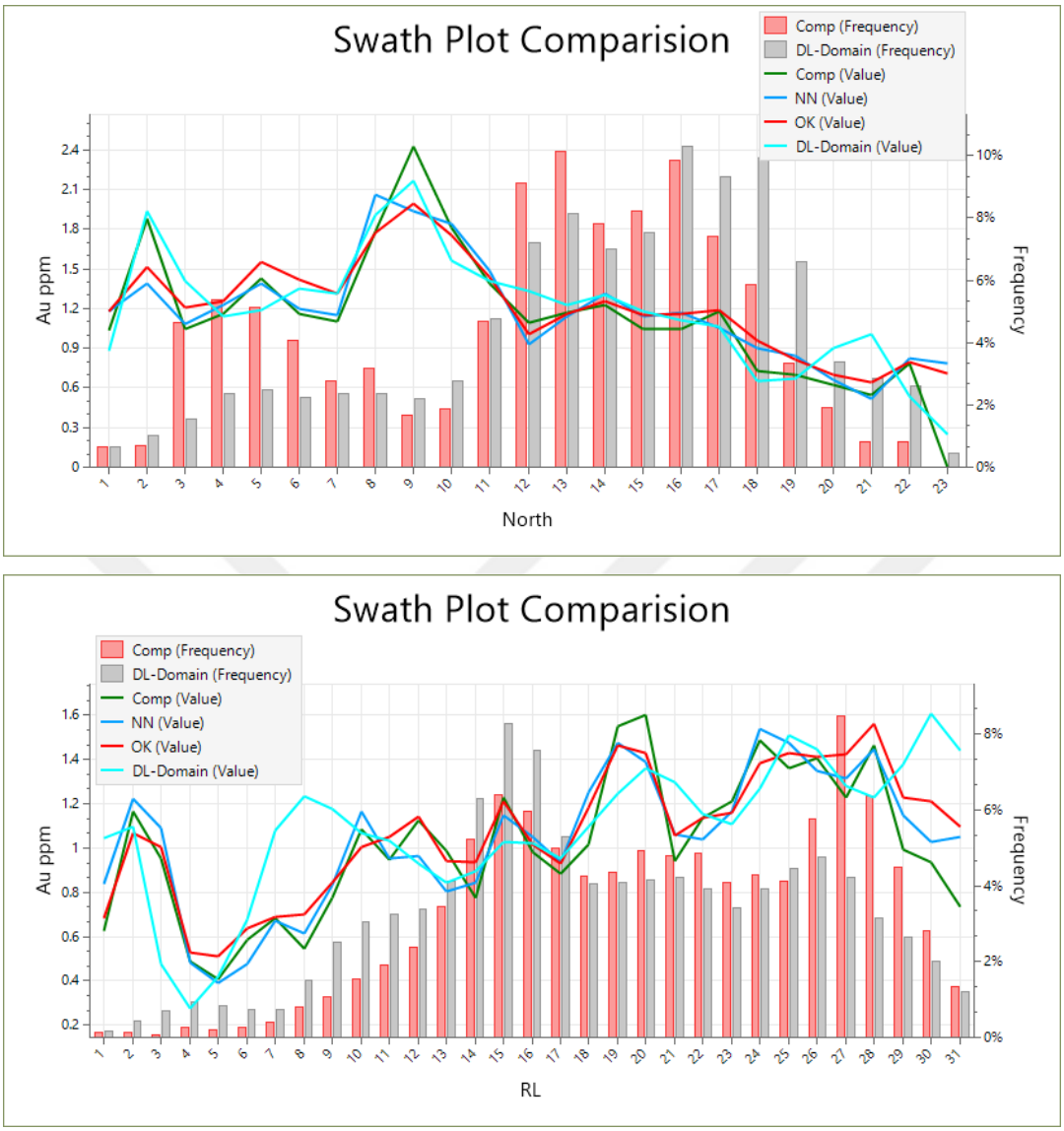
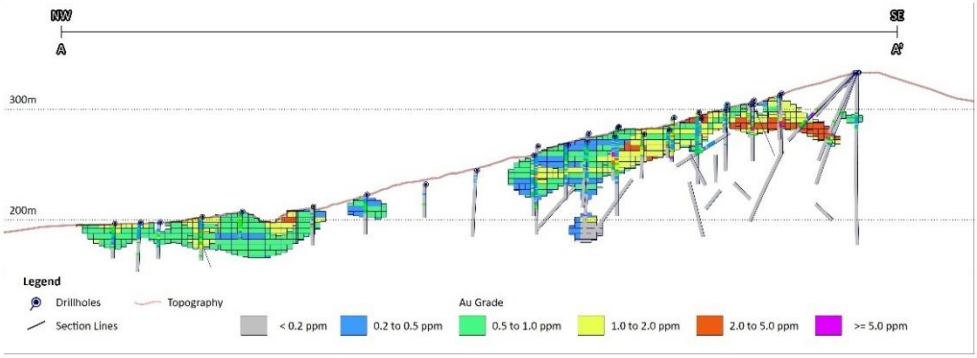


Figure 5.1 continued.



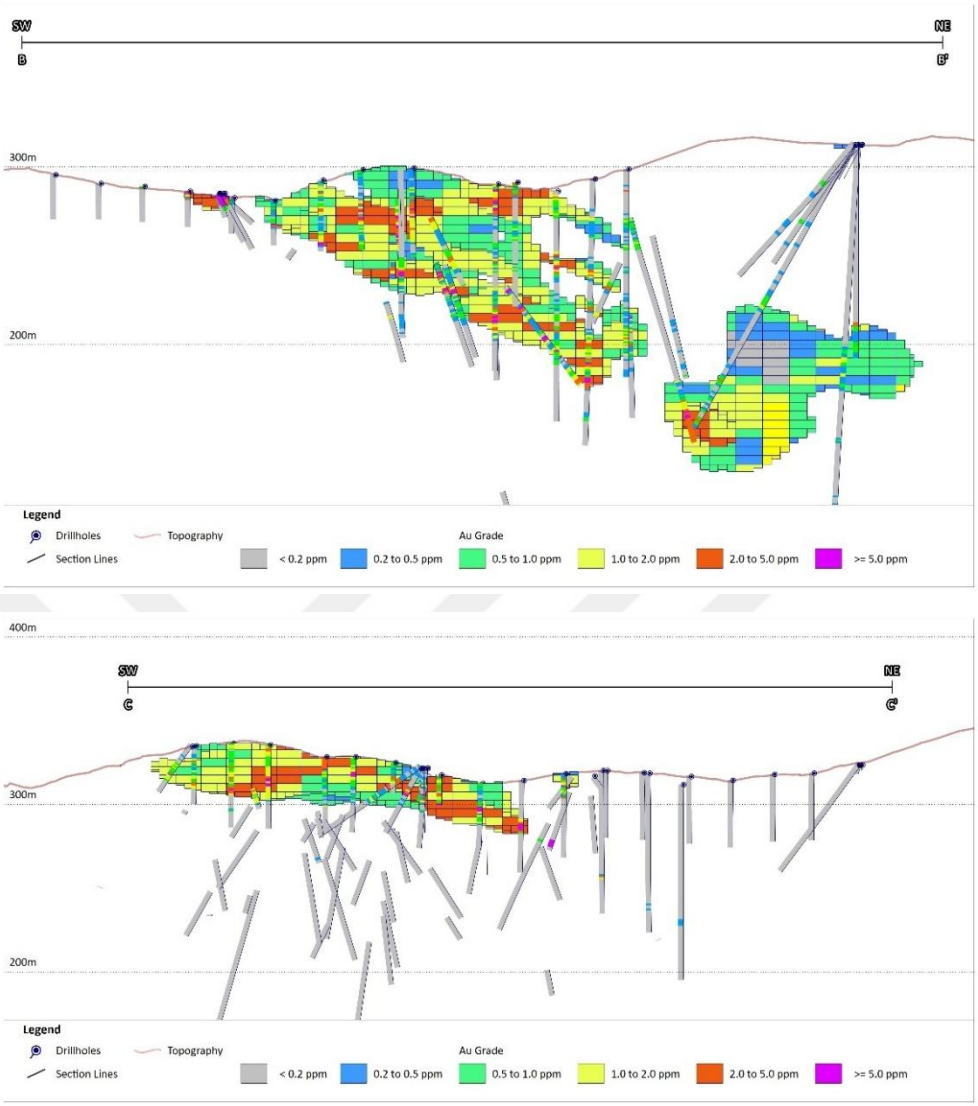


Figure 5.2 30m shaded sections for visual block model and raw assay grade comparison.

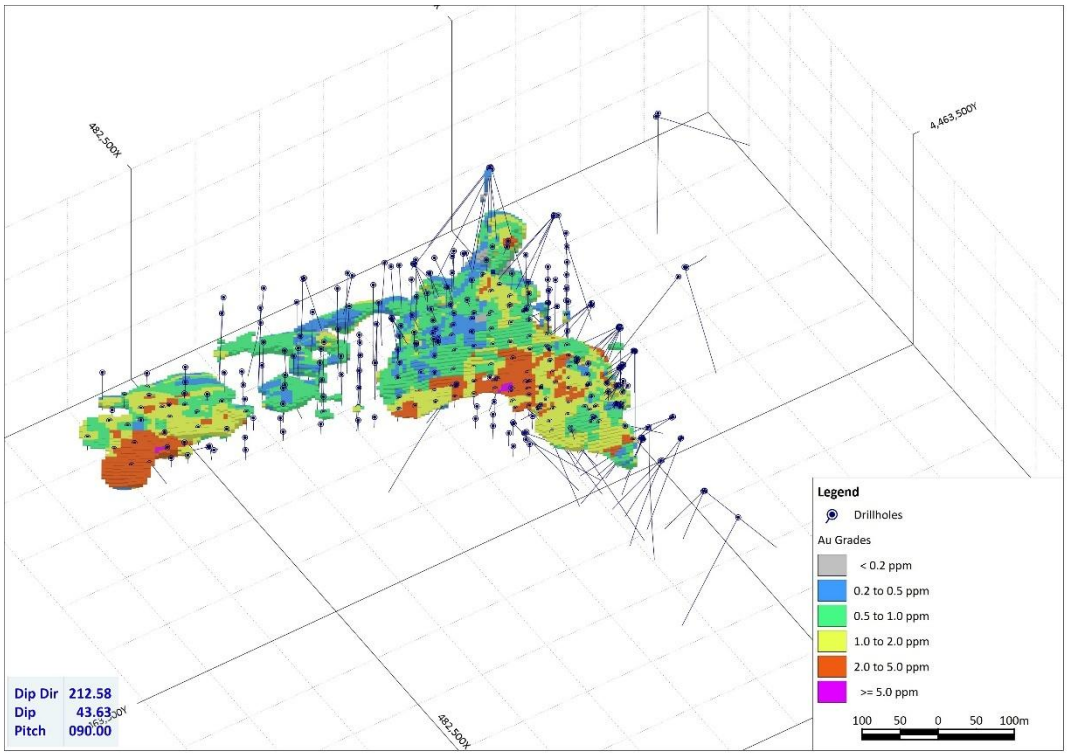


Figure 5.3 3D view of the estimated blocks by using geostatistical approaches.

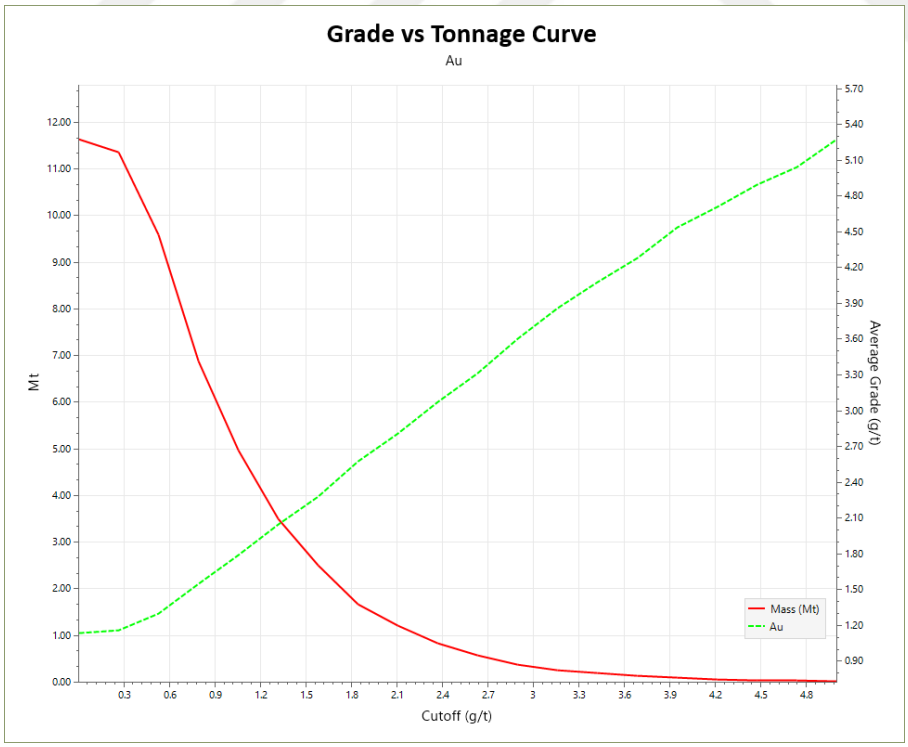


Figure 5.4 Grade vs tonnage curves for comparison to recognize small changes at cut-off grade.

5.2 Deep Learning Estimation Results

5.2.1 Raw Assay Data Application

The same cut-off grades (CoG) were used reporting block models to compare ordinary kriging estimation. Estimation reports of deep learning applications were given through raw and domain assigned data respectively Table 5.2 and Table 5.3.

Table 5.2 Raw Assay Data Application by Deep Learning

CoG (ppm)	Volume (Mm^3)	Tonnes (M)	Grade (ppm)	Au Content (Koz)
1.20	0.07	0.18	1.46	9
1.00	0.66	1.75	1.11	62
0.80	4.52	11.98	0.91	350
0.50	**19.38**	**51.36**	**0.70**	**1,160**
0.30	29.63	78.51	0.60	1,508
0.20	36.68	97.19	0.53	1,654
0.10	132.35	350.72	0.24	2,717
0.00	215.31	570.58	0.18	3,331

Notes:

1. No resource limitations were not applied like frame of license, social boundaries, etc.
2. Any metallurgical domains were not applied.
3. Resource classification was not applied according to national regulations like UMREK, JORC, NI 43-101.
4. Pit optimization was not conducted; all of the resource was assumed as minable with open-pit estimation respectively CoG.
5. This resource statement was conducted in research scope. There is no economic value of them.
6. The numbers were rounded.

In visual validation part for 3D view and sections, raw assay application cannot obey mineralization patterns. As a result, small local differences could be seen at cross sections which are caused by high regularization of data (between Figure 5.5 to 5.9). The summary of input and output BM statistics were given at Table 5.3 (selected final input and out were given as bold).

Table 5.3 Summary Statistic of Input and Output Data for Raw Assay Application

Data Description	Max	No of Points	Mean	Var.	SD	COV
1m Composite	590.0	32,853	0.45	19.17	4.38	9.69
1m Composite with fake points	590.0	48,732	0.31	12.97	3.60	11.78
2m Composite	**295.4**	**16,508**	**0.45**	**10.71**	**3.27**	**7.27**
Over fit BM	8.0	216,333	5.47	5.63	2.37	0.43
Optimal fit BM	**3.4**	**216,333**	**0.19**	**0.04**	**0.20**	**1.02**

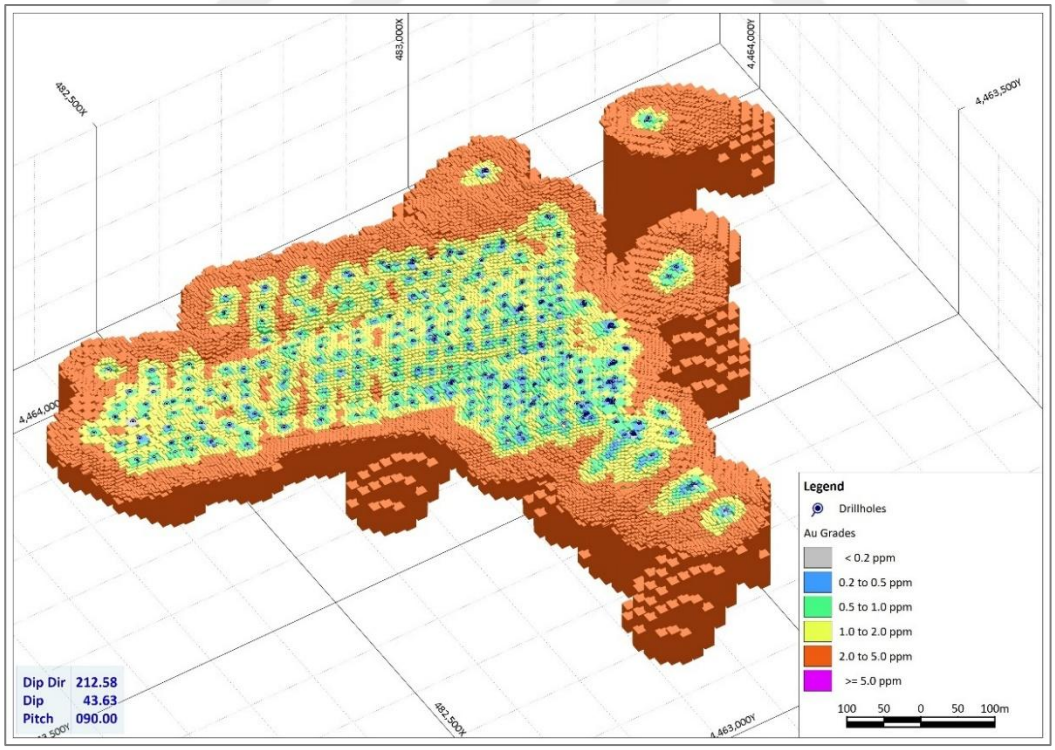


Figure 5.5 Overfit run of the 2m composited data by raw assay application.

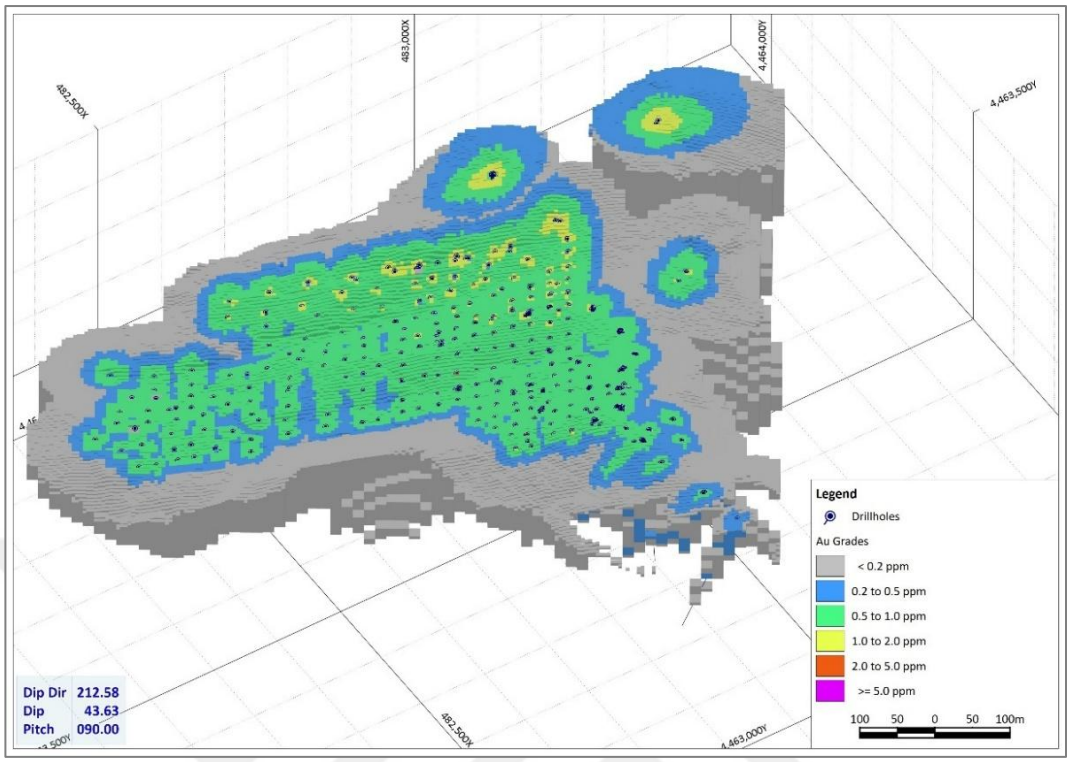


Figure 5.6 Optimal fit run of the 2m composited data by raw assay application.

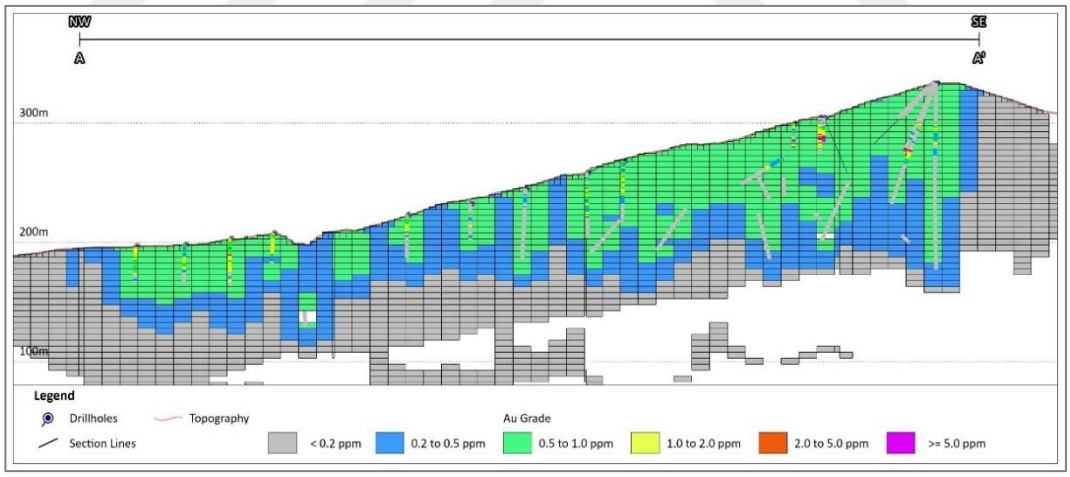


Figure 5.7 A-A' cross-section of raw assay Deep Learning results to compare raw assay data – optimal fit, raw assay application.

In grade vs tonnage curve, any elbow type structure cannot be seen. However, the sudden tonnage changes in between 0 to 2 ppm Au that addresses the sensitivity of the Au grade (Figure 5.10).

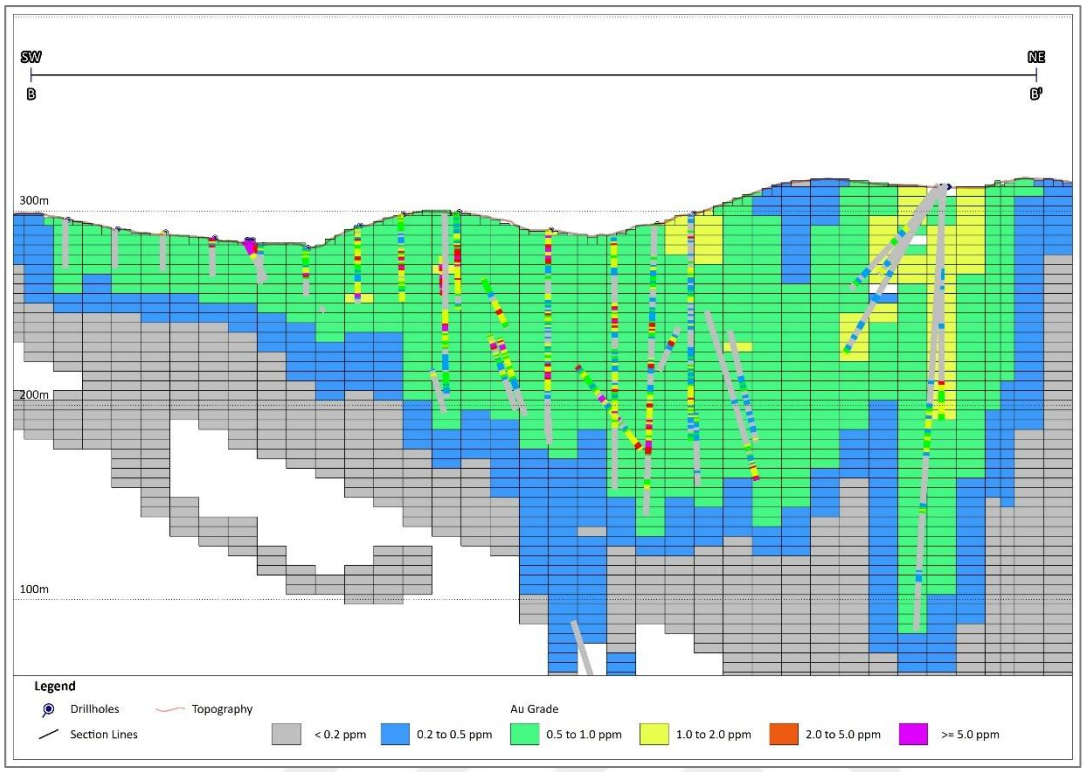


Figure 5.8 B-B' cross-section of raw assay Deep Learning results to compare raw assay data – optimal fit, raw assay application.

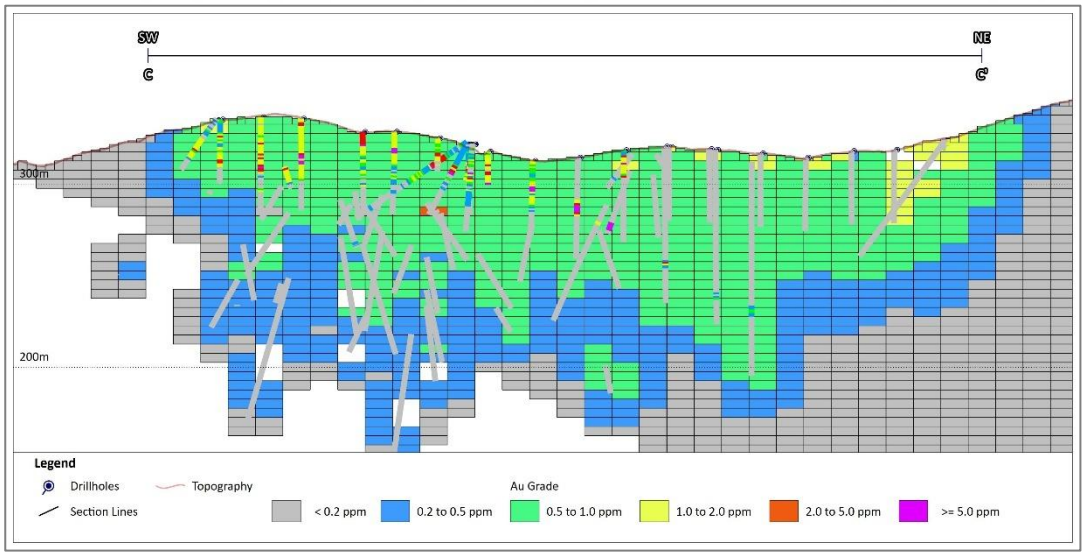


Figure 5.9 C-C' sections of raw assay Deep Learning results to compare raw assay data – optimal fit, raw assay application.

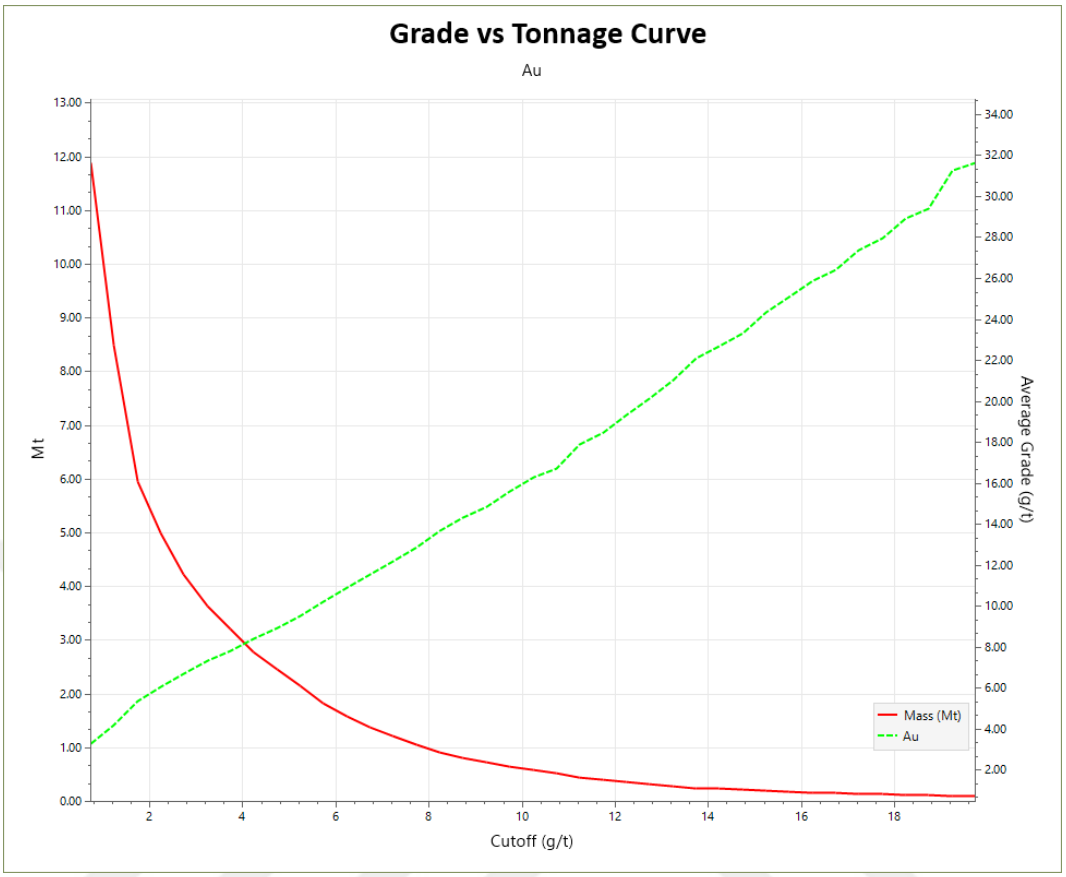


Figure 5.10 Grade vs tonnage curve of Deep Learning approach to comparison to recognize small changes at cut-off grade for raw assay application.

5.2.2 Domain Assigned Assay Application

The resource estimation was reported by using volume, density, and average gold grade in different CoG values as ppm. The resource statement of Sırakayalar mineralization is given Table 5.4 by using DL method.

Table 5.4 Domain Assigned Deep Learning Approach

CoG (ppm)	Volume (Mm^3)	Tonnes (M)	Grade (ppm)	Au Content (Koz)
1.20	1.81	4.81	1.91	297
1.00	2.31	6.11	1.74	343
0.80	2.81	7.45	1.59	382
0.50	**3.35**	**8.87**	**1.44**	**412**
0.30	3.52	9.33	1.39	418
0.20	3.58	9.48	1.38	419
0.10	3.63	9.61	1.36	420
0.00	4.48	11.88	1.10	420

Notes:

1. No resource limitations were not applied like frame of license, social boundaries, etc.
2. Any metallurgical domains were not applied.
3. Resource classification was not applied according to national regulations like UMREK, JORC, NI 43-101.
4. Pit optimization was not conducted; all of the resource was assumed as minable with open-pit estimation respectively CoG.
5. This resource statement was conducted in research scope. There is no economic value of them.
6. The numbers were rounded.

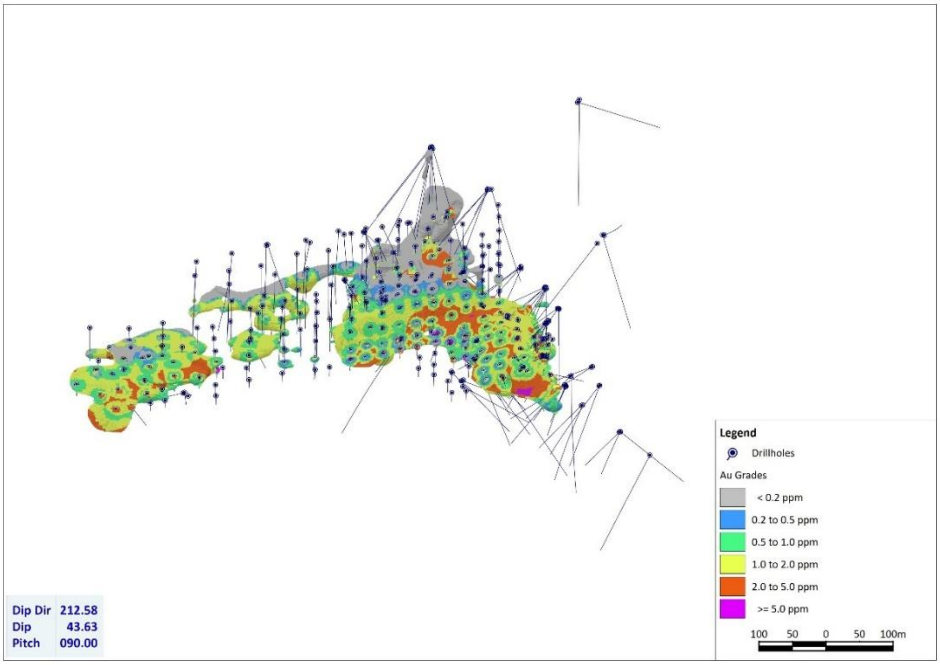


Figure 5.11 3D view of estimated BM for domain assigned DL method.

In the visual validation part, assay grades were amenable to estimated block values. In this part thickness of the sections approximately 15m. Some parts of assay grades were not suited to the estimated blocks significantly, which is caused by the mainly section thickness (between Figure 5.12 to 5.14).

Additionally, in 3D view spotted dog pattern could be seen. This pattern is commonly seen at distance of the informing samples respectively high, and it should be one of the diagnostic features of smaller block sizes (Figure 5.11).

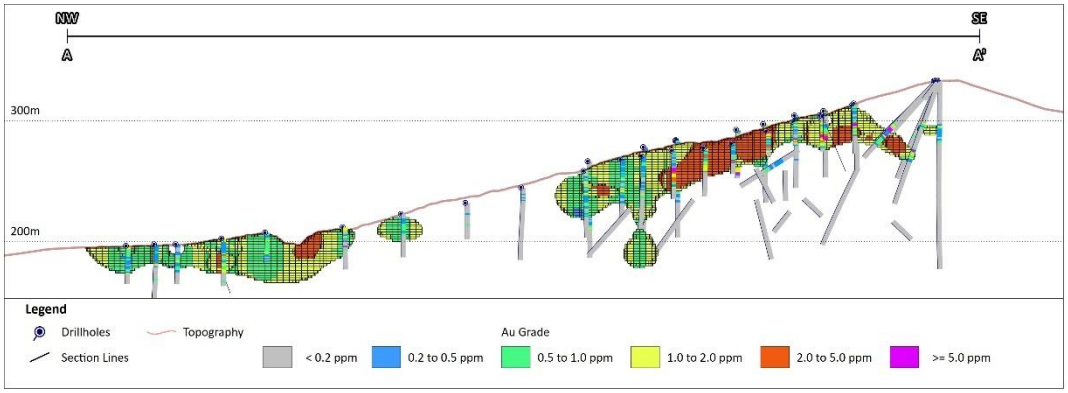


Figure 5.12 A-A' cross-section DL-Domain BM as HG and LG by using Deep Learning approaches.

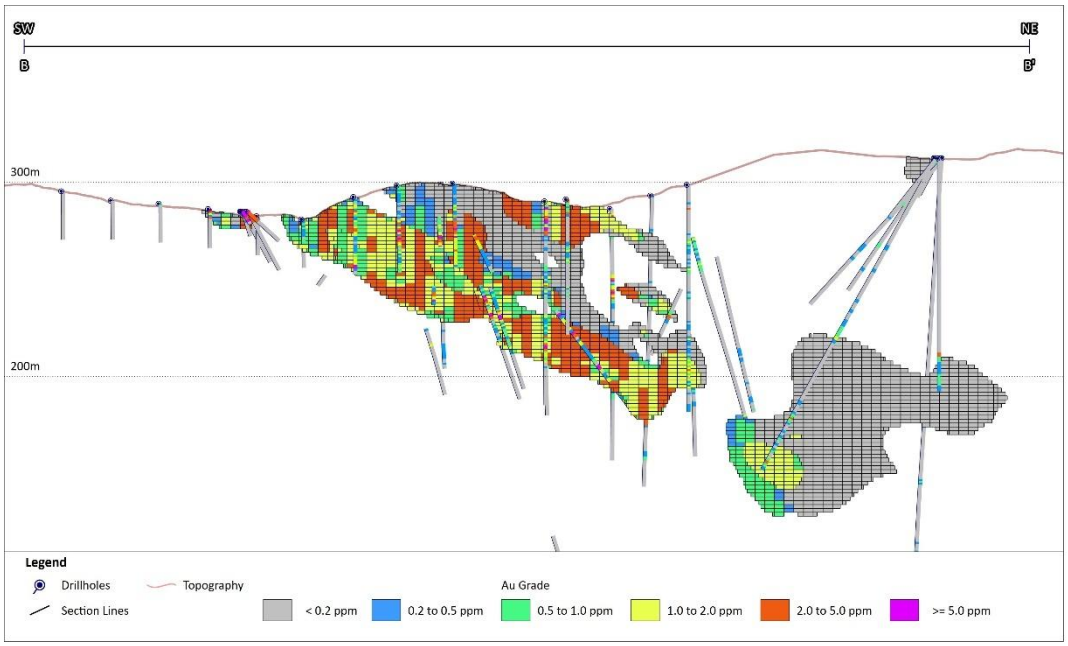


Figure 5.13 B-B' cross-section DL-Domain BM as HG and LG by using Deep Learning approaches.

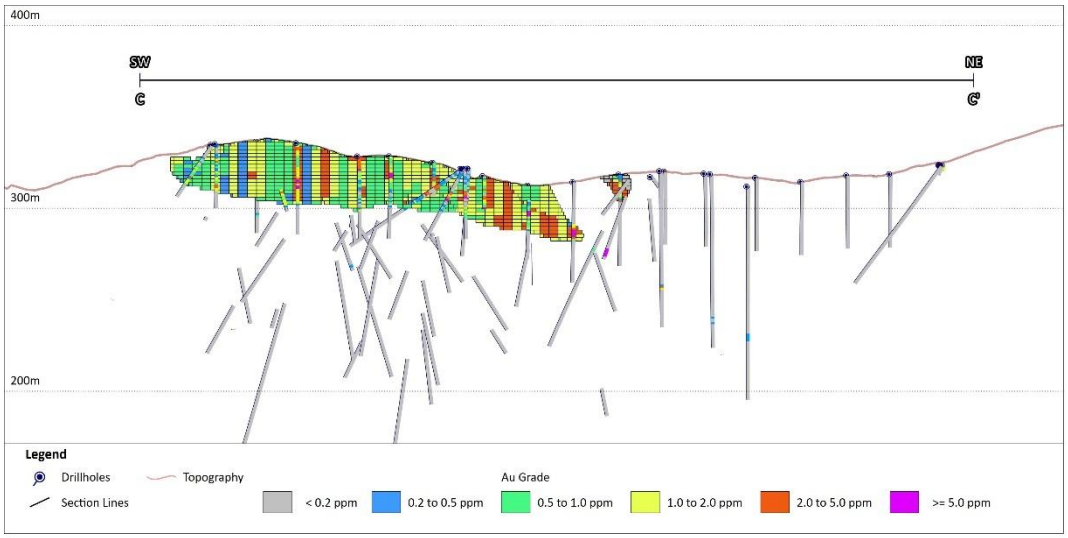


Figure 5.14 C-C' cross-section DL-Domain BM as HG and LG by using Deep Learning approaches.

In grade vs tonnage curve, any elbow type structure cannot be seen (Figure 5.15).

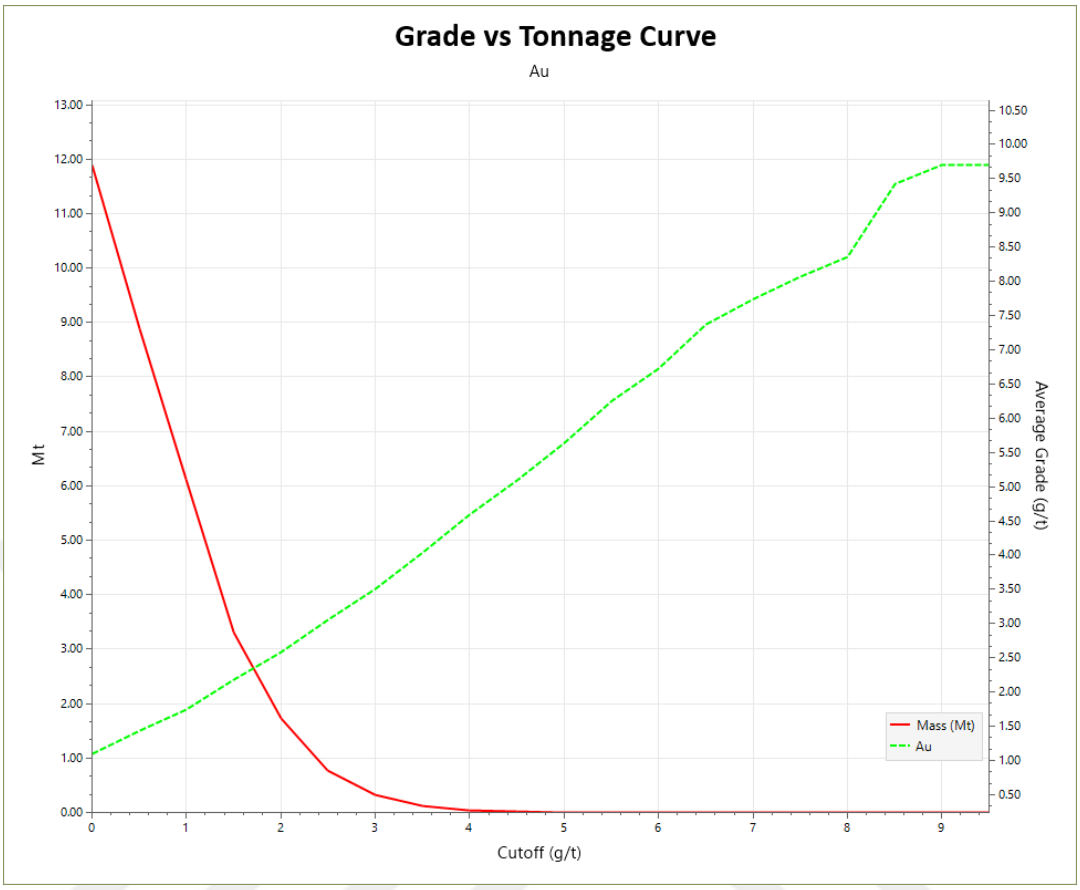


Figure 5.15 Grade vs tonnage curves of domain assigned Deep Learning approach to comparison to recognize small changes at cut-off grade.

The foreground and background block type visualization parts were conducted to comparison. Background blocks represents OK estimation while foreground scaled 0.5 (as size). These sections were given below at Figure 5.16 to 5.18.

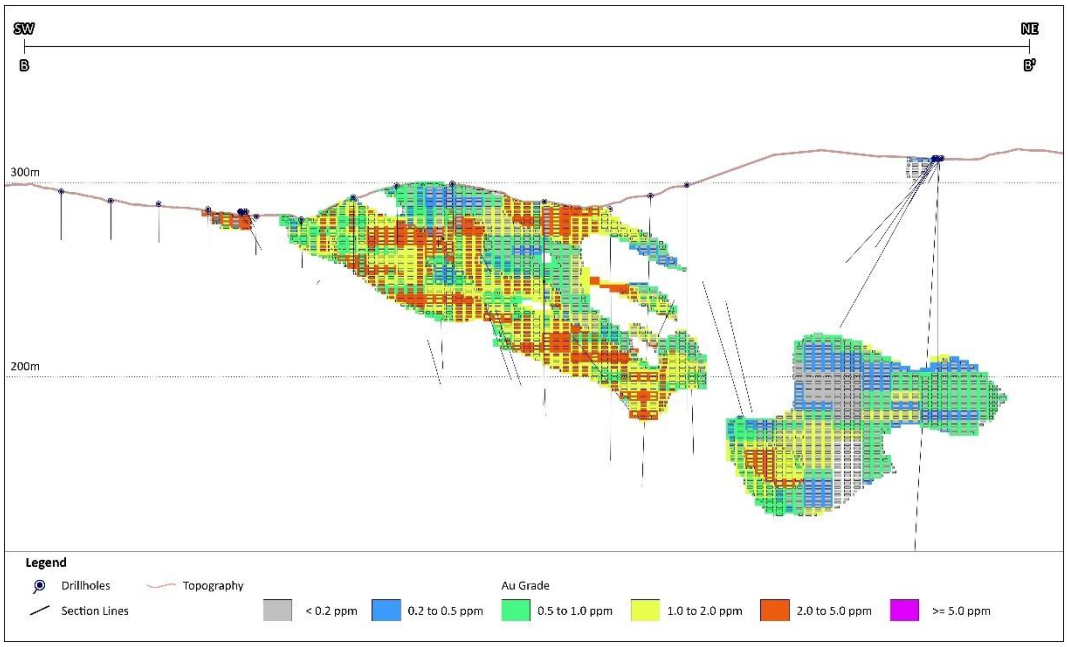


Figure 5.16 Block wise comparison of both methods, B-B' section. The background blocks represent OK, and foreground blocks represent DL.

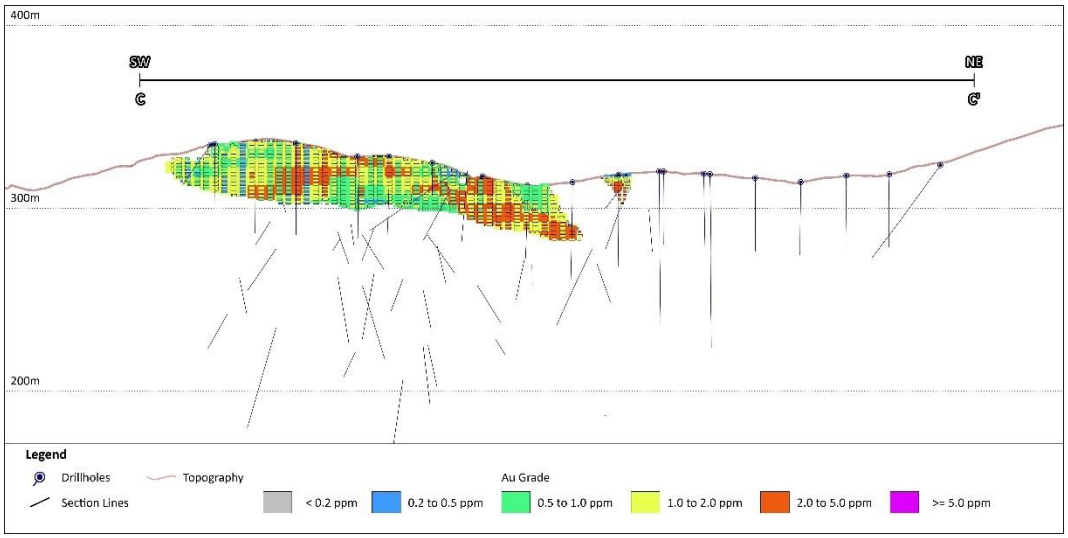


Figure 5.17 Block wise comparison of both methods, C-C' section. The background blocks represent OK, and foreground blocks represent DL.

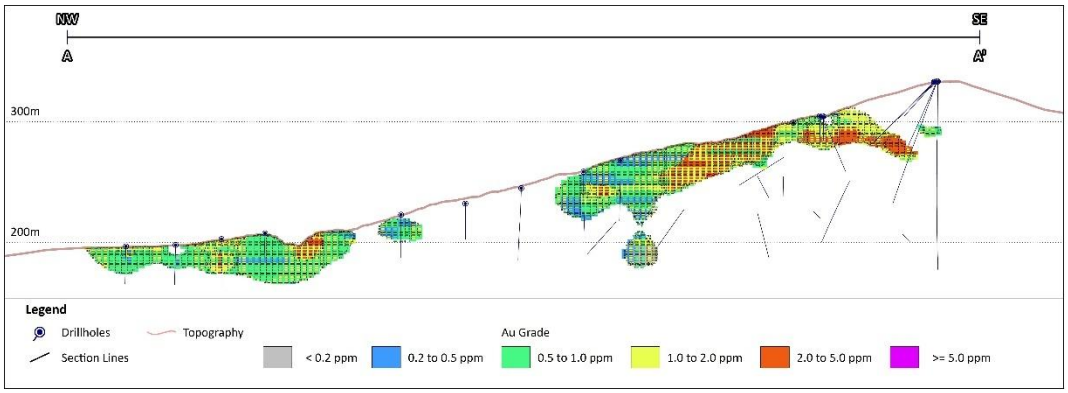


Figure 5.18 Block wise comparison of both methods, A-A' section. The background blocks represent OK, and foreground blocks represent DL.

In Figure 5.19 histogram graphs are shown to compare resulted block models. At the tail part of OK methods, smooth effect could be seen to compare DL-domain, and DL-domain has left skewness log-normal distribution which is not commonly seen at ppm scale estimations. Hence, the tail part of the estimations is below the CoG value. COV values of OK and DL-Domain are respectively 0.82 and 0.72 which are both lover than composite values (Table 4.3).

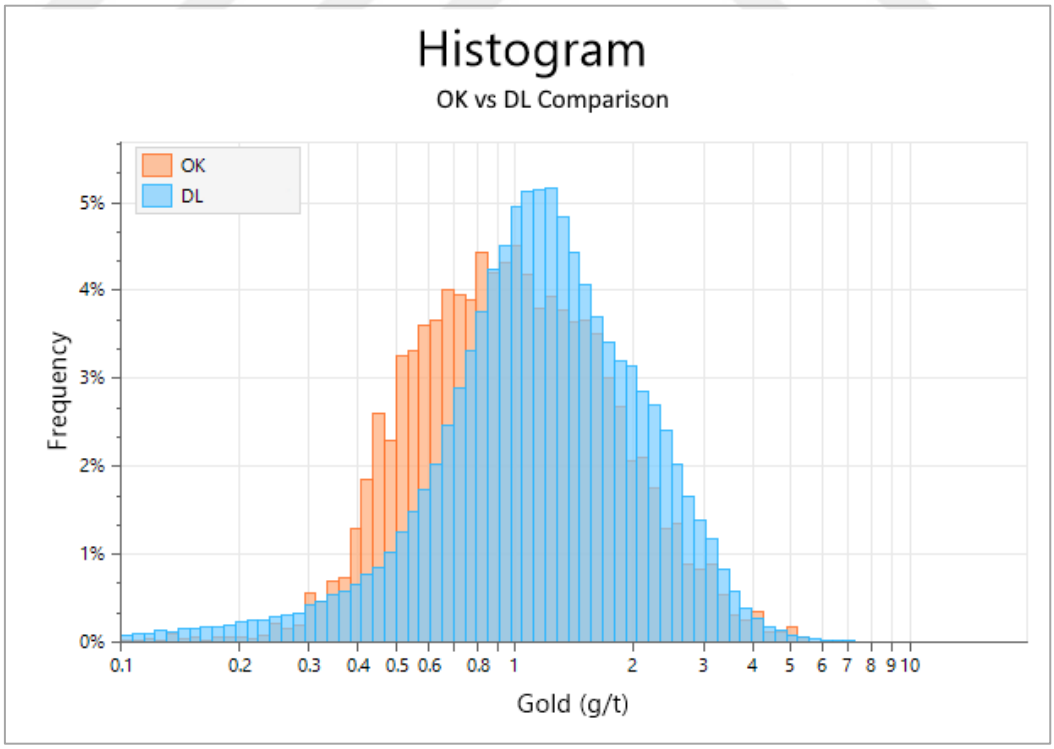


Figure 5.19 Histogram graphs of OK and DL-Domain applications' grades.

To compare the results, regularization of block models was applied by using main block size of the OK application. DL-domain, and OK estimated block were combined as singular BM. The block model factors (factor field represent the volume portion of the mineralization for single block) were written another field. End of the regularization part spotted dog pattern of the DL-domain method had disappeared. 3D view of the block model is given at Figure 5.20.

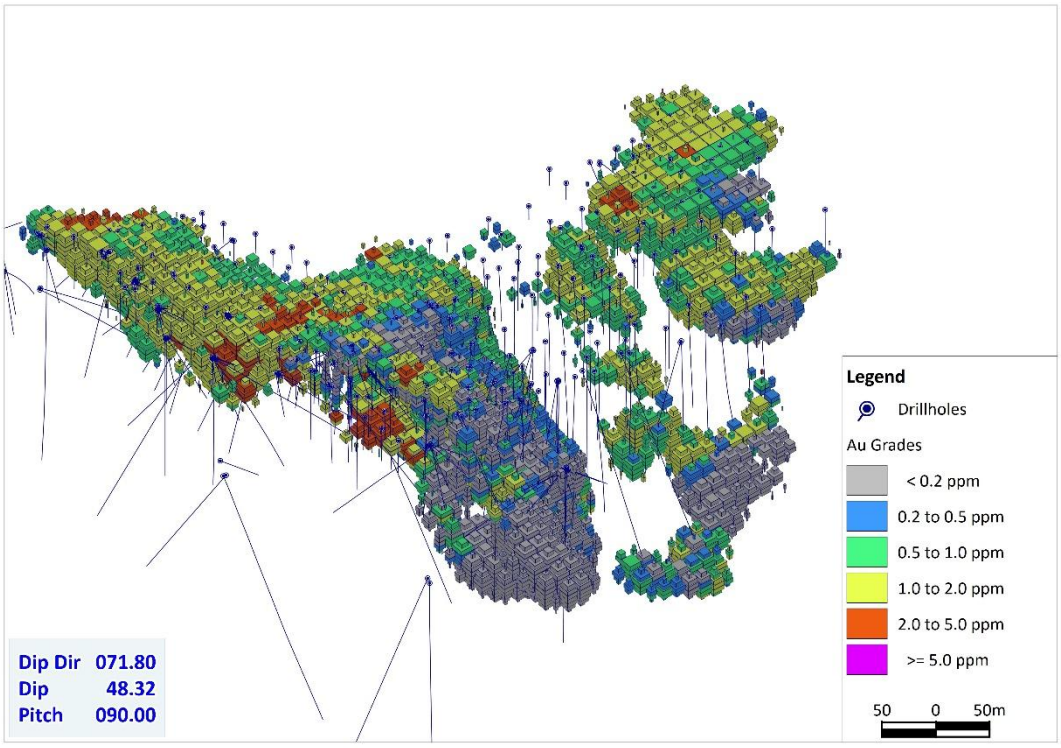
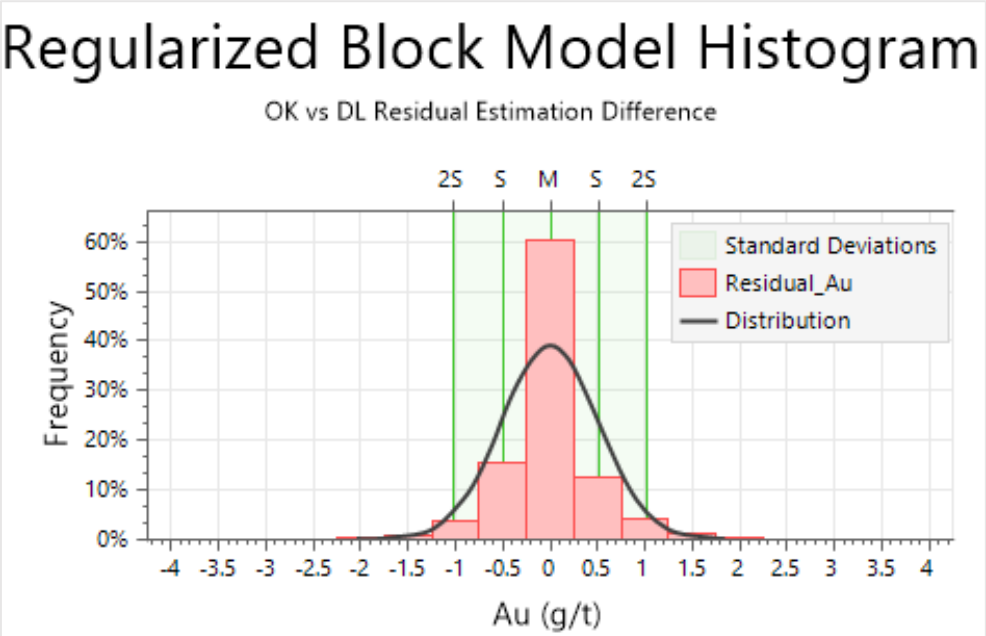


Figure 5.20 3D view of the regularized BM for DL-domain method. Factor fields applied to volume of the blocks and relatively smaller blocks represent smaller portion of mineralization. Original Z dimensions were preserved as location.

Using the regularized BM, a residual estimation analysis was performed by comparing histograms of the differences (obtained by subtraction of OK to DL-domain method and multiplying with the factor field). Results show that 60% of the differences lie within between -0.25 to 0.25 ppm, while 90% lie within -0.75 to 0.75 ppm. No skewness was observed in the histogram. The histogram and related statistical data are presented in Figure 5.21.

To compare the results of OK and DL-domain methods, cross-plot (scatter plot of each record) was performed. The estimated fields were multiplied by factor field, and to eliminate the barren parts 0.1 through 10 ppm were given in log-log plots. The most of the data were accumulated around 1 ppm part with slightly domination of the DL method with some noisy parts. The cross-plot graph is given at Figure 5.22.

The correlations between DL-Domain with OK Au results with and without filtering with 0.1 ppm Au are 0.67 and 0.72 respectively.



Residual_Au		Median	-0.003171
Minimum Value	-3.450522	Lognormal Mean	-1.75225
Maximum Value	4.112118	Lognormal Std Deviation	1.58169
N	7335	Geometric Mean	0.173383
Mean	0.007417	Geometric Std Dev	4.86316
Variance	0.26066	Sichel's Estimator	0.605118
Standard Deviation	0.510548	Sichel's V	2.50089
Coeff. of Variation	68.8355	Sichel's Gamma	3.49006

Figure 5.21 Residual analysis to compare the results of OK and DL-domain methods.

To identify the contrasting areas between the estimated models, residual Au grade differences were conducted. The areas of highest agreement were generally located

in the central portions of the models, where multiple drillholes provided stronger support. In contrast, within sparsely drilled areas and extrapolation zones, the differences between model estimates increased (Figure 5.23).

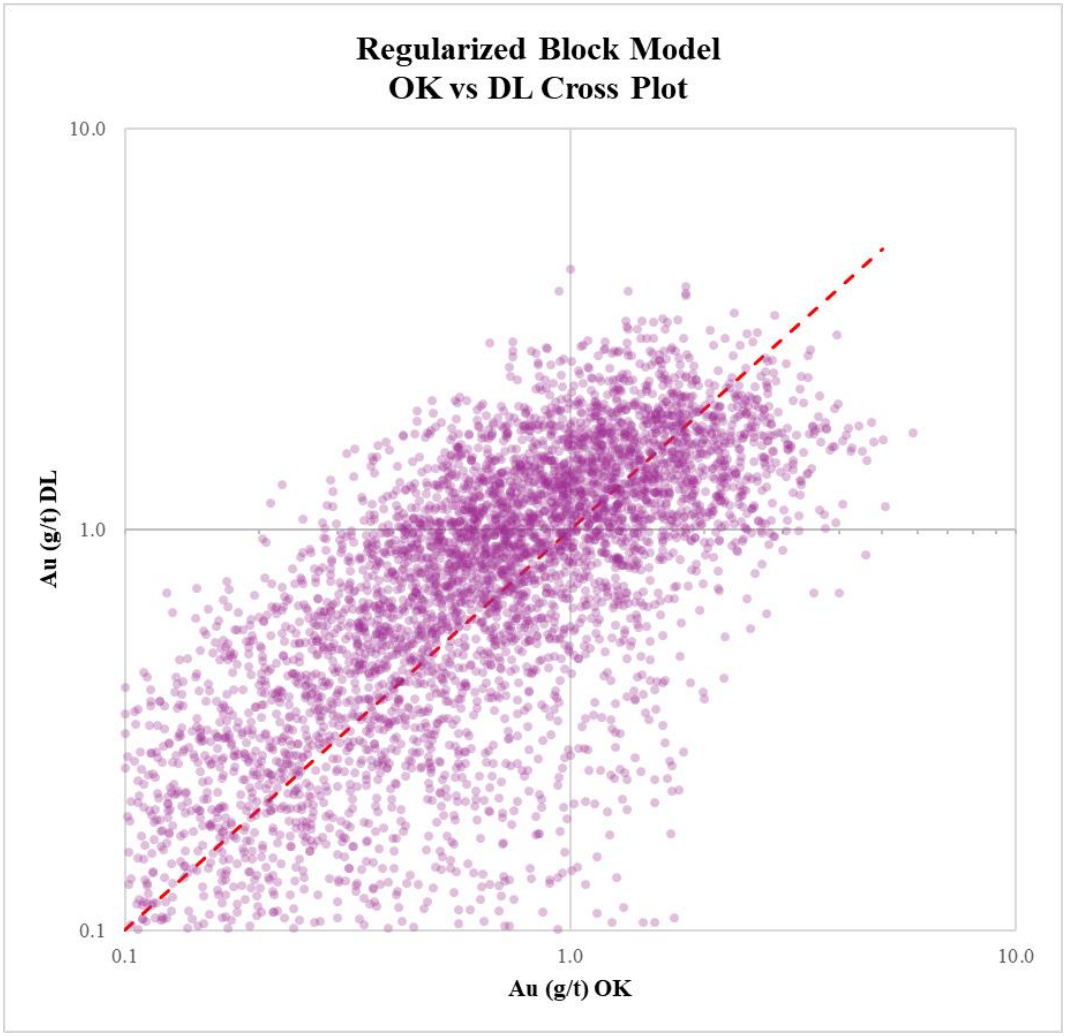


Figure 5.22 Cross plot of OK and DL-domain methods. Red dash line represents 1:1. R^2 value is 0.74 with intersection to zero.

The 3D view of the residual Au-ppm is shown at Figure 5.23. The results indicate that the OK estimation was more dominant in the northwest and southeast portion of the model, whereas the DL-domain estimation dominates along the model edges (edges of both LG and HG), where contrasts were more pronounced. This difference could be explained by usage of smaller block models and sub-blocks for DL method. DL blocks suit the mineralization domain better than OK estimation.

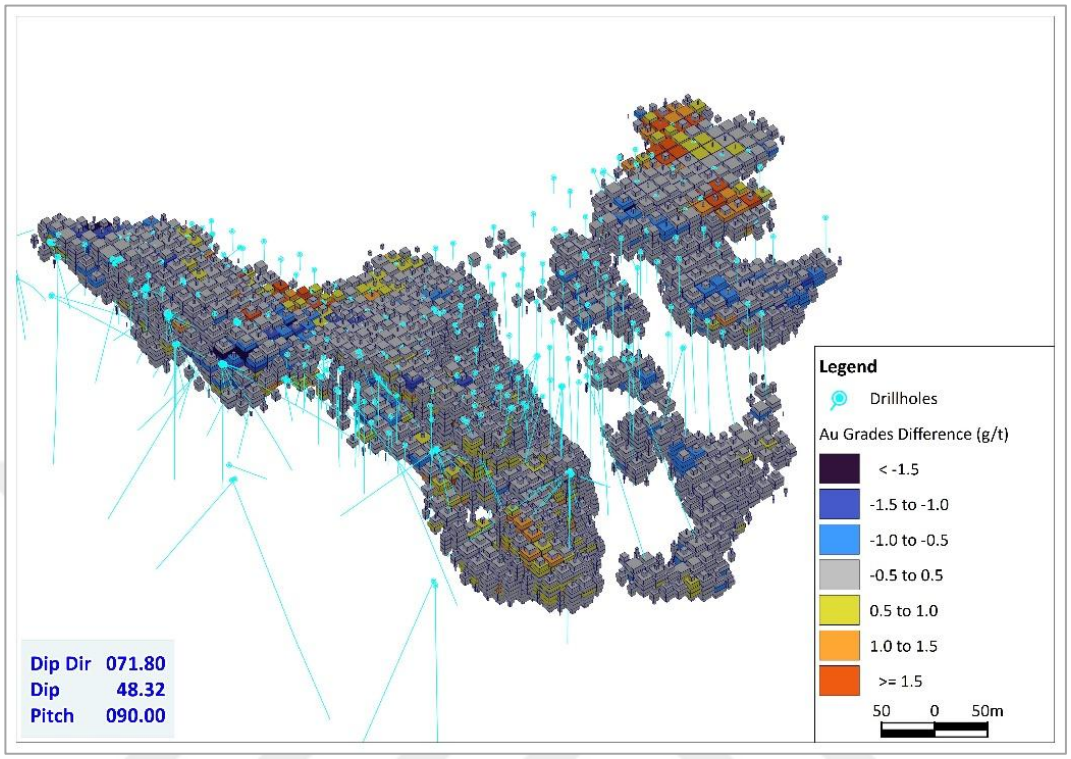


Figure 5.23 3D view of the Au difference in ppm, obtained by OK results subtracted with DL-domain results (block factor applied). The positive and negative values represent respectively domination of OK and DL estimation as grade.

CHAPTER 6

DISCUSSION

6.1 Strengths and Weaknesses of Each Method

Ordinary kriging method is widely accepted and a robust geostatistical method for resource estimation for industrial and scientific purposes. The main strength depends on ability to incorporate spatial correlation structures explicitly via variograms. This makes OK particularly reliable in well-sampled areas with relatively stationary geological features. However, some deficiencies were seen in regions with complex geometries or heteroscedasticity in grade distribution, and it requires extensive variogram modeling, which can be subjective and time consuming.

In contrast, Deep Learning methods, especially neural networks, trained on geological and spatial features, and it offers superior flexibility in modeling non-linear relationships and capturing complex spatial patterns. However, DL estimations depend on model function. External modifications could be needed in different deposits such as defining limitations and extrapolation zones.

Deep learning methods can learn complex patterns from high dimensional datasets (except cases like curse of dimensionality) without using auto-correlation functions like variogram modelling. Moreover, they generally require large amounts of well pre-processed data, and they are untraceable.

6.2 Interpretability vs. Predictive Power

There are trade-offs between interpretability and predictive power. Ordinary kriging is highly interpretable by using followings: creating auto-correlation function due to spatial continuity, kriging variance, kriging efficiency. That means all steps of the applications were almost traceable. In contrast, deep learning methods have higher

prediction accuracy at heterogenous zones (by comparison of visual validation). Unless deep learning methods are untraceable to compare Ordinary Kriging.

6.3 Applicability to Sparse or Noisy Datasets

Sparse and noisy datasets represent a significant challenge in resource estimation. Ordinary Kriging is generally more robust to sparsity, provided the variogram can still be reasonably fitted. However, its assumption of stationarity becomes problematic in sparse datasets where geological trends cannot be adequately captured.

Deep learning methods struggle more with sparse data unless augmented with synthetic data, transfer learning, or data imputation techniques. Nevertheless, DL showed promising results when applied to noisy datasets, where its ability to extract latent features helped reduce the influence of local outliers.

6.4 Literature Comparison of the Study

Three key findings from literature comparing ML-based and OK geostatistical methods are summarized below:

1) Systematic literature review (1990–2019): Summarizes prior studies and shows that ML methods (e.g., ANN, SVR, Random Forest-RF) outperformed OK in many cases, though performance strongly depends on the application context and dataset size (Mahboob et al., 2022).
2) Comparison of modern tree-based methods (XGBoost) with OK: Reports that the results indicate that XGBoost produced more wide-ranged grade estimates, which is a desirable outcome in ore grade prediction. However, the minimum and maximum values of the XGBoost estimates were lower and higher, respectively, than those obtained with kriging. Similar to kriging, the estimation results were smoother than the composite grades, yet the variance of the XGBoost estimates was lower than that of the composites. This

suggests that although XGBoost reduces the smoothing effect to some extent, its estimation results are still influenced by a smoothing effect comparable to that of kriging. (Atalay, 2024).

3) Strengths and limitations of ML vs. geostatistics: ML methods were noted to be strong in incorporating geological parameters and capturing complex nonlinear relationships, whereas geostatistics retains advantages in uncertainty quantification and maintaining spatial consistency (Dumarkor-Dupey & Arya, 2021).

In comparison of ML based algorithms with geostatistics-OK shows that ML algorithms outperformed the non-ML methods. However, the comparison should be carried out with real-case production, statistically, geologically (in different deposit types and models, etc.), geostatistically different datasets. In this study, DL method suits slightly better than OK method composite data well supported locations at 3D space (after the regularization process).

6.5 Lessons Learned and Methodological Reflections

Several methodological insights emerged during the study:

- Data processing is crucial for both methods but especially for deep learning methods such as handling missing values, log-normalized distributions which affected model performance. Even if the same parameters and same portion of the data sets were used for training for raw assay DL application, results are variable. Hence, re-producibility and stationarity are not satisfied.
- Including knowledge of mineralized domains (domain assay data) was found to enhance both ordinary kriging and deep learning applications. In DL applications, the spatial distribution is learned with data by splitting into test and train data. At the end, all of the data are used for the estimation. However, quality of the estimation depends on the selected data which is directly related to frequency of grade distribution. Increasing the number of the domains

enclosed by each other like grade-shells, could increase the estimation quality. Hence, limitation and restriction were essential to modelling.

- Model validation parts were essential to check fitting processes like median-mod collapse of underfits, using different shuffling (repeatability with different random seeds) of data and statistical checks of overfitting. Optimal fits increase robustness of the models.
- Raw assay applications of DL should be clue for the exploration potential rather than robust resource estimation.
- Increasing the number of neurons in a deep learning model may lead to piecewise or cycling (oscillatory) effects. Depending on the acceptable error range of the estimation, this can potentially improve prediction quality. However, this phenomenon should be examined carefully within its specific context.
- Sensitivity of the estimation through elevation dimension by using DL application does not suit well to compare X and Y (even if the swath plots at RL dimension in agreement well). Sampling configuration of elevation dimension is denser than X and Y. The reason is that denser sampling configuration with higher variance parts needs to be regularized more in shorter distances. However, the downhole variance of the samples' grade shows similar behaviors. This phenomenon should be checked with another dataset which shows sequential veins with internal waste and separated as different domains. Secondly, modification of the 3D distribution of data as cubic distribution could be helpful to solve by stabilizing the axes ranges.
- DL applications estimate point-based, and to decrease of this effect smaller block sizes used instead of using virtual block wise estimation (discretization). However, this method still has some deficiencies. In visual validation, high local variance of the blocks could be seen to compare assay results. If this application inserted weight function of DL, the efficiency and robustness of the estimation should be increased. Even if the local variance was decreased and suits better to composite data at the end of regularization part, further studies should be carried out for discretization parts.

- In real life comparisons could be available only, after the mining & reconciliation part. These methods cover long-term resource estimation and generally do not represent short-term mining schedules. After the huge amount of production, reconciliation part could be carried out.

The DL-Domain application results are promising as an alternative for geostatistical applications. As mentioned before, there is no clear evidence that which one is better suits the dataset. Even if there are local differences, OK and DL-Domain applications shows similar trends, global average grade and tonnage.

The comparative analysis also highlighted the importance of hybrid approaches, where deep learning is used to guide or complement traditional geostatistics rather than replace them outright.

CHAPTER 7

CONCLUSIN AND RECOMMENDATIONS

7.1 Summary of Findings

There is a trade-off between usage of both methods. Both methods need to pre-process data preparation. Raw assay data application by using deep learning methods should be clue for the exploration potential rather than proper estimation. During the fitting process, all validation parts like statistical, visual and loss functions should be crucial to eliminating under or overfit. OK and DL applications show similar results in terms of average grade and metal content. The DL-Domain result seems to be promising but DL methods could be risky for the industrial applications which means that hybrid models could be beneficial to increase robustness of the models.

7.2 Contribution to Knowledge

Mineral resource estimation using ordinary kriging and deep learning approaches were applied and results were compared by advantages, limitations and suitable cases were mentioned for mineral resource estimation.

DL applications are conducted both raw assay data and domain data. Hence, pre-processing is interpreted as essential for both methods.

Increasing number of enclosed domains could increase the robustness and quality of the DL-Domain results where each part of the domain-data become more stable.

The challenging part of the study could be defined as short-range auto-correlation at Sırakayalar Au mineralization. Deep learning applications have features like feed-forward and backpropagation. The usage of both techniques on short-range auto-correlated dataset is unique for the grade estimation comparison with OK for this

study. However, there is no clear evidence that shows the DL outperforming the OK method neither vice-versa, except well supported (with drillholes) block results by using visual validation (regularized blocks). Even if regularized block models could be solution for discretization, deficiency of the study could be summarized as discretization part of DL application.

7.3 Recommendations for Future Work

Implementation of block wise estimation directly into weight function is the major gap of DL applications. Deep learning algorithms could handle also polar coordinate systems. Future work could be covering comparison of polar coordinate system based deep learning comparisons. This application has several steps like:

- Defining the mineralized 3D hot spots in different grades,
- Creating network system towards each of the centers,
- Fitting the center of biggest mineralized zone like volume multiplication with average grade,
- Finding relationships between using $r * CosA * CosB$ each of the central relationships and usage of r, CosA and CosB as weights. The rest of the estimation should be halos of the hot spots.

REFERENCES

Addison Mining Services (2019). Resource Estimation of Sırakayalar Mineralization - National instrument NI 43-101 technical report – Internal company report.

Afeni, T. B., Lawal, A. I., & Adeyemi, R. A. (2020). Re-examination of Itakpe iron ore deposit for reserve estimation using geostatistics and artificial neural network techniques. Arabian Journal of Geosciences, 13, 657. https://doi.org/10.1007/s12517-020-05644-9.

Akıska, S., Sayılı, İ.S. and Demirela, G., (2013). Geology, mineralogy and the Pb, S isotope study of the Kalkım Pb-Zn ± Cu deposits, Biga Peninsula, NW Turkey. Journal of Geosciences, 58(4), 379-396.

Almonty Industries Inc. (2025). Company profile. Retrieved from https://almonty.com/ Anatolia, Turkey. Journal of Geology, 115(1), 63–82.

Aluç, A., (2023). Magmatic-hydrothermal evolution and geological framework of the Kirazli epithermal Au and porphyry Cu deposits, Biga Peninsula, Turkey.Muğla Sıtkı Koçman Üniversitesi, Fen Bilimleri Enstitüsü, PhD Thesis, 160p.

Aluç, A., Kuşcu, Į., Ulyanov, A., Selby, D., Antoine, C., Spikings, R. A., & Moritz, R. (2024). Protracted metallogenic and magmatic evolution of the Kirazlı epithermal Au-Ag and porphyry Cu deposits, Biga Peninsula, NW Turkey: Evidence from zircon U–Pb, muscovite $^{140}Ar/^{39}Ar$, and molybdenite Re–Os geochronology. Mineralium Deposita, 59(5), 885–905.

Altunkaynak, Ş. & Genç, Ş.C. (2008). Petrogenesis and time-progressive evolution of the Cenozoic continental volcanism in the Biga Peninsula, NW Anatolia (Turkey). Lithos, 102, 316–340.

Arribas, A., Jr., Hedenquist, J. W., Itaya, T., Okada, T., Concepción, R. A., & García, J. S., Jr. (1995). Contemporaneous formation of adjacent porphyry and epithermal Cu–Au deposits over 300 ka in northern Luzon, Philippines. Geology, 23(4), 337–340. https://doi.org/10.1130/0091-7613(1995)023<0337:CFOAPA>2.3.CO;2.

Aslaner, M. (1965). Etude geologique et petrographique de la region d' Edremit-Havran (Turquie). MTA Bulletin, 119.

Atalay, F. (2024). Estimation of Fe Grade at an Ore Deposit Using Extreme Gradient Boosting Trees (XGBoost). Mining, Metallurgy & Exploration, 41(4), 2119-2128. https://doi.org/10.1007/s42461-024-01010-5.

Aydın, M., Demir, O., Özçelik, Y., Terzioğlu, N. & Satır, M. (1995). A geological revision of İnebolu, Devrekani, Ağlı and Küre areas: new observations in Paleo Tethys - Neo-Tethys sedimentary successions. In: Erler, A., Ercan, T., Bingöl, E., Örçen, S. (Eds.), Geology of the Black Sea Region. MTA Bulletin Special Publication, 33–38.

Aydın,Ü., Şen,P., Özmen, Ö. and Şen, E. (2019). Petrological and geochemical features of Biga Peninsula granitoids, NW Anatolia, Turkey. Bull. of the Mineral Research and Exploration, 160, 81-115.

Bergen, K. J., Johnson, P. A., de Hoop, M. V., & Beroza, G. C. (2019). Machine learning for data-driven discovery in solid Earth geoscience. Science, 363(6433), eaau0323.

Bilgin, İ. (1999). Ezine (Canakkale) Ofiyolit ve Metamorfitlerinin Petrolojisi. Institute of Natural and Applied Sciences, İstanbul University, İstanbul, PhD Thesis, 152 (in Turkish).

Bingöl, E., Akyürek, B., & Korkmazer, B. 1973. Biga Yarımadası'nın Jeolojisi ve Karakaya Formasyonu'nun bazı özellikleri, MTA 50. Anniversary, Proceedings, 71-77 (in Turkish).

Bingöl, E. 1974. Discussions on the metamorphic map of Turkey in a scale of 1:2,500,000 and geotectonic evolution of some metamorphic belts. MTA Bulletin, 83, 119–131.

Breiman, L., Friedman, J. H., Olshen, R. A., & Stone, C. J. (1984). Classification and Regression Trees. Belmont, CA: Wadsworth International Group.

Broomhead, D. S., & Lowe, D. (1988). Multivariable functional interpolation and adaptive networks. Complex Systems, 2(3), 321–355.

Canadian Institute of Mining, Metallurgy and Petroleum. (2019). CIM Estimation of Mineral Resources & Mineral Reserves Best Practice Guidelines. Prepared by the CIM Mineral Resource & Mineral Reserve Committee; Adopted November 29, 2019.

Canadian Securities Administrators. (2001). National Instrument 43-101 – Standards of Disclosure for Mineral Projects (SOR/2001-204). Effective February 1, 2001.

Clark, J. N., Holwell, D. A., Siddle, R. J., & Keser, M. (2014). (rep.). Geochemical and mineralogical characteristics of the Şahinli epithermal Au-Ag deposits, Western Turkey (pp. 1–50).

Clough, R. W. (1960). The finite element method in plane stress analysis. In Proceedings of the 2nd ASCE Conference on Electronic Computation (pp. 345–378).

Cortes, C. and Vapnik, V. (1995). Support vector networks. Machine Learning,20,273–297.

Delaloye, M. & Bingöl, E. (2000). Granitoids from western and northwestern Anatolia: geochemistry and modeling of geodynamic evolution. International Geology Reviews, 42, 241-268.

Demirela, G., Akıska, S., Sayılı, İ. S., & Kuşcu, İ. (2014). Geology and the alteration features of the Çataltepe (Lapseki–Çanakkale) Pb–Zn±Cu±Ag deposit. Yerbilimleri/Hacettepe Üniversitesi Yerbilimleri Uygulama ve Araştırma Merkezi Dergisi, 35(2), 109–136. https://doi.org/10.1501/yerbil_0000000067

Dilekler, G. (2022). Mineralization, textural and alteration characteristics of the Şahinli (Sırakayalar and Karatepe) low-sulfidation epithermal deposit (Lapseki, NW Turkey- M.Sc. thesis). Middle East Technical University-Master Thesis, Ankara.

Dönmez, M., Akçay, A. E., Genç, Ş., & Acar, Ş. (2005). Biga yarımadasında Orta Üst Eosen volkanizması ve denizel ignimbiritler. Maden Tetkik ve Arama Dergisi, (131), 49-61.

Dumakor-Dupey, N.K. ve Arya, S. (2021). Machine Learning—A Review of Applications in Mineral Resource Estimation. Energies 2021, 14(14), 4079; https://doi.org/10.3390/en14144079.

Edwards, A. C. (Ed.). (2001). Mineral Resource and Ore Reserve Estimation (AusIMM Monograph 23). The Australasian Institute of Mining and Metallurgy. Retrieved from https://www.geokniga.org/bookfiles/geokniga-mineralresourceandorereserveestimation.pdf.

Fischer, H. (2011). A History of the Central Limit Theorem. Springer Science+Business Media. doi:10.1007/978-0-387-87857-7. Retrieved from https://www.medicine.mcgill.ca/epidemiology/hanley/bios601/GaussianModel/HistoryCentralLimitTheorem.pdf.

Fix, E., & Hodges, J. L. Jr. (1958). Discriminatory analysis: Nonparametric discrimination—consistency properties (Tech. Rep. No. 4). USAF School of Aviation Medicine.

Fukushima, K. (1975). Cognitron: A self-organizing multilayered neural network. Biological Cybernetics, 20, 121–136.

Fukushima, K. (1980). Neocognitron: A self-organizing neural network model for a mechanism of pattern recognition unaffected by shift in position. Biological Cybernetics,36, 193–202.

Galetakis, M., Vasileiou, A., Rogdaki, A., Deligiorgis, V., & Raka, S. (2021). Estimation of mineral resources with machine learning techniques. Materials Proceedings, 5(1), 122. https://doi.org/10.3390/materproc2021005122.

Glorot, X., Bordes, A., and Bengio, Y. (2011). Domain adaptation for large-scalesentiment classification: A deep learning approach. In ICML'2011.

Goodfellow, I., Bengio, Y., & Courville, A. (2016). Deep Learning. MIT Press. Retrieved from https://www.deeplearningbook.org/.

Gülyüz, N. (2017). Textural and structural characteristics of the Kestanelik epithermal vein system, NW Turkey: implications for permeability enhancement mechanisms and gold exploration in epithermal systems (Doctoral dissertation, University of Strathclyde).

Gülyüz, N., Gülyüz, E., Shipton, Z. K., Kuşcu, İ., & Lord, R. A. (2020). Geological and mineralization characteristics of the Kestanelik epithermal Au-Ag deposit in the Tethyan Metallogenic Belt, NW Turkey. Geosciences Journal, 24(4), 407-424

Gümüş, A. (1964). Contribution a l'etude geologique de secteur serpentrional de Kalabak köy-Eymür Köy region D'Edremit, Turqie, MTA Bulletin, 117, 1-109.

Günaydın, A. (2017). Geology and geochemistry of nodular-phosphate and fault-controlled hydrothermal-phosphate mineralizations in Arıklı and Nusratlı villages (Ayvacık-Çanakkale, NW Turkey). Bulletin of the Mineral Research and Exploration, 155(155), 131–146. https://doi.org/10.19111/bulletinofmre.314197.

Harris, N.B.W., Kelley, S., & Okay, A.I. (1994). Post-collision magmatism and tectonics in northwest Anatolia. Contributions to Mineralogy and Petrography, 117, 241-251.

Harris, C. R., Millman, K. J., van der Walt, S. J., Gommers, R., Virtanen, P., Cournapeau, D., Wieser, E., Taylor, J., Berg, S., Smith, N. J., Kern, R., Picus, M., Hoyer, S., van Kerkwijk, M. H., Brett, M., Haldane, A., del Río, J. F., Wiebe, M., Peterson, P., Gérard-Marchant, P., ... & Oliphant, T. E. (2020). Array programming with NumPy. Nature, 585(7825), 357–362. https://doi.org/10.1038/s41586-020-2649-2.

Hedenquist, J. W., Arribas, A., & González-Urien, E. (2000). Exploration for epithermal gold deposits. In S. G. Hagemann & P. E. Brown (Eds.), Gold in 2000 (Reviews in Economic Geology, Vol. 13, pp. 245–277). Littleton, CO: Society of Economic Geologists.

Hinton, G. E. (1989). Connectionist learning procedures. Artificial Intelligence, 40,185–234.

Hinton, G. E. (2006). To recognize shapes, first learn to generate images. Technical Report UTML TR 2006-003, University of Toronto.

Huijbregts, Ch., Matheron,G., (1977). Universal kriging- an optimal approach to trend surface analysis. Can.Inst.Min.Metall., Spec. Vol.1, 159–169.

Jain, A., & Yellishetty, M. (2021). Machine learning—A review of applications in mineral resource estimation. Energies, 14(14), 4079.

Jarrett, K., Kavukcuoglu, K., Ranzato, M., and LeCun, Y. (2009). What is the best multi-stage architecture for object recognition? In ICCV'09.

Joint Ore Reserves Committee. (2012). Australasian Code for Reporting of Exploration Results, Mineral Resources and Ore Reserves (The JORC Code) (2012 ed.). Retrieved from https://www.jorc.org/docs/jorc_code2012.pdf.

Journel, A.G., 1974, Geostatistics for conditional simulation of ore bodies, Economic Geology 69, 673–687.

Journel, A. G., & Huijbregts, C. J. (1978). *Mining Geostatistics*. Academic Press.

Journel, A.G., (1982). The indicator approach to the estimation of spatial distributions. Proc.17th APCOM,Colorado School of Mines, 793–806.

Isaaks, E. H., & Srivastava, R. M. (1989). *An Introduction to Applied Geostatistics*. Oxford University Press.

Kalafatçıoğlu, A. (1963). Ezine civarının ve Bozcaada'nın jeolojisi, kalker ve serpantinlerinin yaşı. MTA Bulletin, 60, 61-70 (in Turkish).

Kaymakci, N., Aldanmaz, E., Langereis, C., Spell, T.L., Gurer, O.F. & Zanetti, K.A. (2007). Late Miocene transcurrent tectonics in NW Turkey: evidence from palaeomagnetism and 40Ar–39Ar dating of alkaline volcanic rocks. Geological Magazine, 144, 379–392.

Kaymakci, N. Özcelik, Y. White, S.H. & Van Dijk, P.M. (2009). Tectono stratigraphy of the Çankiri Basin: Late Cretaceous to Early Miocene evolution of the Neotethyan Suture Zone in Turkey. In: Van Hinsbergen, D.J.J., Edwards, M.A. & Govers, R. (eds) Geodynamics of Collision and Collapse at the Africa-Arabia-Eurasia subduction zone, Geological Society, London, Special Publications, 311, 67-106.

Kingma, D. and Ba, J. (2014). Adam: A method for stochastic optimization. arXivpreprint arXiv:1412.6980.

Khan, S. U., Khan, A. A., & Mahmood, H. (2022). Machine learning in geosciences: A review of complex environmental monitoring applications. Earth, 6(2), 59–73.

Kuşcu, İ., Tosdal, R. M., & Gençalioğlu-Kuşcu, G. (2019). Episodic porphyry Cu (Mo-Au) formation and associated magmatic evolution in Turkish Tethyan collage. Ore Geology Reviews, 107, 119-154.

Krige, D. G. (1951). A Statistical Approach to Some Basic Mine Valuation Problems on the Witwatersrand. CSIR (Council for Scientific and Industrial Research) Report, South Africa.

Krige, D.G., (1952), A statistical analysis of some of the borehole values in the Orange Free State goldfield. J.Chem. Metall. Min. Soc. S.Afr., Sept. 47 64.

Laramide Resources Ltd. (2025). Company profile. Retrieved from https://laramide.com/.

Lassonde, P. (1990). The Gold Book: The Complete Investment Guide to Precious Metals.

Le Pichon, X., & Angelier, J. (1979). The Hellenic arc and Trench system: a key to the neotectonic Evolution of the Eastern Mediterranean Area. Tectonophysics, 60, 1-42

Li, S., Li, W., Wang, X., & Chen, Y. (2016). Mining land use information from remote sensing images using machine learning algorithms: A case study in northern China. Journal of Remote Sensing, 37(3), 211–225.

Mahboob, M. A., Celik, T., ve Genc, B. (2022). Review of machine learning-based Mineral Resource estimation. The Journal of the Southern African Institute of Mining and Metallurgy, 122(11), 655-664. https://doi.org/10.17159/2411-9717/1250/2022

Matheron, G. (1963). Principles of geostatistics. Economic Geology, 58(8), 1246–1266.

Matheron, G. (1971a). The Intrinsic Random Functions and Their Applications. Advances in Applied Probability, 3(3), 439–468.

Matheron, G. (1971b). The Theory of Regionalized Variables and Its Applications. École des Mines de Paris (Note Géostatistique No. 5).

Meulenkamp, J.E., Wortel, W.J.R., Van Wamel, W.A., Spakman, W., & Hoogerduyn, S.E. (1988). On the Hellenic subduction zone and geodynamic evolution of Crete in the late middle Miocene. Tectonophysics, 146, 203-215.

McKenzie, D.P. (1972). Active tectonics of the Mediterranean region. Geophysical Journal International, 30, 109-185.

Mckenzie, D.P. (1978). Active Tectonics of the Alpine-Himalayan Belt: The Aegean Sea and Surroundings Regions (Tectonics of the Aegean Region). Geophysical Journal International, 55, 217-254

McKinney, W. (2010). Data structures for statistical computing in Python. In S. van der Walt & J. Millman (Eds.), Proceedings of the 9th Python in Science Conference (pp. 51–56). https://doi.org/10.25080/Majora-92bf1922-00a.

Meade, B. J., & Perron, J. T. (2023). Combining physics-based models and machine learning to forecast geophysical phenomena. Journal of Geophysical Research: Solid Earth, 128(2), e2022JB026310.

Mitchell, T. M. (1997). Machine Learning. McGraw-Hill, New York.

Nair, V. and Hinton, G. (2010). Rectified linear units improve restricted Boltzmannmachines. In ICML'2010.

Okay, A.I., Siyako, M. & Bürkan, K.A. (1990). Geology and tectonic evolution of the Biga Peninsula (in Turkish). Bulletin of the Turkish Association of Petroleum Geologists, 2, 83-121.

Okay, A. I., Siyako, M., & Bürkan, K. A. (1991). Geology and tectonic evolution of the Biga Peninsula, northwest Turkey. Bulletin of the Technical University of Istanbul, 44(1-2), 191-256.

Okay, A.I., Satır, M., Maluski, H., Siyako, M., Monie, P., Metzger, R. & Akyüz S. (1996). Paleo- and Neo-Tethyan events in northwest Turkey: geological and geochronological constraints. In: Yin, A. & Harrison, M. (ed.) Tectonics of Asia, Cambridge University Press, Cambridge, 420-441.

Okay, A. I., Harris, N. B. W. & Kelley, S. P. (1998). Exhumatioin of blueschists along a Tethyan suture in northwest Turkey. Tectonophysics, 285, 275–299.

Okay, A.I. & Tüysüz, O. (1999). Tethyan sutures of northern Turkey. In: Durand B., Jolivet, L., Horváthand F. & Séranne, M. (eds) The Mediterranean Basins: Tertiary extension within the Alpine orogen, Geological Society, London, Special Publications, 156, 475-515.

Okay, A. I., & Satır, M. (2000). Upper Cretaceous eclogite-facies metamorphic rocks from the Biga Peninsula, northwest Turkey. Turkish Journal of Earth Sciences, 9, 47–56.

Okay, A. I., & Satır, M. (2000b). Coeval plutonism and metamorphism in a latest Oligocene metamorphic core complex in Northwest Turkey. Geological Magazine, 137, 495–516

Okay, A.I., Tansel, I., Tuysuz, O., (2001). Obduction, subduction and collision as reflected in the Upper Cretaceous–Lower Eocene sedimentary record of western Turkey. Geol. Mag. 138, 117–142.

Okay, A.I., Monod, O., & Monie, P., 2002. Triassic blueschists and eclogites from northwest Turkey: vestiges of the Paleo-Tethyan subduction. Lithos, 64, 155-178.

OpenStreetMap Contributors. (2024). Retrieved from https: //planet.openstreetmap.org.

Özkan, Y.Z. (2025). A Review of Mineral Potential Estimation Methods. Journal of Geological Engineering,49, 63-88. DOI 10.24232/jmd.1633377.

Pedregosa, F., Varoquaux, G., Gramfort, A., Michel, V., Thirion, B., Grisel, O., Blondel, M., Prettenhofer, P., Weiss, R., Dubourg, V., Vanderplas, J., Passos, A., Cournapeau, D., Brucher, M., Perrot, M., & Duchesnay, É. (2011). Scikit-learn: Machine learning in Python. Journal of Machine Learning Research, 12, 2825–2830. http://www.jmlr.org/papers/v12/pedregosa11a.html.

Paszke, A., Gross, S., Massa, F., Lerer, A., Bradbury, J., Chanan, G., ... & Chintala, S. (2019). PyTorch: An imperative style, high-performance deep learning library. In Advances in Neural Information Processing Systems, 32, 8024–8035. https://papers.nips.cc/paper_files/paper/2019/hash/bdbca288fee7f92f2bfa9f7012727740-Abstract.html.

Ramsey, F. P. (1926). Truth and probability. In R. B. Braithwaite, editor, The Foundations of Mathematics and other Logical Essays, chapter 7, pages 156–198. McMaster University Archive for the History of Economic Thought.

Rumelhart, D. E., Hinton, G. E., and Williams, R. J. (1986). Learning internal representations by error propagation. In D. E. Rumelhart and J. L. McClelland, editors, Parallel Distributed Processing, volume 1, chapter 8, pages 318–362. MIT Press, Cambridge.

Rossi, M. E., & Deutsch, C. V. (2014). Mineral Resource Estimation. Springer, Dordrecht.

Sanchez, M. G., McClay, K. R., King, A. R., & Wijbrams, J. R. (2016). Cenozoic Crustal Extension and Its Relationship to Porphyry Cu-Au-(Mo) and Epithermal Au- (Ag) Mineralization in the Biga Peninsula, Northwestern Turkey. Society of Economic Geologists, Inc. Special Publication, 19, 113-156.

Schuiling, R.D. (1959). Uber eine praherzynische faltunggspase im Kazdağ kristallin, MTA Bulletin, 53, 89-93.

Seabridge Gold Inc. (2025). Company profile. Retrieved from https://www.seabridgegold.net/.

Shepard, D. (1968). A two-dimensional interpolation function for irregularly spaced points. In Proceedings of the 1968 ACM National Conference (pp. 517–524).

Şengör, A.M.C. & Yılmaz, Y. (1981). Tethyan evolution of Turkey: A plate-tectonic approach. Tectonophysics, 75(3–4), 181–241. doi:10.1016/0040-1951(81)90275-4.

Şengör, A. M. C., Görür, N. & Şaroğlu, F. (1985). Strike-slip deformation basin formation and sedimentation: Strike-slip faulting and related basin formation in zones of tectonic escape: Turkey as a case study, in Biddle, K.T. and Christie- Blick, N., eds., Strike-slip faulting and basin formation. Society of Economic Paleontologists and Mineralogist Special Publication, 37, 227-264.

Tukey, J. W. (1973). Exploratory Data Analysis. Reading, MA: Addison-Wesley.

Tunç, İ.O., Yiğitbaş, E., Şengün,F., Wazeck, J., Hofmann, M. & Linnemann, U. (2014). U-Pb zircon geochronology of northern metamorphic massifs in the Biga Peninsula (NW Anatolia-Turkey): new data and a new approach to understand the tectonostratigraphy of the region, Geodinamica Acta, 1-24. DOI: 10.1080/09853111.2013.877242.

Türkecan, A. & Yurtsever, A. (2002). 1:500 000 scale geological map of Turkey, İstanbul sheet. General Directorate of Mineral Research and Exploration publications, Ankara.

Werbos, P. J. (1981). Applications of advances in nonlinear sensitivity analysis. InProceedings of the 10th IFIP Conference, 31.8 - 4.9, NYC , pages 762–770.

Verlet, L. (1967). Computer “Experiments” on Classical Fluids. I. Thermodynamical Properties of Lennard-Jones Molecules. Physical Review, 159(1), 98–103.

Yılmaz, Y., & Karacık, Z. (2001). Geology of the northern side of the Gulf of Edremit and its tectonic significance for the development of the Aegean grabens. Journal Name, Volume(Issue), pages.

Yiğit, Ö. (2012). A prospective sector in the Tethyan Metallogenic Belt: Geology and geochronology of mineral deposits in the Biga Peninsula, NW Turkey. Ore Geology Reviews, 46, 118-148

Zhang, L., Zhu, X., Li, Y., & Wu, Y. (2022). GeoAI: Spatially explicit artificial intelligence techniques for geoscience applications. Geoscientific Instrumentation, Methods and Data Systems, 11(2), 195–213. https://doi.org/10.5194/gi-11-195-2022.